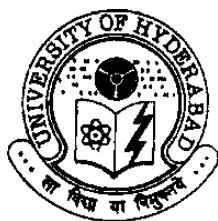# SYNTHESIS AND STUDY OF PHOTOPHYSICAL AND SIGNALING BEHAVIOR OF SOME ELECTRON DONOR-ACCEPTOR SYSTEMS

A Thesis
Submitted for the Degree of
DOCTOR OF PHILOSOPHY

by

Moloy Sarkar

School of Chemistry
University of Hyderabad
Hyderabad 500 046
INDIA

July 2007

To
My parents

"A hundred times every day I remind myself that my inner and outer life depend on the labors of other men, living and dead, and that I must exert myself in order to give in the same measure as I have received and am still receiving."

-Albert Einstein

STATEMENT

I hereby declare that the matter embodied in the thesis entitled **"Synthesis and study of photophysical and signaling behavior of some electron donor-acceptor systems"** is the result of investigations carried out by me in the School of Chemistry, University of Hyderabad, Hyderabad, India under the supervision of **Prof. Anunay Samanta**.

In keeping with the general practice of reporting scientific investigations, due acknowledgements have been made wherever the work described is based on the findings of other investigators. Any omission or error that might have crept in is regretted.

July 2007   **Moloy Sarkar**

SCHOOL OF CHEMISTRY

UNIVERSITY OF HYDERABAD

HYDERABAD-500 046, INDIA

Phone: +91-40-2301 1594 (O)
    +91-40-2301 0715 (R)
Fax: +91-40-2301 2460
Email: assc@uohyd.ernet.in
    anunay_s@yahoo.com

Anunay Samanta, F.A.Sc., F.N.A.Sc.   7th July 2007
Professor

CERTIFICATE

Certified that the work embodied in the thesis entitled *"Synthesis and study of photophysical and signaling behavior of some electron donor-acceptor systems"* has been carried out by **Mr. Moloy Sarkar** under my supervision and that the same has not been submitted elsewhere for any degree.

Anunay Samanta   Dean
(Thesis Supervisor)   School of Chemistry
                                      University of Hyderabad

Acknowledgement

List of Publication

1. Charge-transfer-induced twisting of the nitro group. J. A. Mondal, **M. Sarkar,** A. Samanta, H. N. Ghosh and D. K. Palit, *J. Phys. Chem. A* 2007 (ASAP article; DOI 10.1021/jp0737193).

2. Photophysical and density functional studies of the interaction of a flavone derivative with the halides. **M. Sarkar** and A. Samanta, *J. Phys. Chem. B* 2007, **111**, 7027-7033.

3. Ratiometric-fluorescence signaling of fluoride ions by an amidophthalimide derivative. **M. Sarkar**, R. Yellampalli, B. Bhattacharya, R. K. Kanaparthi and A. Samanta, *J. Chem. Sci.* 2007, **119**, 91-97.

4. Structure-property relationship of aminonitrofluorenes synthesized by copper-mediated Ullmann-type C-N bond formation. **M. Sarkar** and A. Samanta, *Synthesis* 2006, **20**, 3425-3430.

5. A highly selective off-on fluorescence chemosensor for Cr(III). **M. Sarkar**, S. Banthia and A. Samanta, *Tetrahedron Lett.* 2006, **47**, 7575-7578.

6. pH-regulated "off-on" fluorescence signaling of d-block metal ions in aqueous media and realization of molecular IMP logic function. **M. Sarkar**, S. Banthia, A. Patil, Md. B. Ansari and A. Samanta, *New J. Chem.* 2006, **30**, 1557-1560.

7. Size-dependent evolution of optical properties on molecular/nano microcrystals: Manifestation of hierarchical interaction. A. Patra, N. Hebalkar, B. Sreedhar, **M. Sarkar**, A. Samanta and T.P. Radhakrishnan, *Small* 2006**, 5**, 650-659.

8. Charge resonance character in charge transfer state of bianthryls: Effect of symmetry breaking on time-resolved near-IR absorption spectra. T. Takaya, S. Saha, H. Hamaguchi, **M. Sarkar**, A. Samanta and K. Iwata, *J. Phys. Chem. A* 2006**, 110**, 4291-4295.

9. Synthesis, photophysical and metal ion signaling behaviour of mono- and di-azacrown derivatives of 4-Aminophthalimide. N.B. Sankaran, **M. Sarkar** and A. Samanta, *J. Chem. Sci.* 2005**, 117**, 105-110.

10. Photophysical and transition metal ion signalling properties of some 4-amino-1,8-naphthalimide derivatives. S. Banthia, **M. Sarkar** and A. Samanta, *Res. Chem. Interm.* 2005**, 31**, 25-38.

11. Excitation-wavelength-dependent fluorescence behaviour of some dipolar molecules in room-temperature ionic liquids. P. K. Mandal, **M. Sarkar** and A. Samanta *J. Phys. Chem. A* 2004, **108**, 9048-9053.

12. 10,10'-Dibromo-9,9'-bianthryl, **M. Sarkar** and A. Samanta, *Acta Cryst* **E** 2003, **59**, o1764-o1765.

13. Multiple emission of some push-pull aminonitrofluorene derivatives. **M. Sarkar,** P. K. Mandal and A. Samanta (in preparation).

14. Synthesis and photophysical behaviour of some new flavone derivatives. **M. Sarkar,** R. K. Kanaparthi, B. Bhattacharya and A. Samanta (in preparation).

Conference presentations

1. Photophysics of Some Push-Pull Fluorene Derivatives. **M. Sarkar** and A. Samanta. Trombay Symposium for Radiation and Photochemistry, at Bhaba Atomic Research Centre, Mumbai, India, Jan. 2006 (Poster presentation).

2. Base-triggered Signaling of Transition Metal ions, The First fluorescent Molecular IMP Logic Gate, Plus Selective Signaling of Fluoride ions. **M. Sarkar** and A. Samanta. ChemFest – 2006, 3rd annual in-house symposium of the School of Chemistry, University of Hyderabad, Hyderabad, India, Feb. 2006 (Poster presentation).

3. Synthesis and Photophysical Behavior of a New Chromone-based Chemosensor for Fluoride ions: Signaling by both Colorimetric and Fluorescence Responses. **M. Sarkar** and A. Samanta. National Symposium for Radiation and Photochemistry, at National Centre for Ultra Fast Processes, Chennai, India, Jan. 2007 (Poster presentation).

4. Synthesis and Photophysical Behavior of a New Flavone- based Chemosensor for Fluoride ions: Signaling by both Colorimetric and Fluorescence Responses. **M. Sarkar**. ChemFest – 2007, 4th annual in-house symposium of the School of Chemistry, University of Hyderabad, Hyderabad, India, March. 2007 (Oral presentation).

Thesis Layout

The thesis has been divided into eight chapters. ***Chapter 1*** provides a brief introduction on the electron donor-acceptor (EDA) systems and different photophysical phenomena associated with them. The underlying principles of molecular recognition and the design strategies for the development of chemsensors for transition metal ion and anion have been discussed. Further exploration of the sensory actions towards the construction of molecular logic gate has also been illustrated briefly. ***Chapter 2*** provides the details of the experimental procedures and methodologies adopted in this investigation. The instrumental details and methods for theoretical calculations have also been discussed in this chapter. ***Chapter 3*** deals with the synthesis and photophysical behavior of some newly synthesized aminonitrofluorene-based EDA systems. ***Chapter 4*** presents the synthesis and photophysical investigations of another set of amonomethoxyflavone-based EDA systems. ***Chapter 5*** deals with the chromogenic and fluorescence ratiometric responses of a flavone-based chemosensor towards selective signaling of fluoride. ***Chapter 6*** describes the signaling behavior of a simple 4-aminophthalimide-based "off-on" fluoresce sensor system for the selective detection of chromium (III). ***Chapter 7*** delineates the signaling behavior of the nitrobenzoxadiazole-based chemosensor towards both cation and anion. The potential application of the system as a two-input IMP molecular logic gate is also demonstrated. ***Chapter 8*** summarizes the findings of the present investigations by touching upon the achievements and looking into the future scope and upcoming challenges.

Contents

Chapter 1

Introduction

This chapter provides an overview of the electron donor-acceptor (EDA) systems emphasizing on their basic photophysical behavior and potential application towards signaling of cation and anion. Specifically, different photophysical processes associated with the EDA systems, such as reordering of the energy states, radiative and nonradiative phenomena are discussed. The underlying principles and the mechanism of molecular recognition are also discussed giving particular attention to transition metal ions and anions. The systems associated with molecular photonics and electronic devices are also touched upon. The chapter is concluded describing the motivation of the thesis and introducing the systems studied in this work.

1.1. Electron donor-acceptor molecules and their characteristics

Electron donor-acceptor (EDA) molecules have attracted considerable attention in recent years primarily because of the fact that charge separation is one of the most fundamental processes involved in numerous chemical and biological transformations. Understanding of the photoinduced charge separation process, which plays an important role in the primitive photosynthesis phenomenon[1] in plants, helps design and development of efficient systems for solar energy conversions[2-9] in modern days. Moreover, the EDA systems also find their utility in sensing environments,[10] as nonlinear optical materials,[11] molecular electronic

devices,[12] etc. EDA systems also serve as a favorite testing ground for the theories of electron transfer and solvation dynamics.[13]

Mulliken first introduced the concept of charge-transfer transition to describe the spectral and bonding interactions of molecular complexes formed between an electron donor and an acceptor.[14,15] The charge transfer can take place either through bond or through space. In a system where the electron donor and acceptor moieties are connected by a flexible spacer, a charge-transfer complex or exciplex is often formed due to the spatial overlap between the donor and acceptor orbitals.[16] On the other hand, where through-space interaction of the donor and acceptor orbitals is not possible due to limited configurational flexibility, charge separation can take place as a result of through-bond interaction of the two. In both cases, appropriate model systems[17-19] have been used to investigate the dependence of the electron transfer rate on the free energy of reaction, the distance and orientation between the donor and acceptor and the medium. When the charge transfer (CT) state is luminescent, the CT emission provides an excellent opportunity to monitor the dynamics because internal and environmental influences affect this luminescence in such a way that it provides detailed information on their thermodynamic and kinetics of photophysical properties. The simple photophysical techniques such as steady state and time-resolved fluorescence as well as transient absorption studies are useful for the detection of the CT state.

For a majority of the EDA molecules, an appreciable increase in the dipole moment is observed when they are subjected to photoexcitation. The emission maxima and quantum yields of these compounds are often very much sensitive to

the polarity of the medium. This sensitivity is often exploited to determine the polarity of unknown solvent mixtures or to estimate the polarity of the microenvironments in organized assemblies such as micelles and membranes. Examples of these kinds of probes are prodan (**1**)[20,21], ANS (**2**) [22] and hemicyanine dye (**3**).[23]

(1)

(2)   **(3)**
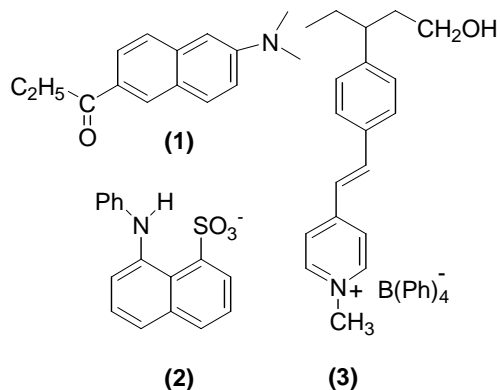
The presence of low-lying closely spaced n-π* and π-π* energy levels is another notable feature for the organic EDA heterocycles. For systems with π-π* state as lowest excited state, a high emission probability for dipole allowed π-π* state with a large emission rate constant can be predicted. On the other hand, for heterocycles with n-π* state as the lowest excited state, a longer lifetime and smaller emission rate constant can be predicted because of the forbidden character

(4)   **(5)**   **(6)**   **(7)**   **(8)**
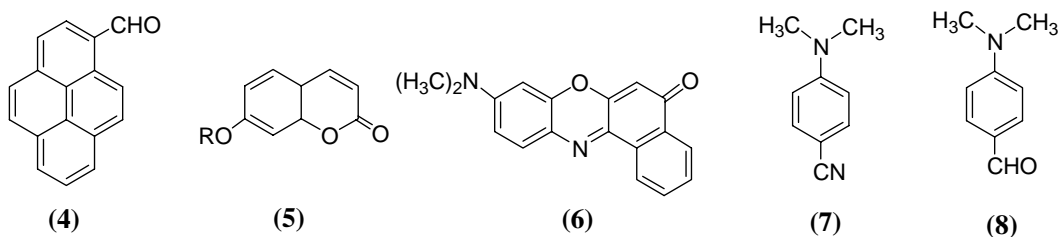
of the transition to the ground state. The response of these two states towards the polarity of the solvents is quite different. Solvent can alter the ordering of the two states or can change the spacing between the states leading to a drastic change in

the fluorescence efficiency. Fluorophore like PyCHO (**4**),[24,25] 7-alkoxycoumarin (**5**) [26] and nile red (**6**) [27] are of these kind. The reversal of the energy levels not only affects the singlet manifold but also the triplet states, thereby causing a change in the rate of intersystem crossing (ISC) process. The dependence of intersystem crossing quantum yield, ϕ_{isc}, of *p*-N,N-dimethylaminobenzonitrile (DMABN) (**7**) and *p*-N,N-dimethylaminobenzaldehyde (DMABA) (**8**) on the solvent polarity has been interpreted by considering the influence of n-π* and π-π* energy states on the nonradiative rate constants of the systems.[28] The observed result of $\phi_{isc} \approx 1.0$ in nonpolar solvent for DMABA has been described as a result of reordering of n-π* and π-π* state.[28]

1.2. Radiative processes: dual emission

A photoexcited molecule when returns to the ground state by radiative transition, *fluorescence emission* is observed. One of the most widely held generalization in solution phase photochemistry has been that photoreaction and luminescence occur from vibrationally relaxed molecule in their lowest singlet or triplet state (Kasha's rule). This implies that irrespective of the excitation energy, polyatomic molecules should emit from the lowest excited state and hence, display a single fluorescence. That most photochemical and luminescent events in solution occur from the lowest vibrational level of the lowest electronic states simply means that the nonradiative decay rate is ordinarily faster than competing radiation or photoreaction from higher excited states.

(9)   (10)   (11)   (12)   (13)
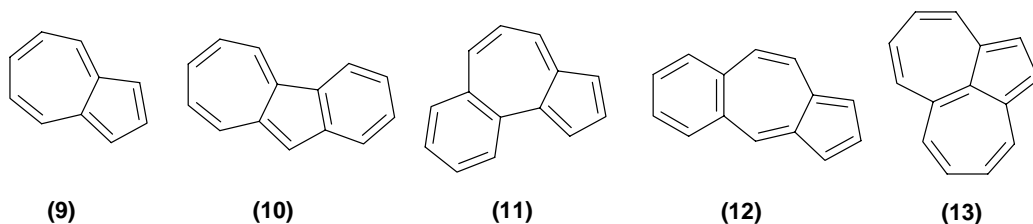
However, this conclusion is not absolute as one expects that photochemistry and luminescence from higher excited states might be most easily observable when radiationless deactivation rates are unusually slow or when radiative or photochemical deactivation rates are unusually fast. Indeed, the best documented example is the dual fluorescence of azulene (**9**).[29] The system emits from both S_1 and S_2 state, as the energy gap between S_2 and S_1 is large making the nonradiative $S_2 \leadsto S_1$ transition slower or comparable to the $S_2 \rightarrow S_0$ fluorescence. Likewise, some benzene annulated azulene derivatives (**10-12**),[30-32] the derivatives of Hafner's hydrocarbon (**13**)[33] exhibit dual fluorescence. S_2 emission from many other systems which include acenaphthylene,[34] ketocyanine dye[35] is also reported.

Multiple emission can also arise due to ground and excited state processes. Ground and excited state complexation of a fluorescent system with other species like DNA,[36] cyclodextrin,[37] solvent[38] may give rise to dual fluorescence. Excited state processes, such as energy transfer,[39-42] exciplex formation,[43-45] excited state proton transfer[46-48] also lead to dual emission. In this context, Twisted Intramolecular Charge Transfer (TICT) phenomenon[49-51] is one of the most extensively studied process. Grabowski and his coworkers introduced the concept of TICT mechanism for a more complete description of the dual fluorescence of 4-dimethylaminobenzonitrile (DMABN).[52,53] According to this concept, the short-

wavelength fluorescence of DMABN originates from the LE state and the long-wavelength band from the TICT state. Complete decoupling of the donor and acceptor orbitals and localization of the transferred electron on the acceptor orbital gives the TICT state a highly dipolar character and accounts for the sensitivity of the TICT emission on the polarity of the medium.

1.3. Nonradiative processes: an overview

The nonradiative electronic processes in isolated molecules and condense phase, which take place without the breaking of any chemical bond, normally involve the conversion of electronic energy to vibrational energy.[54] The nonradiative decay processes have many useful consequences in dye laser operation,[55] efficiency of fluorescence probes,[56] stereomutation of 'push-pull' stilbenes, polyene and rhodopsin,[57-60] light fastness of dyeing agents,[61] effectiveness of photographic sensitizers[62] and molecular switching devices.[63] Radiationless transition between initial and final electronic states normally occurs at the point of intersection of potential energy surfaces. The nonradiative transition occurs irreversibly at this isoenergetic point to the higher vibrational level of the lower energy state and the excess vibrational energy cascades down the vibrational manifold. It is to be noted that efficiency of the radiationless transition increases with the increase in the overlap integral (Franck-Condon integral) value of the two interacting states. However, Franck-Condon integral is not always the sole criterion for efficient crossover from one energy state to another. Symmetry restrictions and spin multiplicity rule impose their own inefficiency factors. In addition to these, *density of state* is another contributing factor for determining the efficiency of the nonradiative process. For example, in

solution, the medium may provide a background of its own energy states in resonance with the initial state, which often facilitates the radiationless transition through the *quasicontinuum* of the final state. These three key factors, (1) energy gap between the interacting electronic states, (2) Franck-Condon overlap integral and (3) density of state, are known to govern the efficiency of the nonradiative processes. Rigid polyatomic systems like naphthalene, anthracene etc. have a finite rate of nonradative process due to these inherent factors. Whereas, structurally flexible systems, which often exhibits unusually high nonradiative rate due to the internal motion of the systems. There are several factors related to the internal motion of the molecule that enhance the nonradiative rate in the systems. These factors are briefly touched upon by illustrating some of the well known fluorescent probes.

1.3.1. Rhodamines

These are a group of popular xanthene dyes (**14**), which show interesting photophysical behavior. Rhodamines in frozen solutions or rhodamines with rigid amino group (such as rhodamine 101) show fluorescence quantum yield close to unity.[64,65] It is found that the internal conversion of these dyes is strongly associated with the rigidity of the xanthene-amine C-N bond. Several models have been proposed to explain the unusual dependence of the internal conversion rate on the solvent and molecular structure of the xanthene dyes. Among them the TICT model[66,67] and umbrella like motion (ULM) model[68-70] are noteworthy. Whereas, the TICT model is mainly governed by the viscosity and polarity of the solvent, the ULM model stresses on the importance of specific solute-solvent interactions for unusually high internal conversion rate. Rettig et al. proposed the

involvement of nonradiative TICT state for rhodamines and few other xanthene dyes.[66,67] A higher quantum yield and lifetime of the monoalkyl derivative compared to dialkyl substituted rhodamine are attributed to a higher energy of the TICT state of the former system. An alternative mechanism by Arbeloa et al.[68] effectively correlates the internal conversion with a change in the amino group configuration from planar to pyramidal one, known as ULM motion.

1.3.2. Coumarins

In order to account for the dependence of the fluorescence property of coumarins (**15**) on the structure of the amino moiety and on the polarity of the medium, Jones II and coworkers have proposed a model,[71-73] according to which the planar intramolecular charge transfer state is highly fluorescent, whereas twisted charge transfer state is nonemissive. Recently, de Melo et al.[26,74] have shown that the photophysical behavior of some coumarin derivatives is essentially determined by the relative location of two energetically close-lying n-π* and π-π* singlet states. A mixing between the two states depending upon the polarity of the media and the nature of the amino substitution controls the magnitude of the nonradiative rates in methoxycoumarin (**16**).

1.3.3. Squaraine

Another class of popular dyes emitting in the visible range, which show interesting nonradiative decay behavior, are squaraine derivatives. The nonfluorescent nature of **17** was interpreted in terms of twisting of the amino moiety around the C-N bond.[75,76] Essentially, the twisting leads to a region close to the funnel of conical intersection, which acts as a nonemissive decay channel.

(14)

(15)

(16)

(17)

(18)

R = H, Me,
Et

(19a)

n = 1-4

(19b)

R = H, Me,
Et

(20a)

n = 1-4

(20b)
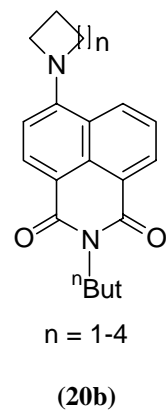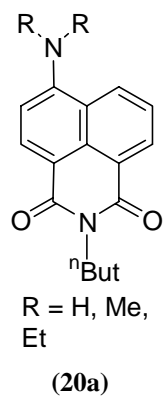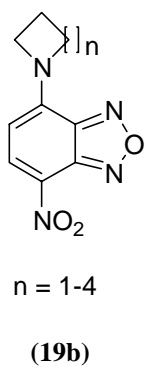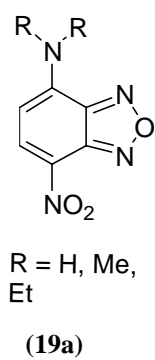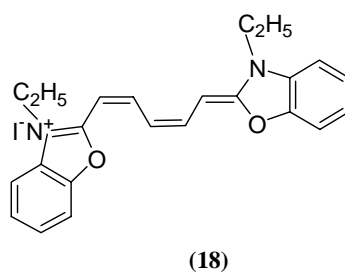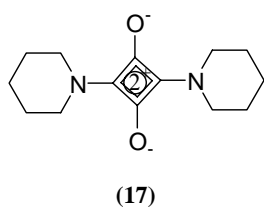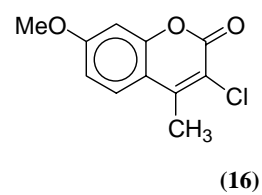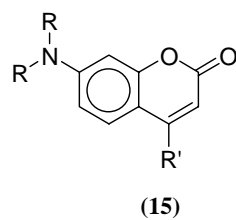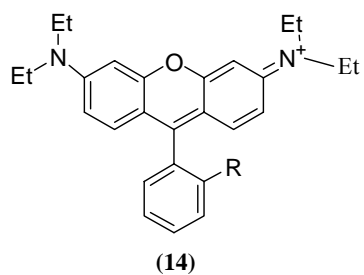
1.3.4. Cyanine dye

Among the large organic molecules, cyanine dyes are interesting systems for the study of solvent and temperature dependence on the radiative and nonradiative processes. Fleming et al. have studied DODCI (**18**), a cyanine dye in a series of polar solvents at different temperatures as well as in rigid matrix and clarified the kinetics for the nonradiative decay.[77] The nonlinear (curved) Arrhenius plot was interpreted by invoking the involvement of a second nonradiative decay channel with a low activation energy barrier (~1.55 kcal/mol). The nonradiative process with low activation barrier can, in principle, be a direct internal conversion which at high temperature cannot compete with the twisting process.

1.3.5. Nitrobenzoxadiazole and naphthalimide derivatives

Recently, two sets of EDA systems, amine-terminated nitrobenzoxadiazole (**19a-b**) and naphthalimide (**20a-b**) derivatives have been studied by Samanta and his coworkers with a view to elucidate the nonradiative pathways in these systems.[78,79] It has been found that the nonradiative rate constants of these systems largely depend on the nature of the amino substituents. An increase in the length of the dialkyl groups connected to the amino nitrogen or an increase in the size of the ring containing the amino nitrogen enhances the nonradiative deactivation of the fluorescence state of the systems. It has also been shown that the variation in the nonradiative rate constants in both cases can be best explained in terms of the nitrogen inversion model.

1.4. Molecular recognition

The process of binding of an analyte to a molecular fragment called receptor is defined as recognition.[80-83] Molecular recognition thus refers to recognition of the substrate by the receptor leading to strong and specific complexation. Sensing typically refers to the monitoring of a chemical species (the analyte) in a given matrix (air, blood, tissue, waste effluents, drinking water, a glass vessel in the lab etc.). However, sensing is not simply recognition, but requires the recognition event to be signaled by a drastic change of a given property, which should be visually and/or instrumentally detectable. Molecular recognition has become an important area of research because of its significance and diverse applications in physical, chemical as well as biological sciences.[84-86]

Chemosensors are molecules capable of binding selectively and reversibly the analyte of interest (molecule, cation, anion) with subsequent change in one or more properties of the system, such as absorption or fluorescence spectrum, redox potential etc.[87,88] The two different processes involved during analyte detection, i.e. molecular recognition and signal transduction, can be visualized[89] by considering three different components: a receptor, which is responsible for selective analyte binding, a signaling unit, which signals the binding event by a change in the property and eventually, a spacer that tunes the electronic interaction between the two former moieties. The binding interactions between receptor and analyte can be of different kinds: hydrogen-bond or π-interactions for molecule, coordinative interactions for cation, hydrogen-bond or coordinative or electrostatic interactions for anion.[90] For an efficient chemosensor, the recognition process has to be fast, guest-selective and reversible.

1.5. Cation sensing

Detection of cation is of immense interest to chemists, biologists, biochemists and environmentalists. Among the cations, protons and the s-block metal ions *viz.* Na^+, K^+, Mg^{2+} and Ca^{2+} have received early attention owing to their importance in biology.[91] In chemical oceanography, it has been demonstrated that some nutrients required for survival of microorganisms in sea water contain zinc, iron and manganese as enzyme cofactors. It is also well known that chromium, mercury, lead and cadmium are toxic for organisms, and early detection of these analytes is highly desirable. Heavy and transition metal (HTM) ions, though important in biology and environment, have been taken up actively only in the recent years.[92-94]

1.5.1. Signaling strategies

Among the numerous analytical methods that are available for detection of cations, flame photometry, atomic absorption spectrometry, ion sensitive electrodes, electron microprobe analysis, neutron activation analysis etc. are expensive, often require samples in large quantity and do not allow continuous monitoring. In contrast, the methods based on colorimetric and fluorescent detection[87-94] offer distinct advantages in terms of sensitivity, selectivity and response time. Several mechanisms have been exploited for fluorescence signaling. These include monitoring of the n-π*,[95,96] π-π*,[97] metal-centered (MC),[98] intramolecular charge transfer (ICT),[99-101] metal to ligand charge transfer (MLCT),[102] twisted intramolecular charge transfer (TICT),[103] triplet[104-106] excited states, monomer-excimer emission bands,[107-110] electronic energy transfer

(EET)[111] and fluorescence resonance energy transfer (FRET)[112]. However, despite the availability of various mechanisms stated above, the most commonly and popularly known mechanism for fluorescence signaling of various guest species is based on photoinduced electron transfer (PET) process.[113]

PET mechanism: The most commonly employed design for "off-on" fluorescence signaling of a guest is based on multi-component molecular system with a *fluorophore-spacer-receptor* architecture (Scheme 1.1).[88]

In this design, the fluorophore and the receptor sites are connected by an intervening spacer unit. This means that these three separate units: guest-binding unit, terminal fluorophore and spacer serve as quantitative predictors for the sensory properties of the multi-component super-molecule.

Thus, a sensor can be designed such that communication between the receptor and the photo-excited fluorophore leads to fluorescence quenching of the system ("off" state) in the absence of any guest. In the presence of a guest, the guest-receptor interaction should lead to a disruption of the communication between the receptor and the fluorophore thereby "switching on" the fluorescence. Sensors based on this mechanism are termed as PET sensors.[88,113] The chosen fluorophore should have high fluorescence efficiency and the receptor should bind the guest strongly and should be optically transparent at the absorbing wavelength of the fluorophore. Finally, the fluorophore and the receptor should be linked through a spacer such that PET is maximized in the *fluorophore-spacer-receptor* system. As PET is a long range interaction process,
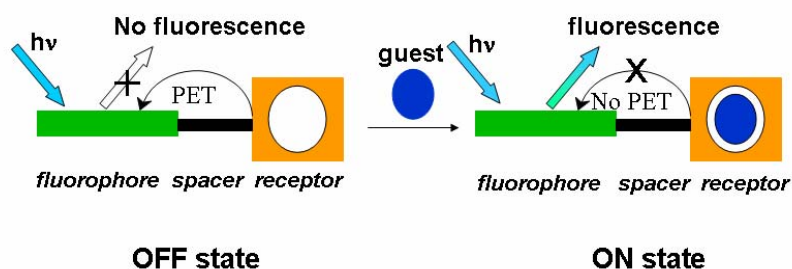
Scheme 1.1 The assembly of functional components in a fluorescent "Off-On" sensor based on PET mechanism.

generally, a short and flexible spacer unit is better than long and rigid ones for an efficient PET in the system.

The thermodynamic criterion for PET can be assessed from the knowledge of the redox potentials of the fluorophore and receptor and the singlet energy of the fluorophore using the following equation.[114,115]

$$\Delta G^* = [E_{ox}\,(\text{receptor}) - E_{red}\,(\text{fluorophore})] - E_{0,0} \qquad (1.1)$$

Where ΔG^* is the free energy of the photoinduced electron transfer process, E_{ox} (receptor) is the oxidation potential of the receptor, E_{red} (fluorophore) is the reduction potential of the fluorophore and $E_{0,0}$ is the singlet energy of the fluorophore. The exothermicity ($\Delta G^* < 0$) is the primary requirement for an efficient electron transfer process. Small exergonic driving force is preferred over a large exergonicity so that it can be easily switched over to an endergonic condition by a suitable charge perturbation. Such a perturbation can occur when a guest binds to the receptor unit causing an increase in the oxidation potential of the guest-bound receptor. A frontier orbital energy diagram of a guest-binding is shown in Scheme 1.2.
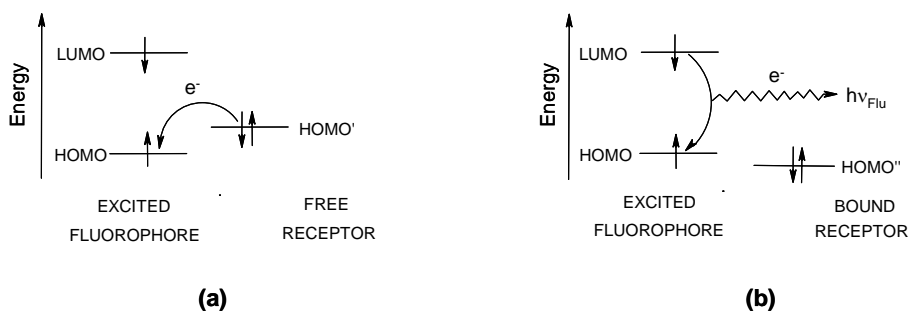
Scheme 1.2 Frontier orbital energy diagram for a fluorophore-receptor pair (a) where PET is feasible, (b) when the receptor is occupied by a cation.

1.5.2. Some examples

Ever since Tsien reported a system for real-time and real-space determination of the activity of Ca^{2+} within living cell by fluorescence microscopy,[116] significant amount of work has been put forward for the design and development of fluorescent PET sensors. Major contributions to the development of this class of fluorosensors have come from the research groups of Lehn, de Silva, Czarnik, Balzani, Fabbrizzi, Shinkai and Valeur.[81-94] Some representative examples of PET sensors developed for various cations have been highlighted here.

Compound **21** is an early example of a fluorescent pH sensor.[117] Then several systems based on anthracene chromophore have followed with improved binding properties of the receptor units. For example, Compound **22** exhibits pH dependent fluorescence in acetonitrile/water solutions.[118] The fluorescence is particularly quenched above pH 4.0 when the amino groups are proton free. With Cu^{2+} and Ni^{2+}, quenching of fluorescence is observed, while Zn^{2+} induces fluorescence enhancement.[118] Compound **23** behaves as more sophisticated 'off-

on-off' switch for protons.[119] This system also exhibits 'off-on' signaling behavior with Zn^{2+}.
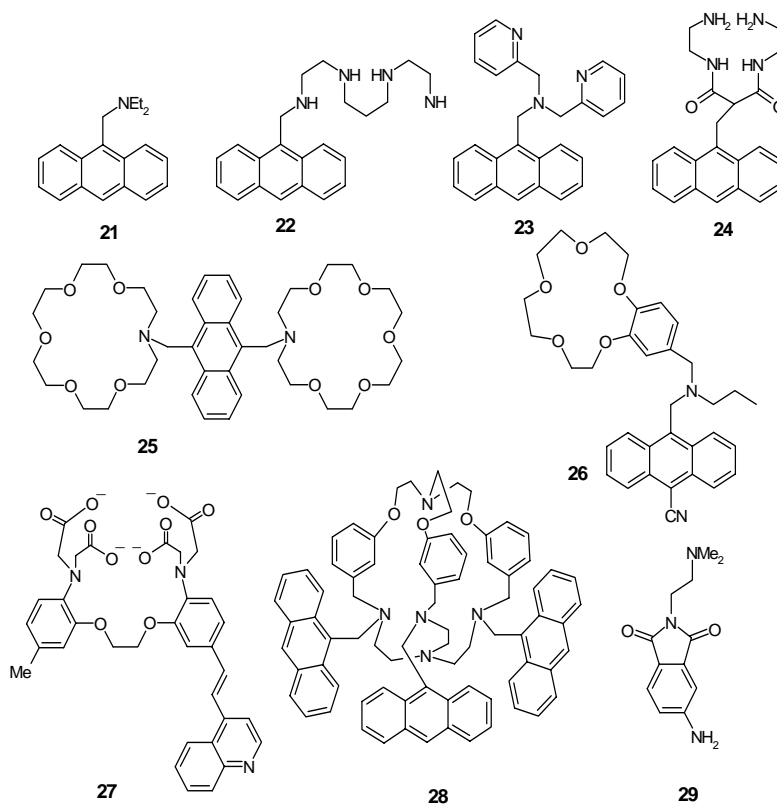
The higher ligand field stabilization energies of Ni^{2+} and Cu^{2+} have been employed in designing selective fluorosensor **24** for these metal ions by using a dioxo-tetramine ligand.[120] Compound **25** employs two PET active receptors. A degree of length recognition is achieved with this system and excellent "switching on" of fluorescence was found with α,ω-alkanediammonium ions.[121] On the other hand, compound **26** is capable of mimicking the switching phenomena based on

molecular logic devices.[122] This system acts as an AND logic gate when H^+ and Na^+ are considered as the two ionic inputs, fluorescence as the output and exciting light as the power supply. Compound **27** mimics the function of XOR logic gate induced by H^+ and Ca^{2+} ions.[123]

In order to develop efficient 'off-on' signaling systems for the transition metal ions, Bharadwaj et al. utilized a tripodal cryptand receptor to develop **28** that not only binds the metal ions tightly but also insulates them from the fluorophore moiety, thereby preventing the quenching interaction between the metal ions and the fluorophore.[124] This system is reported to be the first 'off-on' fluorosensor for transition metal ions, which are notorious for their quenching abilities.

On the other hand, Ramachandram and Samanta used a different strategy for the development of structurally simple 'off-on' sensor systems for the quenching metal ions.[125] Taking into consideration the redox nature of the interaction between the fluorophore and the transition metal ions, electronically deficient fluorophore, 4-aminophthalimide, was employed in the *fluorophore-spacer-receptor* system, **29**, to minimize the quenching interaction of the transition metal ions.[125]

1.6. Anion sensing

Recognition and sensing of anions have become an active area of contemporary research.[126-131] Inorganic anions play an important role in various industrial processes, energy transduction and enzyme activity in organisms, clinical treatment of diseases, etc.[132,133] Anions are ubiquitous throughout biological systems. They carry genetic information (DNA is a polyanion) and the majority of the enzyme substrates and co-factors are anionic. A well known

example is carboxypeptidase A,[134] an enzyme that coordinates to the C-terminal carboxylate group of polypeptides by the formation of an arginine-aspartate salt bridge, and catalyzes the hydrolysis of this residue. This is evident from the availability of large number of contemporary research papers and review articles related to the recognition and sensing of inorganic anions.[126-131] In particular, fluoride ion has occupied the centerstage due to its beneficial (e.g., treatment of osteoporesis)[135,136] as well as detrimental (e.g., fluorosis)[137] roles. Therefore, there is an urgent need to design and develop efficient chemosenosors for detection and reporting anions.

1.6.1. Signaling strategies

The chemosensors for anions can be designed by coupling at least two units, the binding site and the signaling subunit, each one displaying a precise function. In the former, the function of coordination to a certain anion is important, whereas the latter changes some spectroscopic characteristics (color or fluorescence) upon anion coordination. The general designing principle is based on anion coordination events; therefore, both the interaction with the anion and the change in color or fluorescence are in principle reversible. There are several approaches for recognition and sensing of anions. For example, binding sites and signaling units can be covalently linked (binding site-signaling subunit approach)[89] or not (displacement approach).[138] Sometimes, chemodosimetric approach,[139] where an anion-induced chemical reaction gives the output signal, have also been exploited for anion recognition. Recently, PET mechanism has also been exploited for the same purpose.[130] Some of the approaches towards signaling of anions are discussed below.

1.6.1.1. Displacement approach

In this approach, the binding site and the signaling subunit are attached via a coordinative linkage (Scheme 1.3).
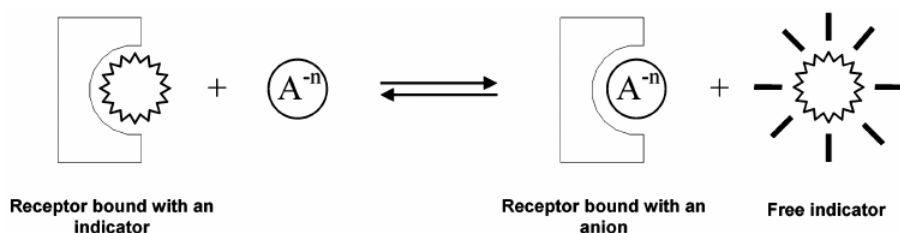
Scheme 1.3 Anion chemosensors based on the displacement approach.

When a target anion is added to an ensemble consisting of the binding site and signaling unit, a displacement reaction takes place; the binding site coordinates the anion whereas signaling unit returns to the solution retrieving its noncoordinated spectroscopic behavior. From this approach it can be inferred that the stability constant for the formation of the complex between the binding site and the signaling subunit has to be lower than that between binding site and the target anion.

1.6.1.2. Chemodosimeter approach

This approach involves the use of specific chemical reaction (usually irreversible) induced by the presence of target anions and is accompanied by a change of color or emission behavior (Scheme 1.4).
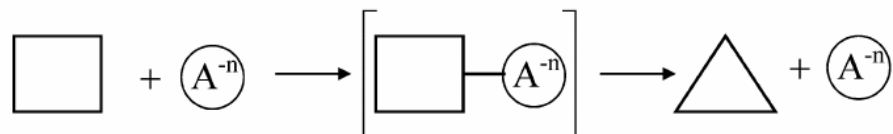
Scheme 1.4 Anion sensors based on the chemodosimeter approach.

In this approach, the anion catalyzes a chemical reaction. As the final product is chemically different from the original one, the spectroscopic property of the solution should change, allowing determination of the anion. If the chemical reaction is irreversible, the use of the term chemosensors cannot be strictly used in this case, rather chemodosimeter or chemoreactants will be more appropriate. The underlying idea of these irreversible systems is to take advantage of the selective reactivity that certain anions may display.

1.6.1.3. Binding site-signaling subunit approach

This has been the most widely used approach in the development of anion chemosensors. In this approach, the binding site and the signaling subunit are attached via a covalent linkage (Scheme 1.5).
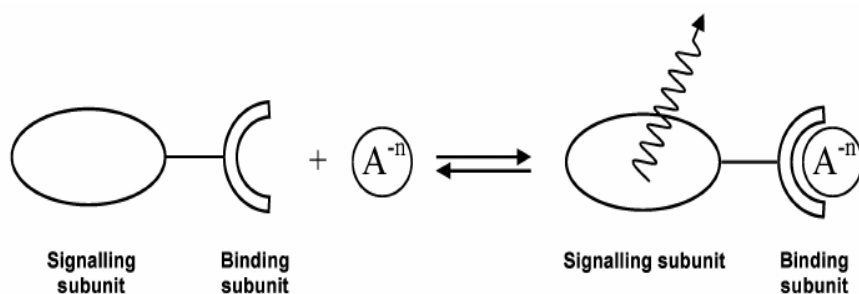
Scheme 1.5 Anion chemosensors based on the binding site-signaling subunit approach.

As can be seen in Scheme 1.5, the coordination site (receptor) binds the anion in such a way that the properties of the signaling subunit are changed giving rise to variations either in the color (chromogenic chemosensor) or in its fluorescence behavior (fluorogenic chemosensor).

Commonly, in this approach, molecular systems containing polarized N-H fragment, which behaves as H-bond donor towards anions, are used as receptors for recognition and sensing purposes in aprotic solvents (CHCl$_3$, MeCN and DMSO).[131] However, the stability of the receptor-anion complex is strictly related to the acidic nature of the receptor and basicity of the target anions.[131] Normally, where the receptor is moderately acidic, the receptor-anion complex is stabilized by H-bonding interaction.[131] However, when the N-H fragment of the receptor is sufficiently polarized by introducing an electron withdrawing substituent (e.g., CO, NO$_2$, CN etc.) to the molecular framework, it might lead to proton transfer to an especially basic anion like fluoride.[131]

1.6.2 Some examples

As mentioned above, receptors containing polarized N-H fragment are commonly used for designing the chemosensors for anions. Some well known examples of this kind have been highlighted below.

Selective sensing of anions was achieved by Sessler and co-workers by utilizing functionalized calix[4]pyrrole or dipyrrolylquinoxaline (DPQ) class of compounds.[140] Anthraquinones linked to calix[4]pyrrole skeleton by C–C triple bond behave as colorimetric anion sensor **30**.[140] It shows a dramatic color change from yellow to red on addition of F$^-$ in CH$_2$Cl$_2$, whereas the color changes from

yellow to reddish-orange for Cl^- or $H_2PO_4^-$ and it requires greater concentration of anions to effect a commensurate change.
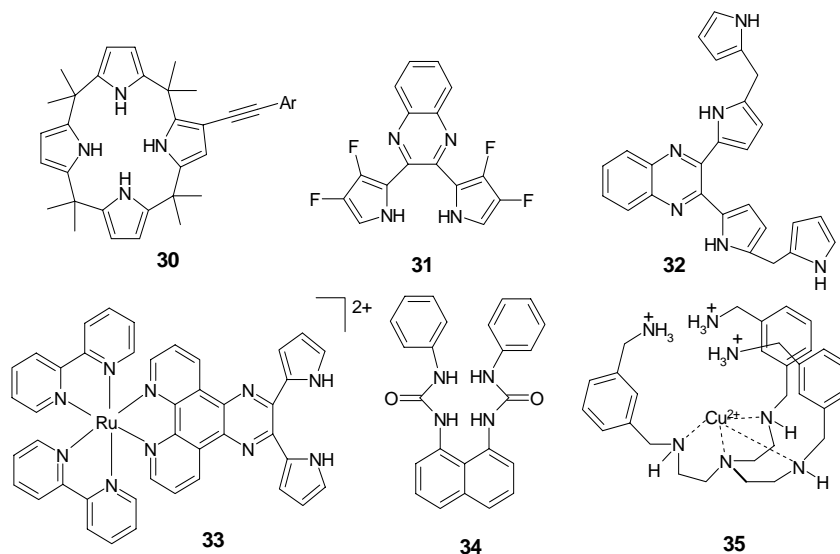
On the other hand, exposure to Br^-, I^- and HSO_4^- ions, which do not bind to calix[4]pyrrole appreciably, no noticeable change in color of **30** could be detected. Anzenbacher et. al. reported anion binding ability of **31** where the β-pyrrolic positions were replaced by electron-withdrawing fluorine substituent.[141] Sessler et al. also reported sensors (**32**) based on quinoxaline derivatives bearing dipyrromethane.[142] The binding constants of **32** with F^-, $H_2PO_4^-$ and Cl^- are of the order of 10^4, 10^3 and 10^2 M^{-1} in CH_2Cl_2 medium.

Sessler and co-workers investigated the anion binding property of Ru(II) (**33**) complex where DPQ moiety is fused with phenanthroline ligand of the metal complexes.[143] The rationale for making **33** was that it contains electron-

withdrawing metal center that would render the pyrrole NH protons more acidic, thereby promoting the key anion-to-DPQ interactions.

Cho et al. studied anion binding properties of a urea based anion sensor (**34**) containing naphthalene fluorophore.[144] The anion sensor **34** shows almost 40-fold selective binding of F^- compared to Cl^- in CH_3CN/DMSO (9:1, v/v). On addition of F^-, a new emission peak at 445 nm is observed; on the other hand, only changes in intensity of the original band are observed in presence of Cl^-, Br^- or I^-. Although, the selectivity for F^- over Cl^- is not that high, the appearance of a new peak in the presence of F^- provides a great advantage for detecting F^- ion.

Tobey and Anslyn reported receptors containing a Cu(II) binding site with appended ammonium groups (**35**).[145] The receptor **35** shows high affinities (10^4 M^{-1}) and selectivities for phosphate over other anions in water/methanol (98:2, v/v) at biological pH. The binding of the host-guest pairs is proposed to proceed through ion-pairing interactions between the charged functional groups on both the host and the guest.

1.7. Molecular photonics and electronics

The relatively recent development of supramolecular chemistry along with the cutting-edge technologies such as scanning probe microscopy and surface spectroscopic techniques, which allow the design, characterization and manipulation of new devices, has stimulated interest in the construction of simple electronics or photonics driven systems and networks that function as molecular-level devices.[146-148] Examples include simple host–guest complexes as well as more advanced molecular wires,[149] gates,[150] switches,[151] etc.

Arithmetic and logic operations are the twin platforms on which the entire information technology has been built. Molecular-level devices that perform elementary arithmetic and logic operations are thus gaining increasing importance and are being taken up as a challenge of today. In this direction, mimicking the functions of semiconductor logic gates used in modern computing is of particular interest.[152]

Logic gates: A logic gate performs a logical operation on one or more logic inputs and produces a single logic output. The logic normally performed is Boolean logic and is most commonly found in digital circuits.[153] Because the output of a logic operation is also a logic level, an output of one logic can connect to the input of one or more other logic gates. Two outputs are never connected together as they could produce conflicting logic values. In electronic logic gates, this would cause a short circuit.[153]
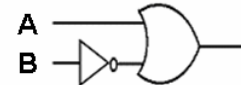
In electronic logic, a logic level is represented by certain voltage, which depends on the type of electronic logic in use. Each logic gate requires power so that it can source and sink currents to achieve the correct voltage. In logic circuit diagram the power is not shown, but in a full electronic schematic, power connections are required.[153]

The relationship between the input and the output, which are the necessary components for various kind of logic operation, is described by truth tables. In the truth table, "1" represents an active input/output and "0" represents an inactive one.[154] NAND and NOR logic gates are the two pillars of logic, in that all other types of Boolean logic gates, (i.e., AND, OR, YES, NOT, XOR, XNOR) can be created from a suitable network of just NAND or just NOR gate(s). They can be

built from relays or transistors, or any other technology that can create an inverter and a two-input AND or OR gate. Hence the NAND and NOR gates are called universal gates.[153]

Some of the logic functions such as the YES,[155] OR,[156] NOR,[157] AND,[158] XOR[159] and INH[160] functions have recently been demonstrated where ions and molecules are used as inputs and changes in the optical properties of the system are used as outputs. Some of the logic representations are shown below.

Type	Distinctive shape	Boolean algebra between A&B	Truth table		
			INPUT	OUTPUT	
			A	YES A	
YES		A			
			0	0	
			1	1	
			INPUT	OUTPUT	
			A	NOT A	
NOT		$\overline{A}$			
			0	1	
			1	0	
			INPUT		OUTPUT
			A	B	A OR B
			0	0	0
OR		$A + B$	0	1	1
			1	0	1
			1	1	1

			INPUT		OUTPUT
			A	B	A AND B
			0	0	0
AND		$A \cdot B$	0	1	0
			1	0	0
			1	1	1

			INPUT		OUTPUT
			A	B	A NAND B
			0	0	1
NAND		$\overline{A \cdot B}$	0	1	1
			1	0	1
			1	1	0

			INPUT		OUTPUT
			A	B	A NOR B
			0	0	1
NOR		$\overline{A + B}$	0	1	0
			1	0	0
			1	1	0

			INPUT		OUTPUT
			A	B	A IMP B
			0	0	1
IMP		$A + B'$	0	1	0
			1	0	1
			1	1	1

1.8 Motivation behind the thesis

The work embodied in this thesis has been undertaken with a two-dimensional objective: firstly, to understand the basic photophysics relating to the charge/electron transfer phenomenon of some new electron donor-acceptor (EDA) systems and secondly, to envisage the utility of some EDA systems in recognition

and sensing of metal ions and anions exploiting the charge/electron transfer phenomenon. It is evident from the above discussions that EDA systems are important components in contemporary research both from the view point of fundamental research and real application. It is also quite clear that the effective use of the EDA systems for different purposes such as solvent polarity indicator, reporter molecules for microhetrogeneous media, probe for studying solvation dynamics and electron transfer processes, lasing efficiency applications and sensor molecules for metal ions and anions requires a detailed knowledge of their photophysical behavior.

Among the various applications of the EDA systems, the recognition and sensing of the cations and anions have gathered huge attention. This is mainly because of the fact that these metal ions and anions represent an environmental and health concern when present in uncontrollable amount. In this regard, a large number of PET sensor molecules are available in the literature.[91,92] However, development of efficient "off-on" fluorescent signaling systems for selective detection of transition metal ions still remains a challenge because of inherent quenching nature of these species. The primary disadvantage of single wavelength intensity-based sensing is the problem of referencing the intensity measurements. The efficiency of light transmission and collection can fluctuate from one instrument to another, and a constant intensity reference is often unavailable. The fluorescence intensity can also vary due to light scattering and/or absorption characteristics of the sample. Moreover, very often photobleaching of the fluorophores happens rapidly thereby complicating the quantitative intensity measurements. These effects require frequent recalibration and other corrections.

As a result of these difficulties, alternative fluorescent probes and sensing methods are highly desirable. Therefore, sensing by wavelength ratiometric fashion, i.e. by monitoring the ratio of the fluorescence intensities at two different wavelengths as a function of the analyte concentration, is advantageous compared to the single wavelength intensity-based measurements as it offers a built-in correction to the above mentioned problems. Though several fluorescent ratiometric sensors for cations are reported in the literature,[161-163] very few such systems are available for anions[164,165] .

Construction of molecular level devices, which mimic the functions of semiconductor logic gates used in modern computing, is also an area of thrust in modern day research. Though several kinds of molecular level logic gates are available in the literature, the sensory actions can further be exploited in the direction to construct new kind of molecular logic gate.

Keeping these aspects in mind, several new EDA systems have been synthesized and their photophysical properties have been investigated. Subsequently, attempts have been made to design and develop chemosensors for selective detection of cations and anions by exploiting the charge transfer character of the EDA systems. Sensory actions have also been exploited further for designing new kind of molecular logic gate.

Specifically, we have synthesized several amine-terminated nitrofluorene derivatives (Chart 1) with a view to examine the influence of various amino functionalities on the energetics and consequent changes in the radiative and nonradiative processes of the systems.

Chart 1

Chart 2

Chart 3
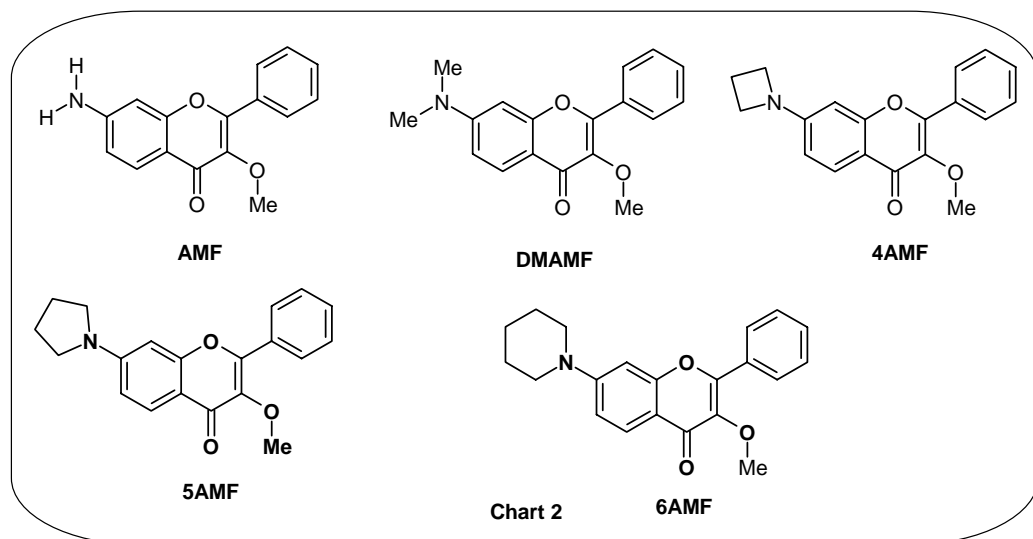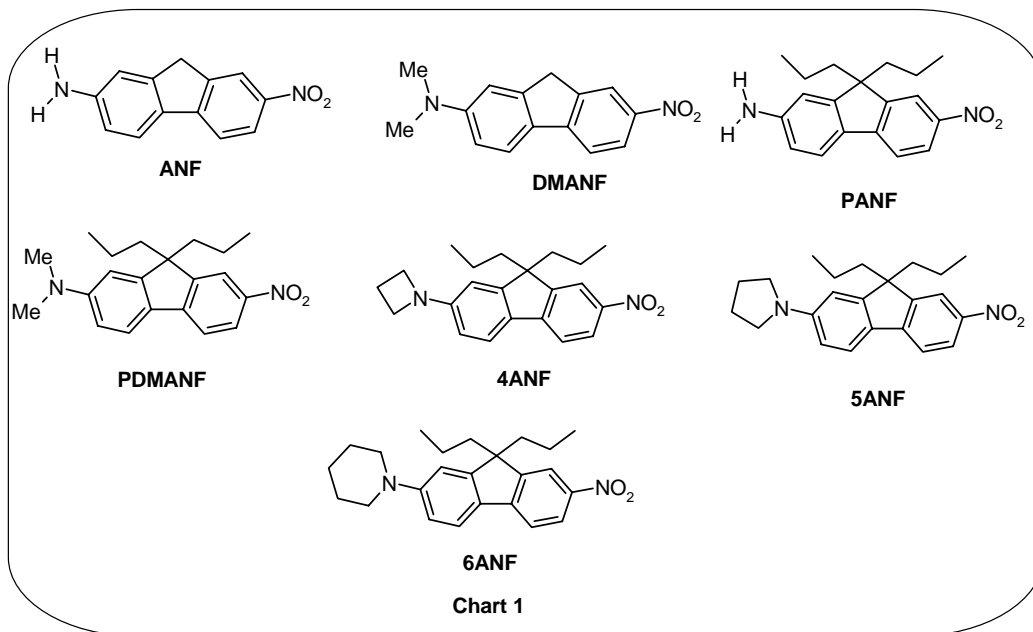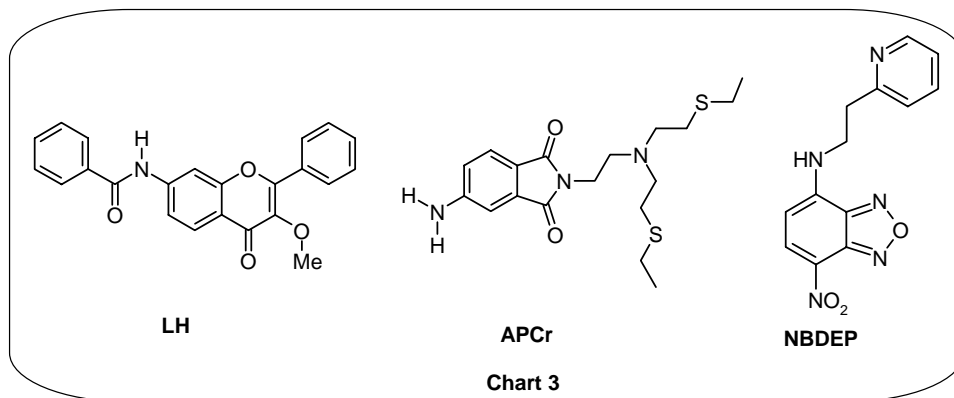
While targeting the systems we have kept in mind the fact that except for a few studies, which suggest a huge change in the dipole moment (25 D) upon photoexcitation of 2-amino-7-nitrofluorene,[166,167] this system has not received the attention it deserves in comparison to other EDA systems. The systems have been synthesized and fully characterized by conventional techniques and X-ray crystallography. Photophysical behavior of the systems has been carried out as a function of the polarity of the media. Theoretical calculations based on semi-empirical and density functional studies have also been carried out to obtain a better understanding of the photophysical behavior of the systems (Chapter 3).

Very little attention has been given to the photophysical properties of the EDA flavone derivatives. To explore charge/electron transfer behavior of the EDA flavone derivatives, we have synthesized a series of amine-terminated methoxyflavone derivatives, where an amino group serves as the donor and carbonyl group of the flavone moiety serves as the acceptor (Chart 2). Spectral and temporal behavior of these systems has been carried out in solvent of varying

polarity. Excited state calculations of the frontier orbitals based on the TD-DFT have been carried out to rationalize the experimental findings (Chapter 4).

Flavones have not been used so far in anion signaling process. In this perspective, we have synthesized a flavone-based chemosensor (**LH**, Chart 3) with a view to sense fluoride ion selectively. In this direction, chromogenic and fluorescence ratiometric responses of **LH** in the presence of different anions have been carried out. Density functional calculations have been executed to rationalize the signaling mechanism (Chapter 5).

Chromium is an environmental pollutant and increase of its concentration due to industrial activities is a matter of great concern. Moreover, "off-on" fluorosensors for Cr(III) ion is very rare. A 4-aminophthalimide-based fluorosensor (**APCr**, Chart 3) for selective detection of Cr(III) ion has been designed and developed. The signaling behavior of this system with different metal ions has been investigated (Chapter 6).

With a view to sense cations and anions within a same molecular entity, a nitrobenzoxadiazole-based chemosensor (**NBDEP**, Chart 3) has been designed and developed. The cation and anion signaling behavior and the potential of this system as a two-input IMP molecular logic gate have been shown (Chapter 7).

References

1. Michel-Beyerle, M. E. *The Reaction Centre of Photosynthetic Bacteria*; Springer Verlag: Berlin, 1995.

2. Michel-Beyerle, M. E.; Finckh, P.; Heitele, H.; Volk, M. *J. Phys. Chem.* **1988**, *92*, 6584.

3. Wasielewski, M. R. *Chem. Rev.* **1992**, *92*, 435.

4. Gust, D.; Moore, T. A.; Moore, A. L. *Acc. Chem. Res.* **1993**, *26*, 198.

5. Kurreck, H.; Huber, M. *Angew. Chem. Int. Ed. Engl.* **1995**, *34*, 849.

6. Bard, A.; Fox, M. A. *Acc. Chem. Res.* **1995**, *28*, 141.

7. Memming, R. *Photochemical Conversion and Storage of Solar Energy*; Pelizetti, E. and Schiavello, M., Ed.; Kluwer: Holland, 1991, pp 193.

8. Meyer, T. J. *Acc. Chem. Res.* **1989**, *22*, 163.

9. Diner, B. A.; Babcock, G. T. *Structure, Dynamics and Energy Conversion Efficiency in Photosystem II*; Diner, B. A. and Babcock, G. T., Ed.; Kluwer: Dordrecht, 1996, pp 213.

10. Fabbrizzi, L.; Poggi, A. *Chem. Soc. Rev.* **1995**, *24*, 197.

11. Shelton, D. B.; Rice, J. E. *Chem. Rev.* **1994**, *94*, 3.

12. Carter, F. L.; Siatoski, R. E.; Woltjen, H. *Molecular Electronic Devices*; North-Holland: Amsterdam, 1988.

13. Barbara, P. F.; Jarzeba, W. *Acc. Chem. Res.* **1988**, *21*, 195.

14. Mulliken, R. S. *J. Am. Chem. Soc.* **1950**, *72*, 600.

15. Mulliken, R. S. *J. Phys. Chem.* **1952**, *56*, 801.

16. Birks, J. B. *Photophysics of Aromatic Molecules*; Wiley-Interscience: New York, 1970.

17. Jordan, K. D.; Paddon-Row, M. N. *Chem. Rev.* **1992**, *92*, 395.

18. Verhoeven, J. W.; Scherer, T.; Willemse, R. J. *Pure Appl. Chem.* **1993**, *65*, 1717.

19. Fox, M. A.; Galoppini, E. *J. Am. Chem. Soc.* **1997**, *119*, 5277.

20. Yazdi, P.; McFann, G. J.; Fox, M. A.; Johnston, K. P. *J. Phys. Chem.* **1990**, *94*, 7224.

21. Zhang, J.; Bright, F. V. *J. Phys. Chem.* **1992**, *96*, 5633.

22. Slavik, J. *Biochem. Biophys. Acta* **1982**, *1*, 694.

23. Narang, V.; Zhav, C. F.; Bhawalkar, J. D.; Bright, F. V.; Prasad, P. N. *J. Phys. Chem.* **1996**, *100*, 4521.

24. Kalyanasundaram, K.; Thomas, J. K. *J. Phys. Chem.* **1977**, *81*, 2176.

25. Turro, N. J.; Okubo, T. *J. Phys. Chem.* **1982**, *86*, 159.

26. de Melo, J. S.; Becker, R. S.; Elisei, F.; Macanita, A. L. *J. Chem. Phys.* **1997**, *107*, 6062.

27. Datta, A.; Mandal, D.; Pal, S. K.; Bhattacharyya, K. *J. Phys. Chem. B* **1997**, *101*, 10221.

28. Purkayastha, P.; Bhattacharyya, P. K.; Bera, S. C.; Chattopadhyay, N. *Phys. Chem. Chem. Phys.* **1999**, *1*, 3253.

29. Birks, J. B. *Chem. Phys. Lett.* **1972**, *17*, 370.

30. Binsch, G.; Heilbronner, E.; Kankow, R.; Schmidt, D. *Chem. Phys. Lett.* **1967**, *1*, 135.

31. Eaton, P. F.; Evans, T. R.; Lennakers, P. A. *Mol. Photochem.* **1969**, *1*, 347.

32. Turro, N. J.; Ramamurthy, V.; Cherry, W.; Farneth, W. *Chem. Rev.* **1978**, *78*, 125.

33. Dhingra, R.; Poole, J. A. *Chem. Phys. Lett.* **1968**, *2*, 108.

34. Samanta, A.; Devadoss, C.; Fessenden, R. W. *J. Phys. Chem.* **1990**, *94*, 7106.

35. Mondal, J. A.; Ghosh, H. N.; Mukherjee, T.; Palit, D. K. *J. Phys. Chem. A* **2005**, *109*, 6836.

36. BÎrlă, L.; Bertorelle, F.; Rodrigues, F.; Badré, S.; Pansu, R.; Fery-Forgues, S. *Langmuir* **2006**, *22*, 6256.

37. Agbaria, R. A.; Butterfield, T.; Warner, I. M. *J. Phys. Chem.* **1996**, *100*, 17133.

38. Valentium, R.; Gehlen, M. W. *J. Phys. Chem. A* 2006, *110*, 7539.

39. Tsourkas, A.; Bhelke, M. A.; Xu, Y.; Bao, G. *Anal. Chem.* **2003**, *75*, 3697.

40. Getz, D.; Ron, A.; Rubin, M. B.; Speiser, S. *J. Phys. Chem.* **1980**, *84*, 768.

41. Wilson, G. J.; Launikonis, A.; Sasse, W. H. F.; Mau, A. O. -H. *J. Phys. Chem. A* **1997**, *101*, 4860.

42. Liu, J.; Lu, Y. *J. Am. Chem. Soc.* **2002**, *124*, 15208.

43. Bhattacharya, K.; Chowdhury, M. *Chem. Rev.* **1993**, *93*, 507.

44. Weigel, W.; Wagner, P. J. *J. Am. Chem. Soc.* **1996**, *118*, 12858.

45. Yip, W. T.; Levy, D. H. *J. Phys. Chem.* **1996**, *100*, 11539.

46. Kasha, M. *J. Chem. Soc., Faraday, Trans. 2* **1986**, *82*, 2379.

47. Ormson, S. M.; Brown, R. G.; Vollmer, F.; Rettig, W. *J. Photochem. Photobiol. A: Chem.* **1994**, *81*, 65.

48. Das, K.; Sarkar, N.; Mazumder, D.; Bhattacharya, K. *Chem. Phys. Lett.* **1992**, *198*, 443.

49. Rettig, W. *Angew. Chem. Int. Ed. Engl.* **1986**, *25*, 971.

50. Grabowski, Z. R.; Dobkowski, J. *Pure. Appl. Chem.* **1983**, *55*, 245.

51. Grabowski, Z. R.; Rotkiewicz, K.; Rettig, W. *Chem. Rev.* **2003**, *103*, 3899.

52. Rotkiewicz, K.; Grellmann, K. H.; Grabowski, Z. R. *Chem. Phys. Lett.* **1973**, *19*, 315.

53. Rotkiewicz, K.; Grabowski, Z. R.; Krowczynski, A.; Kühnle, W. *J. Lumin.* **1976**, *12*, 877.

54.   Jortner, J.; Levine, R. D. *Adv. Chem. Phys.* **1981**, *47*, 1.

55.   Fletcher, A. N. *Appl. Phys.* **1983**, *B31*, 19.

56.   Kosower, E. M. *Acc. Chem. Res.* **1982**, *15*, 259.

57.   Gorner, H.; Schulte-Frohlinde, D. *J. Mol. Struct.* **1982**, *84*, 227.

58.   Baretz, B. H.; Singh, A. K.; Liu, R. S. H. *Nouv. J. Chim.* **1981**, *5*, 297.

59.   Keery, K. M.; Fleming, G. R. *Chem. Phys. Lett.* **1982**, *93*, 322.

60.   Salem, L. *Science* **1976**, *191*, 822.

61.   Allen, N. S.; Bentley, P.; McKellar, J. F. *J. Photochem.* **1976**, *5*, 225.

62.   O'Brien, D. F.; Kelly, T. M.; Costa, L. F. *Photogr. Sci. Eng.* **1974**, *18*, 76.

63.   Carter, F. L. *Optical Information Processing Fundamentals*; Lee, S. H., Ed.; Springer-Verlag: New York, 1981.

64.   Drexhage, K. H. *Dye Laser*; Schäfer, F. P., Ed.; Springer: Berlin, 1977.

65.   Kubin, R. F.; Fletcher, A. N. *J. Lumin.* **1982**, *27*, 455.

66.   Vogel, M.; Rettig, W.; Sens, R.; Drexhage, K. H. *Chem. Phys. Lett.* **1988**, *147*, 461.

67.   Vogel, M.; Rettig, W.; Sens, R.; Drexhage, K. H. *Chem. Phys. Lett.* **1988**, *148*, 452.

68.   Arbeloa, F. L.; Aguirresacona, U. I.; Arbeloa, I. L. *Chem. Phys.* **1989**, *130*, 371.

69.   Arbeloa, F. L.; Arbeloa, T. L.; Arbeloa, I. L.; De Schryver, F. C. *J. Photochem. Photobiol. A: Chem.* **1991**, *56*, 313.

70.   Onganer, Y.; Quitevis, E. L. *J. Phys. Chem.* **1992**, *96*, 7996.

71.   Jones II, G.; Jackson, W. R.; Kanoktanaporn, S.; Halpern, A. M. *Opt. Commun.* **1980**, *33*, 315.

72.   Jones II, G.; Jackson, W. R.; Choi, C.-Y.; Bergmark, W. R. *J. Phys. Chem.* **1985**, *89*, 294.

73.   Jones II, G.; Jackson, W. R.; Halpern, A. M. *Chem. Phys. Lett.* **1980**, *72*, 391.

74.   de Melo, J. S.; Becker, R. S.; Macanita, A. L. *J. Phys. Chem.* **1994**, *98*, 6054.

75.   Cornelissen-Gude, C.; Rettig, W.; Lapouyade, R. *J. Phys. Chem. A* **1997**, *101*, 9673.

76.   Gude, C.; Rettig, W. *J. Phys. Chem. A* **2000**, *104*, 8050.

77.   Velsko, S. P.; Fleming, G. R. *Chem. Phys.* **1982**, *65*, 59.

78.   Saha, S.; Samanta, A. *J. Phys. Chem. A* **1998**, *102*, 7903.

79.   Saha, S.; Samanta, A. *J. Phys. Chem. A* **2002**, *106*, 4763.

80.   Vögtle, F. *Supramolecular Chemistry*; John Wiley & Sons: Chichester, 1991.

81.   Lehn, J.-M. *Supramolecular Chemistry*; VCH, Weinheim, 1995.

82.   Steed, J. W.; Atwood, J. L. *Supramolecular Chemistry*; John Wiley & Sons: New York, 2000.

83.   *Chemosensors of Ion and Molecular Recognition*; Desvergene, J. P.; Czarnik, A. W., Eds.; Kluwer Academic: Dordrecht, 1997; Vol. C492.

84.   *Supramolecular Photochemistry*; Balzani, V., Ed.; Reidel Publishing Company.: Dordrecht, 1987.

85.   Lehn, J.-M. *Angew. Chem., Int. Ed.* **1990**, *29*, 1304.

86.   Spichiger-Keller, U. S. *Chemical Sensors and Biosensors for Medical and Biological Applications*; Wiley-VCH: Weinheim, 1998.

87.   *Fluorescent Chemosensors of Ion and Molecule Recognition*. Czarnik, A. W., Ed.; ACS Symp. Ser. 538; American Chemical Society: Washington DC, 1993.

88.   de Silva, A. P.; Gunaratne, H. Q. N.; Gunnlaugsson, T.; Huxley, A. J. M.; McCoy, C. P.; Rademacher, J. T.; Rice, T.E. *Chem. Rev.* **1997**, *97*, 1515.

89.   Bissell, R. A.; de Silva, A. P.; Gunaratne, H. Q. N.; Lynch, P. L. M.; Maguire, G. E. M.; Sandanayake, K. R. A. S. *Chem. Soc. Rev.* **1992**, *21*, 187.

90.   Fabbrizzi, L.; Poggi, A. *Chem. Soc. Rev.* **1995**, *24*, 197.

91. de Silva, A. P.; Fox, D. B.; Huxley, A. J. M.; Moody, T. S. *Coord. Chem. Rev.* **2000**, *205*, 41.

92. Valeur, B.; Leray, I. *Coord. Chem. Rev.* **2000**, *205*, 3.

93. Prodi, L.; Bolletta, F.; Montalti, M.; Zaccheroni, N. *Coord. Chem. Rev.* **2000**, *205*, 59.

94. Rurack, K. *Spectrochim. Acta, Part A.* **2001**, *57*, 2161.

95. Kalyanasundaram, K.; Thomas, J. K. *J. Phys. Chem.* **1977**, *81*, 2176.

96. Ogawa, S.; Tsuchiya, S. *Chem. Lett.* **1996**, 709.

97. Nagasaki, T.; Tajirl, Y.; Shinkai, S. *Rec. Trav. Chim. Pays Bas* **1993**, *112*, 407.

98. Bunzli, J.-C. G. In *Lanthanide Probes in Life, Chemical and Earth Sciences*; Bunzli, J.-C. G., Choppin, G. R., Eds.; Elsevier: Amsterdam, 1989.

99. Martin, M. M.; Plaza, P.; Meyer, Y. H.; Badaoui, F.; Bourson, J.; Lefebvre, J. P.; Valeur, B. *J. Phys. Chem.* **1996**, *100*, 6879.

100. Létard, J.-F.; Lapouyade, R.; Rettig, W. *Pure Appl. Chem.* **1993**, *65*, 1705.

101. Mathevet, R.; Jonasauskas, G.; Rullière, C.; Létard, J.-F.; Lapouyade, R. *J. Phys. Chem.* **1995**, *99*, 15709.

102. Demas, J. N.; DeGraff, B. A. In *Topics in Fluorescence Spectroscopy*; Lakowicz, J. R., Ed.; Plenum Press: New York, 1994; Vol. 4.

103. Rettig, W.; Lapouyade, R. In *Topics in Fluorescence Spectroscopy*; Lakowicz, J. R., Ed.; Plenum Press: New York, 1994; Vol. 4.

104. Sousa, L. R.; Larson, J. M. *J. Am. Chem. Soc.* **1977**, *99*, 307.

105. Larson, J. M.; Sousa, L. R. *J. Am. Chem. Soc.* **1978**, *100*, 1943.

106. Shirai, M.; Tanaka, M. *Chem. Commun.* **1988**, 381.

107. Nishizawa, N.; Watanabe, M.; Uchida, T.; Terame, N. *J. Chem. Soc. Perkin Trans. 2* **1999**, 141.

108. Marquis, D.; Desvergne, J.-P.; Bouas-Laurent, H. *J. Org. Chem.* **1995**, *60*, 1784.

109. Kubo, K.; Sakurai, T. *Chem. Lett.* **1996**, 959.

110. Strauss, J.; Daub, J. *Org. Lett.* **2002**, *4*, 683.

111. Harriman, A.; Sauvage, J.-P. *Chem. Soc. Rev.* **1996**, *25*, 41.

112. Szmacinski, H.; Lakowicz, J. R. In *Topics in Fluorescence Spectroscopy*; Lakowicz, J. R., Ed.; Plenum Press: New York, 1994; Vol. 4.

113. Bissel, R. A.; de Silva, A. P.; Gunaratne, H. Q. N.; Lynch, P. L. M.; Maguire, G. E. M.; McCoy, C. P.; Sandanayake, K. R. A. S. *Top. Curr. Chem.* **1993**, *168*, 223.

114. Rehm, D.; Weller, A. *Isr. J. Chem.* **1970**, *8*, 259.

115. Weller, A. *Pure Appl. Chem.* **1968**, *16*, 115.

116. Grynkiewicz, G.; Poenie, M.; Tsien, R. Y. *J. Biol. Chem.* **1985**, *260*, 3440.

117. de Silva, A. P.; Rupasinghe, R. A. D. *Chem. Commun.* **1985**, 1669.

118. Fabbrizzi, L.; Lichelli, M.; Pallavicini, P.; Perotti, A.; Taglietti, A.; Sacchi, D. *Chem. Eur. J.* **1996**, *2*, 75.

119. de Silva, S. A.; Zaveleta, A.; Baron, D. E.; Allam, O.; Isidor, E. V.; Kashimura, N.; Percarpio, J. M. *Tetrahedron Lett.* **1997**, *38*, 2237.

120. Fabbrizzi, L.; Licchelli, M.; Pallavicini, P.; Perroti, A.; Sacchi, D. *Angew. Chem., Int. Ed.* **1994**, *33*, 1975.

121. de Silva, A. P.; Sandanayake, K. R. A. S. *Angew. Chem., Int. Ed.* **1990**, *29*, 1173.

122. de Silva, A. P.; Gunaratne, H. Q. N.; McCoy, C. P. *Nature* **1993**, *364*, 42.

123. de Silva, A. P.; McClenaghan, N. D. *J. Am. Chem. Soc.* **2000**, *122*, 3965.

124. Ghosh, P.; Bharadwaj, P. K.; Roy, J.; Ghosh, S. *J. Am. Chem. Soc.* **1997**, *119*, 11903.

125. Ramachandram, B.; Samanta, A. *Chem. Commun.* **1997**, 1037.

126. Martinez-Manez, R.; Sancenon, F. *Chem. Rev.* **2003**, *103*, 4419.

127. Suksai, C.; Tuntulani, T. *Chem. Soc. Rev.* **2003**, *32*, 192.

128. Beer, P. D.; Gale, P. A. *Angew. Chem., Int. Ed.* **2001**, *40*, 486.

129. Fabbrizzi, L.; Licchelli, M.; Rabaioli, G.; Taglietti, A. *Coord. Chem. Rev.* **2000**, *205*, 85.

130. Gunnlaugsson, T.; Glynn, M.; Tocci (née Hussey), G. M.; Kruger, P. E.; Pfeffer, F. M. *Coord. Chem. Rev.* **2006**, *250*, 3094.

131. Amendola, V.; Esteban-Gomez, D.; Fabbbrizzi, L.; Lecchelli, M. *Acc. Chem. Res.* **2006**, *39*, 343.

132. *Reigel's Handbook of Industrial Chemistry*, 9th ed.; Kent, J. A., Ed.; Van Nostrad Reihold-International Thomson Publising: New York, 1992.

133. Stryer, L. *Biochemistry;* 4th Ed.; W. H. Freeman & Co.: New York, 1995.

134. Christianson, D. W.; Lipscomb, W. N. *Acc. Chem. Res.* **1989**, *22*, 62.

135. Kirk, K. L. *Biochemistry of the Halogens and Inorganic Halides*; Plenum Press: New York, 1991; p 58.

136. Kleerekoper, M. *Endochrinol. Metab. Clin. North Am.*, **1998**, *27*, 441.

137. Wiseman, A. *Handbook of Experimental Pharmacology XX/2, Part 2*; Springer- Verlag: Berlin, 1970; pp. 48–97.

138. Wiskur, S. L.; Aït-Haddou, H.; Lavigne, J. J.; Anslyn, E. V. *Acc. Chem. Res.* **2001**, *34*, 963.

139. Dujols, V.; Ford, F.; Czarnik, A. W. *J. Am. Chem. Soc.* **1997**, *119*, 7386.

140. Miyaji, H.; Sato, W.; Sessler, J. L. *Angew. Chem. Int. Ed. Engl.* **2000**, *39*, 1777.

141. Anzenbacher, P., Jr.; Try, A. C.; Miyaji, H.; Jursikova, K.; Lynch, V. M.; Marquez, M.; Sessler, J. L. *J. Am. Chem. Soc.* **2000**, *122*, 10268.

142. Sessler, J. L.; Maeda, H.; Mizuno, T.; Lynch, V. M.; Furuta, H. *Chem. Commun.* **2002**, 862.

143. Mizuno, T.; Wei, W.-H.; Eller, L. R.; Sessler, J. L. *J. Am. Chem. Soc.* **2002**, *124*, 1134.

144. Cho, E. J.; Moon, J. W.; Ko, S. W.; Lee, J. Y.; Kim, S. K.; Yoon, J.; Nam, K. C. *J. Am. Chem. Soc.* **2003**, *125*, 12376.

145. Tobey, S. L.; Anslyn, E. V. *J. Am. Chem. Soc.* **2003**, *125*, 14807.

146. *Molecular Electronic Devices*; Carter, F. L.; Siatkowski, R. E.; Wohltjen, H., Eds.; Elsevier: Amsterdam, 1988.

147. de Silva, A. P.; McClenaghan, N. D.; McCoy, C. P. *Molecular Switches*; Wiley-VCH: Weinheim, 2000.

148. Balzani, V.; Venturi, M.; Credi, A. *Molecular Devices and Machines*; Wiley-VCH: Weinheim, 2003.

149. Bumm, L. A.; Arnold, J. J.; Cygan, M. T.; Dunbar, T. D.; Burgin, T. P.; Jones II, L.; Allara, D. L.; Tour, J. M.; Weiss, P. S. *Science* **1996**, *271*, 1705.

150. Wagner, R. W.; Lindsey, J. S.; Seth, J.; Palaniappan, V.; Bocian, D. F. *J. Am. Chem. Soc.* **1996**, *118*, 3996.

151. Raymo, F. M.; Giordani, S. *J. Am. Chem. Soc.* **2001**, *123*, 4651.

152. de Silva, A. P.; McClenaghan, N. D. *Chem. Eur. J.* **2004**, *10*, 574.

153. http://en.wikipedia.org/wiki/Logic_gate

154. Burger, P. *Digital Design: A Practical Course*; Wiley: New York, 1988.

155. de Silva, A. P.; de Silva, S. A. *Chem. Commun*. **1986**, 1709.

156. de Silva, A. P.; Gunaratne, H. Q. N.; Maguire, G. E. M. *Chem. Commun.* **1994**, 1213.

157. de Silva, A. P.; Dixon, I. M.; Gunaratne, H. Q. N.; Gunnlaugsson, T.; Maxwell, P. R. S.; Rice, T. E. *J. Am. Chem. Soc.* **1999**, *121*, 1393.

158. de Silva, A. P.; Gunaratne, H. Q. N.; McCoy, C. P. *J. Am. Chem. Soc.* **1997**, *119*, 7891.

159. Credi, A.; Balzani, V.; Langford, S. J.; Stoddart, J. F. *J. Am. Chem. Soc.* **1997**, *119*, 2679.

160. Gunnlaugsson, T.; Mac Donail, D. A.; Parker, D. *Chem. Commun.* **2000**, 93.

161. Taki, M.; Wolford, J. L.; O'Halloran, T. V. *J. Am. Chem. Soc.* **2004**, *126*, 712.

162. Paker, J.; Glass, T. E.; *J. Org. Chem.* **2001**, *66*, 6505.

163. Banthia, S.; Samanta, A. *J. Phys. Chem. B* **2006**, *110*, 6437.

164. Coskun, A.; Akkaya, E. *Tetrahedron Lett.* **2004**, *45*, 4947.

165. Liu, B.; Tian, H. *J. Mater. Chem.* **2005**, *15*, 2681.

166. Baumann, W.; Bischof, H. *J. Mol. Struct.* **1985**, *129*, 125.

167. Catalán, J.; López, V.; Pérez, P.; Martin-Villamil, R.; Rodriguez, J-G. *Liebigs, Ann.* **1995**, 241

Chapter 2

Materials, Methods and Instrumentation

This chapter lists the materials used in this study procured from various commercial sources followed by the methods of solvent purification. Various methodologies employed in the present investigation, such as measurements of fluorescence quantum yield and lifetime, estimation of excited state dipole moment, evaluation of efficiency of the sensor systems and estimation of the binding constants, have been discussed. Theoretical methods for semi-empirical and density functional studies, based on which the ground and excited state properties of different systems have been evaluated, are discussed. The instrumental details, strategies for crystal growth and details concerning single crystal structure determination are also described at the end of this chapter.

2.1. Materials

2-nitrofluorene and azetidine were purchased from Acros organics and used as received. 3-iodophenol and cesium acetate were obtained from Lancaster. The amines, e.g. ammonia, dimethyl amine, pyrrolidine and piperidine were procured from Loba chemicals and used after dry distillation. 4-Aminophthalimide (AP) was obtained from TCI (Japan). AP was recrystallized twice from ethanol/water mixture prior to photophysical experiments but used as received for synthesis. Ethanethiol, bis(2-chloroethyl)-amine hydrochloride were procured from Lancaster. 4-Chloro-7-nitrobenzoxadiazole, 2-(2-aminoethyl)pyridine were

procured from Acros. N-propyl bromide, benzaldehyde, acetyl chloride, 1,2-dibromoethane were obtained from Sisco Chem. Industries. Common chemicals such as sodium hydride, cuprous iodide, sodium hydroxide, potassium hydroxide, potassium permanganate, potassium carbonate, iodine, aluminium chloride and dimethyl sulphate were obtained either from Rankem or Loba. Silica gel and alumina (neutral and basic), used for thin-layer and column chromatography, were purchased from Acme Scientifics (India). HEPES buffer salt was obtained from Lancaster. The various drying agents such as sodium sulphate, calcium oxide, magnesium turnings, sodium metal. and synthesis grade solvents were procured from local companies. Calcium hydride was obtained from Spectrochem (India). GR grade solvents were obtained from Merck (India) for spectroscopic purposes and were dry-distilled before use. Deuteriated solvents, chloroform-d, methanol-d_4, acetonitrile-d_3, dimethyl sulfoxide (DMSO)-d_6 and D_2O used for NMR spectral measurements were obtained either from Aldrich or from Merck (India). All the metal salts described in the investigation were hydrated perchlorate salts and were obtained either from Aldrich or Acros Organics. Tetrabutyl ammonium salts of different halides, perchlorate, acetate and nitrate were obtained from Aldrich chemicals.

2.2. Purification of solvents

The solvents used at various stages of the study were purified using the general procedures available in the literature.[1] We adopted the following procedures for the purification of various solvents. The purified solvents were optically transparent in the spectral region of interest.

Cyclohexane, toluene, 1,4-dioxane and tetrahydrofuran: The solvent was refluxed over metallic sodium for 3-4 h and added benzophenone. The dark blue solution was refluxed for another one hour and collected under dry conditions.

Acetonitrile, dichloromethane, acetone: The solvents were stirred with calcium hydride for 5-6 h and then distilled. The distilled solvent was collected and stored under dry conditions.

Methanol: After the initial drying over CaH_2 by keeping overnight, 50-75 mL of methanol was added to clean dry magnesium turnings (5 g) and iodine (0.5 g) and warmed until all magnesium was converted into magnesium methoxide. About 1 L of methanol was added to this, refluxed for 2-3 h and distilled out.

Ethanol: Ethanol was refluxed with stirring over anhydrous calcium oxide for 6 h The solution was left at room temperature overnight. This was then distilled and dried over magnesium and iodine and collected under dry atmosphere.

N,N-dimethyl formamide: The solvent was stirred with calcium hydride for 5-6 h and distilled under vacuum at 80°C. Precautions were taken to store the solvent under dry conditions.

Dimethyl sulfoxide: The solvent was stored on dry molecular sieves for overnight and distilled under vacuum. Precautions were taken to store the solvent under dry conditions.

Water: Water was initially distilled using potassium permanganate and potassium hydroxide. This was subsequently distilled twice before taken to study.

2.3. Sample preparation for spectral measurements

The solutions of the systems were prepared such that the absorbance of the solution (1 cm path length) at the excitation wavelength was between 0.1 and 0.2.

The concentration of the systems corresponding to an absorbance value of 0.2 was found to be in the range of 1×10^{-6} – 1×10^{-4} M. In case of sensing experiments, concentrated stock solutions of the salts were prepared in a given solvent and a few microlitres of this solution (not more than 150 μL) were added using a microlitre syringe to 3 mL solution of the sensor molecule, taken in a quartz cuvette. All the time freshly prepared solutions of the salts were used prior to titration.

2.4. Measurement of the fluorescence quantum yield

For quantum yield measurements, optically matched solutions (or solutions with very similar ODs) of the sample and the standard at a given absorbing wavelength were prepared. The quantum yield was calculated by measuring the integrated area under the emission curves and by using the following equation.[2]

$$\Phi_{sample} = \frac{I_{sample} \times OD_{standard} \times \eta^2_{sample}}{I_{standard} \times OD_{sample} \times \eta^2_{standard}} \times \Phi_{standard} \qquad (2.1)$$

Where, Φ is the quantum yield, I is the integrated emission intensity, OD is the optical density at the excitation wavelength, and η is the refractive index. The subscripts 'sample' and 'standard' refer to the fluorophore of unknown quantum yield and the reference fluorophore of known quantum yield, respectively.

Fluorescence quantum yield of aminonitrofluorene and aminomethoxyflavone derivatives were measured using quinine sulphate (ϕ_f in 1N H_2SO_4 is 0.546)[3] as the reference compound. Fluorescence quantum yield of AP-substituted compound was measured with reference to that of **AP** (ϕ_f in acetonitrile is 0.63).[4] In the case of **NBDDEP**, the fluorescence quantum yield was determined with

reference to that of 4-amino-7-nitrobenzoxadiazole (**ANBD**) fluorophore (ϕ_f in acetonitrile is 0.70).[5]

2.5. Excited state dipole moment calculations

Four different methods were employed for the estimation of the excited dipole moments of the systems.[6-11]

The first method utilized the Lippert-Mataga equation,[6-8] which relates the difference between the wavenumbers corresponding to the absorption and fluorescence maxima with the solvent polarity parameter (Δf) as shown below:

$$\overline{v}_a - \overline{v}_f = \frac{2(\mu_e - \mu_g)^2}{hca^3} \times \Delta f + \text{constant} \tag{2.2}$$

where, Δf is defined as $\left[\dfrac{\varepsilon - 1}{2\varepsilon + 1} - \dfrac{n^2 - 1}{2n^2 + 1}\right]$, μ_e and μ_g are the excited state and ground state dipole moments respectively. 'a' is Onsager cavity radius and other terms have their usual meaning. The change in dipole moment can be estimated from the slope of the $(\overline{v}_a - \overline{v}_f)$ vs. Δf plot.

It is well known that $(\overline{v}_a - \overline{v}_f)$ correlates better with the microscopic solvent polarity parameter, E_T^N, where E_T^N is defined as[12]

$$E_T^N = \frac{E_T(solvent) - E_T(TMS)}{E_T(water) - E_T(TMS)} = \frac{E_T(solvent) - 30.7}{32.4} \tag{2.3}$$

where, E_T is defined as the transition energy of the dissolved pyridinium-N-phenoxide betaine dye measured in kcal/mole:[12]

$$E_T = hc\,\overline{v}N_A = 2.859 \times \overline{v} \tag{2.4}$$

here, h is Planck's constant, c is the velocity of light, $\bar{v}$ is the wavenumber of the photon in cm^{-1} which produces the electronic transition, and N_A is Avogadro's number.

The second method adopted for the evaluation of the change of dipole moment is based on the following relation between ($\bar{v}_a - \bar{v}_f$) and E_T^N.[9]

$$\bar{v}_a - \bar{v}_f = 11307.6[(\Delta\mu / \Delta\mu_D)^2 (a_D / a)^3]E_T^N + \text{constant} \qquad (2.5)$$

$\Delta\mu_D$ and a_D represent the dipole moment change and Onsager cavity radius respectively for pyridinium-N-phenoxide betaine dye.[12] The change in dipole moment ($\Delta\mu$) of the given system could be extracted from the slope of the plot when $\Delta\mu_D$ and a_D are known.

The estimation of $\Delta\mu$ values by the two methods mentioned above requires the use of Onsager cavity radius (a), which cannot be measured directly and hence, this quantity is often chosen arbitrarily. Quite obviously, the estimated $\Delta\mu$ value is subjected to uncertainty. To avoid this problem, two more 'a' independent methods were also employed to calculate the $\Delta\mu$ values.

The third method[10] employed for the estimation of $\Delta\mu$ value is based on the following equations:

$$\bar{v}_a - \bar{v}_f = m_1 \times \Delta f + \text{constant} \qquad (2.6)$$

$$\bar{v}_a + \bar{v}_f = -m_2 \times \Delta f' + \text{constant} \qquad (2.7)$$

where, $m_1 = \dfrac{2(\mu_e - \mu_g)^2}{hca^3}$, $m_2 = \dfrac{2(\mu_e^2 - \mu_g^2)}{hca^3}$,

$$\Delta f = \left[\frac{\varepsilon - 1}{2\varepsilon + 1} - \frac{n^2 - 1}{2n^2 + 1} \right] \text{ and } \Delta f' = \left[\frac{\varepsilon - 1}{2\varepsilon + 1} + \frac{n^2 - 1}{2n^2 + 1} \right]$$

The $\Delta\mu$ values can be estimated from the ratio of the slopes, m_1 and m_2 of the two plots obtained from Eq. 2.5 and Eq. 2.6 respectively. It is evident that m_1 / m_2 is independent of the 'a' term.

The fourth method,[11] which is also an 'a' independent method, utilizes two different solvent polarity functions, $f(\varepsilon, n)$ and $g(n)$ for the estimation of $\Delta\mu$. These solvent polarity functions are related to the absorption and emission energies in the following manner:

$$\bar{v}_a - \bar{v}_f = m_1 . f(\varepsilon, n) + \text{constant} \tag{2.8}$$

$$\bar{v}_a + \bar{v}_f = -m_2 [f(\varepsilon, n) + 2g(n)] + \text{constant} \tag{2.9}$$

where, $f(\varepsilon, n) = \dfrac{2n^2 + 1}{n^2 + 2} \left(\dfrac{\varepsilon - 1}{\varepsilon + 2} \right) - \dfrac{n^2 - 1}{n^2 + 2}$, $g(n) = \dfrac{3}{2} . \dfrac{n^4 - 1}{(n^2 + 2)^2}$,

$$m_1 = \frac{2(\mu_e - \mu_g)^2}{hca^3} \text{ and } m_2 = \frac{2(\mu_e^2 - \mu_g^2)}{hca^3}$$

$\Delta\mu$ is estimated from m_1 / m_2, ratio of the two slopes.

2.6. Estimation of fluorescence enhancement

The magnitude of fluorescence enhancement (FE) was calculated from the following equation, using the integrated area of the fluorescence curves.

$$\text{FE} = I_F / I_F (\text{zero}) \tag{2.10}$$

Where, I_F is the integrated area of the fluorescence curve obtained in the presence of a given quantity of the guest species and I_F (zero) is the corresponding area in

the absence of the guest. Both I_F and I_F (zero) were measured under identical experimental conditions.

2.7. Estimation of binding constant

Binding affinity of a sensor system for the transition metal ions was investigated from the changes in the absorption spectrum induced by these metal ions[13] assuming 1:1 complex formation using the following method.

At equilibrium, the association constant (K) is given by

$$K = \frac{[C]}{([F]_0 - [C])([M]_0 - [C])} \tag{2.11}$$

where, $[C]$ is the equilibrium concentration of the complex, $[F]_0$ is the initial concentration of the fluorosensor, and $[M]_0$ is the initial concentration of the metal salt.

By substituting $\Delta A/\Delta\varepsilon$ for $[C]$ (for a path length of 1 cm) the following equation can be derived,

$$\frac{[F]_0[M]_0}{\Delta A} = \left([F]_0 + [M]_0 - \frac{\Delta A}{\Delta\varepsilon}\right)\frac{1}{\Delta\varepsilon} + \frac{1}{K\Delta\varepsilon} \tag{2.12}$$

where, ΔA is the change in absorbance due to the addition of metal salts, and $\Delta\varepsilon$ is the difference between the molar extinction coefficient of the complex and the fluorosensor.

A plot of $\dfrac{[F]_0[M]_0}{\Delta A}$ vs. $\left([F]_0 + [M]_0 - \dfrac{\Delta A}{\Delta\varepsilon}\right)$ would therefore yield a straight line with slope $1/\Delta\varepsilon$ and intercept $1/K\Delta\varepsilon$.

However, a knowledge of the unknown quantity $\Delta\varepsilon$ was needed to make this plot. Consequently, a tentative value of $\Delta\varepsilon$ was determined by using data from two solutions and solving equation (2.12) simultaneously for $\Delta\varepsilon$ and K. Using this value of $\Delta\varepsilon$ a plot was made, employing data from a series of solutions, and a new value of $\Delta\varepsilon$ was determined along with a new value of K. This procedure was repeated until a consistent set of values for both $\Delta\varepsilon$ and K were obtained from two successive plots.

2. 8. Theoretical calculations

2.8.1. Semi-empirical calculations

Calculations based on semi-empirical AM1 (Austin Model 1) method[14,15] were performed either using HyperChem package (Release 5.0) for Windows obtained from Hypercube, Inc. or using Material Studio (MS Modelling v.3.0) program package. Unrestricted geometry optimization of the molecular structure was performed at the semi-empirical level using conjugate gradient (Polak-Ribiere) type of algorithm with root-mean-square (rms) gradient as the convergence criterion. The rms gradient was kept below 0.001 kcal/(Åmol) in all the cases. The ground state dipole moments of the systems were also obtained from these calculations. The excited state properties were also determined in certain cases by ZINDO/S-CI method using configuration interaction (singly excited, orbital criterion: HOMO = 8, LUMO = 8).

The effect of solvent on the energy states was estimated using Onsager's formulation.[16] The solvation energy of a fully relaxed state was estimated using the following relation.[17]

$$\Delta E_{sf} = -\ \frac{2\mu_i^2}{a^3}\ \frac{\varepsilon - 1}{2\varepsilon + 1} \qquad\qquad (2.13)$$

Where μ_i represents the dipole about which the solvent is fully equilibrated, a is the Onsager cavity radius and ε is the dielectric constant of the solvent.

When the dipole moment of the solutes changes from μ_i to μ_f so rapidly that the solvent molecules do not have sufficient time to reorient themselves (as is the case of electronic excitation) then one needs to calculate the energy of the partially solvated state. The solvation energy of the partially solvated state was calculated using the following relation.[18]

$$\Delta E_{sp} = -\ \frac{2}{a^3}\ \mu_f \cdot \mu_i \left(\frac{\varepsilon - 1}{2\varepsilon + 1} - \frac{n^2 - 1}{2n^2 + 1} \right) - \frac{2\mu_f^2}{a^3}\ \frac{n^2 - 1}{2n^2 + 1} \qquad (2.14)$$

The solvent stabilized state energies were obtained by adding the solvation energies and gas phase energies.

2.8.2. Calculations based on density functional theory

For most of the systems, structural parameters and ground state dipole moments were calculated by using density functional theory (DFT),[19-21] which is a more improved method of calculations than the Hartree-Fock theory in the sense that it includes terms for both exchange energy and the electron correlation. Instead of a pure DFT method, a hybrid method in which the exchange functional is a linear combination of the Hartree-Fock exchange and a functional integral was employed in the calculations. The structural parameters and energies of the various systems were determined using the hybrid DFT functional B3LYP[22,23] at the B3LYP/6-31G* level.

Charge density analysis was performed using the natural bond orbital (NBO) approach based on the B3LYP/6-31G* wave function.[24] NBO atomic charges of the small molecules have recently been demonstrated to agree well with the experimental values obtained from X-ray diffraction data.[25]

Excited state calculations were performed within the time-dependent (TD-DFT) framework[26,27] in both vacuo and in presence of solvents. The excited state calculations incorporating the solvents were carried out by self-consistent reaction field (SCRF) method[28] and using polarized continuum (PCM) model.[29] All these calculations were performed using the Gaussian 03 program package.[30]

2.9. Instrumentation

IR spectra were recorded on a Jasco FT-IR/5300 spectrometer. NMR spectra were recorded on a Brucker AVANCE 400 MHz spectrometer at ambient temperature and were referenced to the internal ^{1}H and ^{13}C solvent peaks.

LC mass were recorded on a Shimadzu LCMS-2010A mass spectrometer. Elemental analyses were carried using on a Thermo Finnigan Flash EA 1112 series CHNS analyzer.

The UV-vis absorption spectral measurements were carried out either on a Shimadzu UV-3101PC or on a Cary 100 (varian) spectrophotometer. The fluorescence spectra were recorded either on a Spex FluoroMax-3 or Spex FluoroLog-3 spectrofluorimeter.

The transient absorption measurements were performed by a laser flash photolysis setup, which was equipped with a laser system (Q switched Nd:YAG, pulse width ~8 ns) from Spectra Physics (Quanta-Ray INDI series) and a spectrometer from Applied Photophysics (model LKS.60). The spectrometer

consisted of a 150 W pulsed xenon lamp, a programmable f/3.4 grating monochromator, a digitized oscilloscope (Agilent, 600 MHz), and an R-928 photomultiplier tube. The solutions were excited by the third harmonic (355 nm) of the laser. A perpendicular configuration was chosen for the excitation of the sample. Quartz cuvettes with a path length of 0.3 cm were used. The optical densities of the sample solutions were kept near about 0.1 at the excitation wavelength (355 nm). Applied Photophysics LKS.60 Kinetic Spectrometer workstation software was used for the collection and analysis of the data.

Time-resolved fluorescence measurements were carried out using a time-correlated single-photon counting (TCSPC) spectrometer (5000, IBH). Diode laser (λ_{exc} = 374 nm, FWHM = 65 ps), nano LED (λ_{exc} = 281 nm, FWHM = 1.0 ns) were used as the excitation sources and an MCP photomultiplier (Hamamatsu R3809U-50) as the detector. The lamp profile was recorded by placing a scatterer (dilute solution of Ludox in water) in place of the sample. Decay curves were analyzed by nonlinear least-squares iteration procedure using IBH DAS6 (Version 2.2) decay analysis software.

Data Analysis: The program used for the estimation of fluorescence lifetimes from the fluorescence decay curves was based on reconvolution least squares method.[31] When the decay time is long compared to the pulse-width of the excitation pulse, the excitation may be described as a δ-function. However, when the lifetime is short, distortion of the experimental data occurs by the finite decay time of the lamp pulse and response time of the photomultiplier and associated electronics. Since the measured decay function is convolution of the true

fluorescence decay, it is necessary to analyze the data by deconvolution in order to get the fluorescence lifetime. The mathematical statement of the problem is given by the following equation:

$$D(t) = \int\limits_{0}^{t} P(t')G(t-t')dt' \qquad (2.15)$$

where, D(t) is the fluorescence intensity at time t, P(t') is the intensity of the exciting light at time t' and G(t-t') is the response function of the experimental system. The experimental data D(t) and P(t') from the MCA were fed into a personal computer (PC) to determine the lifetime. We used the IBH program to analyze the multi-exponential decays. An excitation pulse profile was recorded and then deconvolution started with mixing of the excitation pulse and a projected decay to form a new reconvoluted set. The data was compared with the experimental set and the difference between the data points summed, generating χ^2 function for the fit. The deconvolution proceeded through a series of such iterations until an insignificant change of χ^2 occurred between iterations. The inspection of reduced χ^2, a plot of weighted residuals and autocorrelation function of the residuals, assessed the quality of the fit.

2.10. X-ray crystallography

Single crystals of the compounds, suitable for X-ray diffraction studies, were grown from the slow evaporation of their dilute solutions. The raw data were collected on Bruker CCD X-ray diffractometer. The details of the collection and reduction of data for various compounds are as follows:

Collection and reduction of X-ray data from CCD diffractometer: A tiny single crystal was mounted on the tip of glass fiber and transferred to a Bruker CCD X-ray diffraction system, which was equipped with a graphite-monochromatized Mo Kα radiation (λ = 0.71073 Å) source controlled by a Pentium-based PC running the SMART software package.[32] Data were collected either at room temperature or at 100 K and the raw data frames were integrated by the SAINTPLUS program package.[33] Empirical absorption corrections were applied with the SADABS program[34] and the space group was determined by examining systematic absences and confirmed by the successful solution and refinement of the structure.

The structures were solved by direct methods and refined by full matrix least-squares and difference Fourier techniques with SHELXTL program package.[35] All non-hydrogen atoms were refined anisotropically. Hydrogen atoms attached to amine nitrogen atoms and water molecules were introduced as found on the Fourier difference maps and refined with restraint N–H = 0.87 Å with displacement parameter equal to 1.5 times that of the parent atom. All other hydrogen atoms were introduced geometrically and refined using a riding model with a displacement parameter equal to 1.2 (CH, CH_2) or 1.5 (CH_3) times that of the parent atom. Multipurpose crystallographic tools, PLATON,[36] ORTEP-3[37] and MERCURY,[38] were used for molecular graphics. Relevant crystallographic parameters and thermal ellipsoid plots for various compounds are presented in the respective chapters.

2.11. Standard error limits

Standard error limits involved in the measurements are:

λ_{max} (abs./fluo.)	± 2 nm
ϕ_f	$\pm 10\%$
FE	$\pm 10\%$
τ_f (> 1 ns)	$\pm 5\%$
τ_f (< 1 ns)	$\pm 5\text{-}15\%$ (depending on the excitation source used)

References

1. Perrin, D. D.; Armerego, W. L. F.; Perrin, D. R. *Purification of Laboratory Chemicals*; Pergamon Press: New York, 1980.

2. Austin, E.; Gouterman, M. *Bioinorg. Chem.* **1978**, *9*, 281.

3. Demas, J. N.; Crosby, G. A. *J. Phys. Chem.* **1971**, *75*, 991.

4. Soujanya, T.; Fessenden, R. W.; Samanta, A. *J. Phys. Chem.* **1996**, *100*, 3507.

5. Ramachandram, B.; Samanta, A. *J. Phys. Chem. A* **1998**, *102*, 10579.

6. Lippert, V. E. *Z. Electrochem.* **1957,** *61*, 962.

7. Mataga, N.; Kaifu, Y.; Koizumi, M. *Bull. Chem. Soc. Jpn.* **1956**, 29, 465.

8. Mataga, N. *Bull. Chem. Soc. Jpn.* **1963**, *36*, 654.

9. Ravi, M.; Samanta, A.; Radhakrishnan, T.P. *J. Phys. Chem.* **1994**, *98*, 9133.

10. Koti, A. S. R.; Bhattacharjee, B.; Haram, N. S.; Das, R.; Periasamy, N.; Sonawane, N. D.; Rangnekar, D.W. *J. Photochem. Photobiol., A* **2000**, *137*, 115.

11. Kawski, A. *Z. Naturforsch*. **1999,** *54a,* 379.

12. Reichard, C. *Solvents and solvent Effects in Organic Chemistry;* VCH Publishers: Weinheim, Germany, 1988.

13. Connors, K. A. *Binding Constants*; Wiley: New York, 1987.

14. Dewar, M. J. S.; Zoebisch, E. G.; Healy, E. F.; Stewart, J. J. P. *J. Am. Chem. Soc.* **1985**, *107*, 3902.

15. Dewar, M. J. S.; Dieter, K. M. *J. Am. Chem. Soc.* **1986**, *108*, 8075.

16. Soujanya. T.; Saroja, G.; Samanta, A. *Chem. Phys. Lett.* **1995**, *236*, 503.

17. Böttcher, C. J. F. In *Theory of Electronic Polarization* Elsvier: Amsterdam, 1973, Vol. 1, p. 153.

18. Mazumdar, D.; Sen, R.; Bhattacharya, K.; Bhattacharya, S. P. *J. Phys. Chem.* **1991**, *95*, 3424.

19. Hohenberg, P.; Kohn, W. *Phys. Rev.* **1964**, *B864*, 136.

20. Kohn, W.; Sham, L. J. *Phys. Rev.* **1965**, *A1133*, 140.

21. Parr, R. G.; Yang, W. *Density-functional theory of atoms and molecules;* Oxford Univ. Press: Oxford, 1989.

22. Becke, D. A. *J. Chem. Phys.* **1993**, *98*, 5648.

23. Lee, C.; Yang, W.; Parr, R. G. *Phys. Rev. B* **1988**, *37*, 785.

24. Reed, A. E.; Curtiss L. A.; Weinhold, F. *Chem. Rev.* **1988**, *88*, 899.

25. Messerschmidt, M.; Wagner, A.; Wong M. W.; Luger, P. *J. Am. Chem. Soc.* **2002***, *124*, 732.

26. Bauernschmitt, R.; Ahlrichs, R. *Chem. Phys. Lett.* **1996**, *256*, 454.

27. Casida, M. E.; Jamorski, C.; Casida, K. C.; Salahub, D. R. *J. Chem. Phys.* **1998**, *108*, 4439.

28. Wong, M. W.; Frish M. J.; Weiberg, K. B. *J. Am. Chem. Soc.* **1991**, *113*, 4776.

29. Cossi, M.; Barone, V. *J. Chem. Phys.* **2000**, *112*, 2427.

30. Frisch, M. J.; Trucks, G. W.; Schlegel, H. B.; Scuseria, G. E.; Robb, M. A.; Cheeseman, J. R.; Zakrzewski, V. G.; Montgomery, J. A. Jr.; Stratmann, R. E.; Burant, J. C.; Dapprich, S.; Millam, J. M.; Daniels, A.D.; Kudin, K. N.; Strain, M. C.; Farkas, O.; Tomasi, J.; Barone, V.; Cossi, M.; Cammi, R.; Mennucci, B.;

Pomelli, C.; Adamo, C.; Clifford, S.; Ochterski, J.; Petersson, G. A.; Ayala, P. Y.; Cui, Q.; Morokuma, K.; Malick, D. K.; Rabuck, A. D.; Raghavachari, K.; Foresman, J. B.; Cioslowski, J.; Ortiz, J. V.; Stefanov, B. B.; Liu, G.; Liashenko, A.; Piskorz, P.; Komaromi, I.; Gomperts, R.; Martin, R. L.; Fox, D. J.; Keith, T.; Al-Laham, M. A.; Peng, C. Y.; Nanayakkara, A.; Gonzalez, C.; Challacombe, M.; Gill, P. M. W.; Johnson, B.; Chen, W.; Wong, M. W.; Andres, J. L.; Gonzalez, C.; Head-Gordon, M.; Replogle, E. S.; Pople, J. A. *Gaussian 98*; Gaussian,Inc.: Pittsburgh, PA, 1998.

31. Bevington, P. R. *Data Reduction and Error Analysis for the Physical Sciences*; McGraw-Hill: New York, 1969.

32. *SMANTPLUS*; 6.45 ed.; Bruker AXS, Inc.: Madison, WI, 2003.

33. *SADABSRT*; 5.629 ed.; Bruker AXS, Inc.: Madison, WI, 2003.

34. *SAI*; 2.10 ed.; Bruker AXS, Inc.: Madison, WI, 2003.

35. *SHELXTL*; 6.14 ed.; Bruker AXS, Inc.: Madison, WI, 2003.

36. Spek, A. L.; Utrecht University: Utrecht, The Netherlands, 1998.

37. Farrugia, L. J. *J. Appl. Cryst.* **1997**, *30*, 565.

38. *MERCURY*; 1.2.1 ed.; CCDC: UK, 2004.

Photophysical Behavior of Aminonitrofluorene Derivatives

Synthesis, characterization and photophysical behavior of several amine-terminated nitrofluorene derivatives have been described in this chapter. Copper-mediated Ullmann-type C-N bond formation reaction protocol has been employed for the synthesis of most of the derivatives. The systems have been characterized by conventional analytical and single crystal X-ray diffraction techniques. Photophysical behavior of the systems has been studied as a function of the polarity of the medium using steady state and time-resolved spectroscopic techniques. Theoretical calculations have also been carried out with a view to rationalize the experimental findings.

3.1. Introduction

As stated earlier, the electron donor acceptor (EDA) systems have been the focus of contemporary research owing to their importance in biological and materials sciences. We have been interested in push-pull fluorene derivatives, in particular, the 2-amino-7-nitro derivatives, as these are known to be attractive candidates for studying solvation dynamics,[1] two-photon absorption phenomena[2] and pH sensing[3]. However, except for a few studies, which suggest a huge change in the dipole moment (25 D) upon photoexcitation of 2-amino-7-nitrofluorene,[4,5] this system has not received the attention it deserves compared to other EDA systems.

In this work, we have concentrated ourselves on several amine-terminated nitrofluorene derivatives (Chart 3.1), where different amino groups serve as donor and a nitro group as common acceptor.
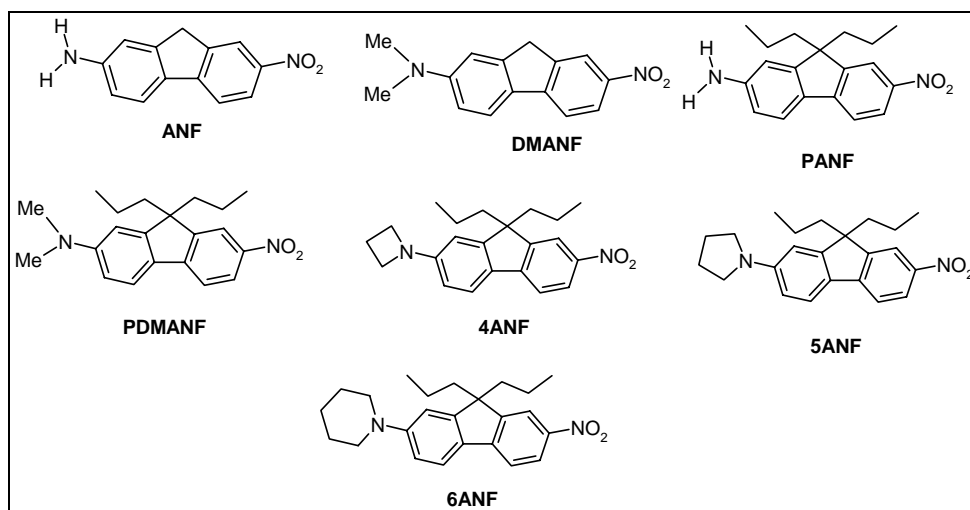
Chart 3.1

The first two systems of the set, **ANF** and **DMANF,** differ from the remaining systems in respect of not having the dipropyl groups at the ninth position. Replacement of the two hydrogens at 9-position by two alkyl groups was necessary prior to incorporation of the desired amino-functionality in the systems to avoid deprotonation of these acidic hydrogens (*vide* section 3.2.3). It must be noted, however, this replacement does not significantly affect the photophysical behavior of the systems.

The fluorescence behavior of all the systems is found to be strongly dependent on the polarity of the solvent. Unlike commonly encountered EDA systems,

several fluorescence bands have been identified under various experimental conditions for these systems. It is to be noted in this context that several structurally similar di-propyl group containing systems have been synthesized primarily to confirm that the multiple emissions are real and that they do not come from the impurities.

3.2. Synthesis of the systems
ANF

ANF was synthesized by following a literature procedure.[6] A mixture of 2,7-dinitrofluorene (4 g, 0.015 mol), 10% palladium on carbon (0.25 g), and triethylamine (20 mL, 0.140 mol) was placed in a two-necked round-bottomed flask which was equipped with a reflux condenser. The mixture was heated to boiling, and formic acid (2.56 mL, 0.067 mol) was added drop-wise with stirring. The mixture was boiled for about 30-40 min. The reaction mixture turned dark reddish a few minutes after addition of formic acid. Later, the reaction mixture was cooled, dichloromethane was added and the catalyst was removed by filtration. The solvent and excess triethylamine were removed under reduced pressure, and the reddish residue was chromatographed on alumina (EtOAc-Hexane, 20:80) to give a bright red solid. Yield: 1.94 g (57%).

The compound was characterized by the following analytical data.

Mp: 228-230 $^{\circ}$C.

^{1}H NMR (400 MHz, DMSO-d_6): δ 3.93 (s, 2 H), 5.74 (s, 2 H), 6.71 (d, J = 7.9 Hz, 1 H), 6.85 (s, 1 H), 7.74 (d, J = 8.3 Hz, 1 H), 7.82 (d, J = 8.7 Hz, 1 H), 8.23 (d, J = 7.9 Hz, 1 H), 8.31 (s, 1 H).

DMANF

   DMANF was synthesized from **ANF** by following a literature procedure.[6] To the stirred mixture of **ANF** (100 mg, 0.442 mmol) and paraformaldehyde (148 mg, 0.005 mmol) in 99% glacial acetic acid (4 mL) was added sodium cyano borohydride (140 mg, 2.25 mmol) in one portion at room temperature under nitrogen atmosphere. The resulting mixture was stirred at room temperature for 24 h and then poured into cold water. A bright orange-red solid precipitated. It was filtered off and re-crystallized from MeCN/water. Yield: 91 mg (81%).

   The compound was characterized by following analytical data.
^{1}H NMR (400 MHz, CDCl$_3$): δ 3.05 (s, 6 H), 3.88 (s, 2 H), 6.75 (dd, J_1 = 2.6 Hz, J_2 = 2.2 Hz, 1 H), 6.89 (d, J = 1.9 Hz, 1 H), 7.61 (d, J = 8.7 Hz, 1 H), 7.67 (d, J = 8.7 Hz, 1 H), 8.22 (d, J = 8.7 Hz, 1 H), 8.26 (s, 1 H).

3.2.1. Fluorene derivatives bearing n-propyl groups

   The starting material for the C-N coupling reaction, 2-iodo-7-nitro-9H-fluorene (**INF**) was obtained from 2-nitrofluorene by an iodination reaction following a literature method.[7] However, since Leibscher et al. had shown recently that acidity of the C-9 hydrogen atoms of fluorene leads to deprotonation in the presence of the reactant base (in our case, cesium acetate), generating an fluorenyl anion that deactivates the nucleophilic substitution reaction[6] leading to the failure of C-N bond formation, it was necessary to block this position before going to the main reaction. This was accomplished by introducing two n-propyl groups following a literature method[8] to obtain 2-iodo-7-nitro-9,9-dipropyl-9H-fluorene (**PINF**). The syntheses of **INF** and **PINF** have been described in Scheme 3.1. Finally, **PINF** was treated with appropriate amines, using cuprous iodide and

cesium acetate in dry DMSO with close control of the reaction temperature and stirring for 24-48 h under nitrogen atmosphere to obtain two acyclic amine analogues, **PANF, PDMANF** and three cyclic analogues, **4ANF, 5ANF** and **6ANF**. The C-N bond formation reaction has been described in Scheme 3.2.

INF

To 2-nitrofluorene (12.8 g, 0.06 mol) in 400 mL of glacial acetic acid was added iodine (7.58 g, 0.03 mol). The solution was stirred at room temperature for about 10 min, after which 60 mL of *conc.* H_2SO_4 and $NaNO_2$ (4.4 g, 0.06 mol) were added. The solution was heated under reflux for 30 min and poured into 200 g of ice. The yellow solid that formed was collected by filtration. Recrystallization from dioxane and water mixture afforded nice yellow material. Yield: 13.62 g (67%).

The compound was characterized by following analytical data.
Mp: 245 °C. Anal calc. for $C_{13}H_8O_2NI$: C, 46.32; H, 2.39; N, 4.15. Found: C, 45.89; H, 2.43; N, 4.55.

PINF

A mixture of **INF** (2 g, 5.9 mmol), propylbromide (1.83 g, 15 mmol), KI (0.11 g, 0.66 mmol) and DMSO (12 mL) was stirred at room temperature, to which powdered KOH (1.5 g, 27 mmol) was slowly added under nitrogen. The color of the reaction mixture changed to dark green immediately after the addition of KOH. After 3-4 h of stirring, the reaction mixture was poured into water. A somewhat greenish colored precipitate that formed was collected by filtration and dried to get the product. Yield: 2.42 g (96%).

The compound was characterized by following analytical data.

^{1}H NMR (400 MHz, CDCl$_3$): δ 0.62–0.66 (m, 10 H, 2 × CH$_2$C*H*$_2$C*H*$_3$), 1.82–2.02 (m, 4 H, 2 × C*H*$_2$CH$_2$CH$_3$), 7.50 (d, *J* = 8.0 Hz, 1 H, H-6), 7.72 (d, *J* = 8.8 Hz, 1 H, H-5), 7.75 (br, 1 H, H-8), 7.78 (d, *J* = 9.0 Hz, 1 H, H-4), 8.20 (br, 1 H, H-1), 8.27 (d, *J* = 1.6 Hz, 1 H, H-3).
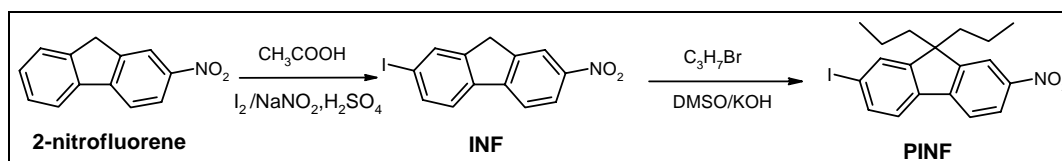
Scheme 3.1 Synthetic route to precursor fluorene.

3.2.1.1. Synthesis of Acyclic analogues: general procedure

To a solution of **PINF** (100 mg, 0.273 mmol) in dry DMSO (1.5 mL), were added the corresponding amine (1.2 mmol), CsOAc (120 mg, 0.62 mmol) and CuI (5 mol%) and the solution was heated to 40–90 °C (according to the boiling point of the corresponding amine) under N$_2$ atmosphere for 24 h. The color changed to reddish brown during this time. After cooling to room temperature, the reaction was quenched with H$_2$O (20 mL), extracted with EtOAc (50 mL) and the organic layer was washed with brine (100 mL). The organic layer was dried over Na$_2$SO$_4$ and concentrated through evaporation. The products were purified by column chromatography (basic alumina, EtOAc–hexane, 30:70).

The compounds were characterized from the following analytical data.

PANF

Yield: 55 mg (74.8%).

Mp: 120-124 ˚C.

IR (KBr): 3090, 1512, 1319 cm^{-1}.

^{1}H NMR (400 MHz, CDCl$_3$): δ 0.64–0.67 (m, 10 H, 2 × CH$_2$C*H$_2$*C*H$_3$*), 1.71–1.91 (m, 4 H, 2 × C*H$_2$*CH$_2$CH$_3$), 3.96 (s, 2 H, NH$_2$), 6.66 (br, 1 H, H-8), 6.68 (d, *J* = 2.0 Hz, 1 H, H-6), 7.56 (d, *J* = 8.8 Hz, 1 H, H-5), 7.58 (d, *J* = 8.8 Hz, 1 H, H-4), 8.12 (br, 1 H, H-1), 8.22 (d, *J* = 8.8 Hz, 1 H, H-3).

LCMS: m/z 311 (M+H$^+$).

Anal calc. for C$_{19}$H$_{22}$N$_2$O$_2$: C, 73.54; H, 7.14; N, 9.02. Found: C, 73.71; H, 7.21; N, 9.10.

PDMANF

Yield: 50 mg (52.0%).

Mp: 125-130 ˚C.

IR (KBr): 1508, 1312 cm^{-1}.

^{1}H NMR (400 MHz, CDCl$_3$): δ 0.64–0.68 (m, 10 H, 2 × CH$_2$C*H$_2$*C*H$_3$*), 1.71–1.91 (m, 4 H, 2 × C*H$_2$*CH$_2$CH$_3$), 3.08 (s, 6 H, 2 × NMe), 6.62 (br, 1 H, H-8), 6.63 (d, *J* = 2.2 Hz, 1 H, H-6), 7.55 (d, *J* = 8.0 Hz, 1 H, H-5), 7.57 (d, *J* = 8.8 Hz, 1 H, H-4), 8.11 (br, 1 H, H-1), 8.12 (d, *J* = 1.6 Hz, 1 H, H-3).

^{13}C NMR (400 MHz, CDCl$_3$): δ 14.38 (CH$_3$), 17.09 (CH$_2$), 24.64 (CH$_2$), 42.70 (CH$_3$), 55.5 (C), 106.1 (CH), 111.8 (CH), 117.6 (CH), 117.9 (CH), 122.3 (CH), 123.6 (CH), 128.4(CH), 143.3 (C), 148.8 (C), 150.5 (C), 150.9 (C), 154.8 (C).

LCMS: m/z 339 (M+H$^+$). Anal calc. for C$_{21}$H$_{26}$N$_2$O$_2$: C, 74.53; H, 7.74; N, 8.28. Found: C, 74.72; H, 7.91; N, 8.40.
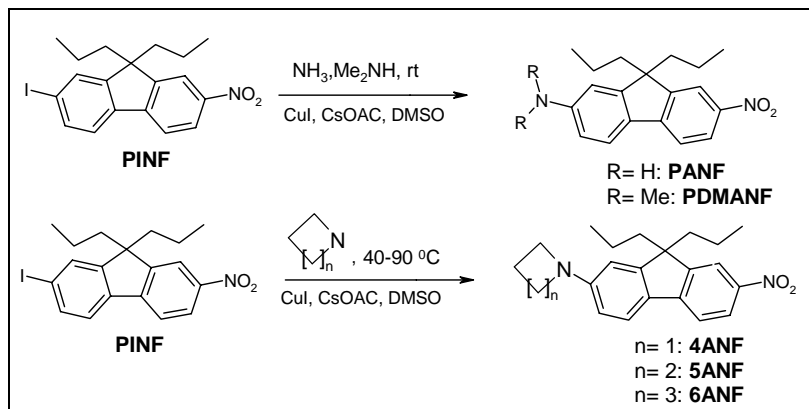
Scheme 3.2 C-N bond formation reaction by Cu-catalyzed amination of **PINF**.

3.2.1.2. Synthesis of cyclic analogues: general procedure

To a solution of **PINF** (100 mg, 0.273 mmol) in dry DMSO (1.5 ml) the corresponding amine (1.2 mmol) and cesium acetate (120 mg, 0.62 mmol), CuI (5 mol%) were added and the solution was heated to 40-90°C (according to the boiling point of the corresponding amines) under N_2 atmosphere for 24 h, the color changed to reddish brown. After being cooled to room temperature, the reaction was quenched with water and extracted with EtOAc (50 mL) and organic layer was washed with brine solution (100 mL). The organic layer was dried over anhydrous Na_2SO_4 and concentrated through evaporation. The product was purified through column chromatography (basic alumina, EtOAc/hexane = 30/70) as a bright red solid.

The compounds were characterized from the following analytical data.

4ANF

Yield: 65 mg (78.3%).

Mp: 105-109 °C.

IR (KBr): 1506, 1310 cm^{-1}.

^{1}H NMR (400 MHz, CDCl$_3$): δ 0.64–0.69 (m, 10 H, 2 × CH$_2$C*H*$_2$C*H*$_3$), 1.71–1.92 (m, 4 H, 2 × C*H*$_2$CH$_2$CH$_3$), 2.31–2.52 (m, 2 H, azetidine CH$_2$), 4.12 (t, *J* = 6 Hz, 4 H, azetidine CH$_2$), 6.42 (br, 1 H, H-8), 6.51 (d, *J* = 2.0 Hz, 1 H, H-6), 7.63 (d, *J* = 8.0 Hz, 1 H, H-5), 7.65 (d, *J* = 8.2 Hz, 1 H, H-4), 8.21 (br, 1 H, H-1), 8.30 (d, *J* = 1.6 Hz, 1 H, H-3).

^{13}C NMR (400 MHz, CDCl$_3$): δ 14.4 (CH$_3$), 17.1 (CH$_2$), 25.6 (CH$_2$), 42.5 (CH$_2$), 48.9 (CH$_2$), 55.5 (C), 104.9 (CH), 111.5 (CH), 116.1 (CH), 116.9 (CH), 122.1 (CH), 123.4 (CH), 127.2 (CH), 144.5 (C), 148.2 (C), 148.3 (C), 150.1 (C), 154.3 (C).

LCMS: m/z 351 (M+H$^+$).

Anal calc. for C$_{22}$H$_{26}$N$_2$O$_2$: C, 75.40; H, 7.48; N, 7.99. Found: C, 75.69; H, 7.57; N, 8.21.

5ANF

Yield: 60 mg (69.5%).

Mp: 115-118 °C.

IR (KBr): 1502, 1304 cm^{-1}.

^{1}H NMR (400 MHz, CDCl$_3$): δ 0.64–0.69 (m, 10 H, 2 × CH$_2$C*H*$_2$C*H*$_3$), 1.67–1.85 (m, 4 H, 2 × C*H*$_2$CH$_2$CH$_3$), 2.04–2.08 (m, 4 H, pyrrolidine CH$_2$), 3.42 (t, *J* = 5.6 Hz, 4 H, pyrrolidine CH$_2$), 6.49 (br, 1 H, H-8), 6.60 (d, *J* = 2.0 Hz, 1 H, H-6),

7.54 (d, *J* = 8.4 Hz, 1 H, H-5), 7.62 (d, *J* = 8.4 Hz, 1 H, H-4), 8.13 (br, 1 H, H-1), 8.21 (d, *J* = 1.6 Hz, 1 H, H-3).

^{13}C NMR (400 MHz, CDCl$_3$): δ 14.4 (CH$_3$), 17.1 (CH$_2$), 25.5 (CH$_2$), 42.8 (CH$_2$), 47.92 (CH$_2$), 55.4 (C), 105.4 (CH), 111.2 (CH), 117.3 (CH), 117.9 (CH), 122.3 (CH), 123.7 (CH), 126.6(CH), 144.9 (C), 149.2 (C), 149.3 (C), 150.4 (C), 154.7 (C).

LCMS: m/z 365 (M+H$^+$).

Anal calc. for C$_{23}$ H$_{28}$ N$_2$ O$_2$: C, 75.79; H, 7.74; N, 7.69. Found: C, 75.65; H, 7.62; N, 7.81.

6ANF

Yield: 50mg (55.8%).

Mp: 117-122 °C.

IR (KBr): 1507, 1301 cm^{-1}.

^{1}H NMR (400 MHz, CDCl$_3$): δ 0.63–0.66 (m, 10 H, 2 × CH$_2$C*H$_2$*C*H$_3$*), 1.64–1.81 (m, 4 H, 2 × C*H$_2$*CH$_2$CH$_3$), 1.74 (m, 2 H, piperidine CH$_2$), 1.83–1.87 (m, 4 H, piperidine CH$_2$), 3.32 (t, *J* = 5.3 Hz, 4 H, piperidine CH$_2$), 6.87 (br, 1 H, H-8), 6.95 (d, *J* = 2.8 Hz, 1 H, H-6), 7.50 (d, *J* = 8.0 Hz, 1 H, H-5), 7.60 (d, *J* = 8.4 Hz, 1 H, H-4), 8.12 (br, 1 H, H-1), 8.20 (d, *J* = 2 Hz, 1 H, H-3).

^{13}C NMR (400 MHz, CDCl$_3$): δ 14.39 (CH$_3$), 17.1 (CH$_2$), 24.29 (CH$_2$), 25.7 (CH$_2$), 42.62 (CH$_2$), 50.22 (CH$_2$), 55.6 (C), 109.9 (CH), 115.1 (CH), 118.03 (CH), 118.09 (CH), 121.9 (CH), 123.5 (CH), 129.6 (CH), 145.6 (C), 148.4 (C), 151.1 (C), 153.4 (C), 154.1 (C).

LCMS: m/z 379 (M+H$^+$).

Anal calc. for $C_{24} H_{30} N_2 O_2$: C, 76.16; H, 7.99; N, 7.40. Found: C, 76.1; H, 8.03; N, 7.64.

3.3. X-ray crystallographic measurements

Among the aminonitrofluorenes, good single crystals suitable for X-ray diffraction could be obtained for **PDMANF**, **5ANF** and **6ANF** (from chloroform). ORTEP diagrams of the systems are shown in Figure 3.1. The essential crystallographic data are presented in Table 3.1.
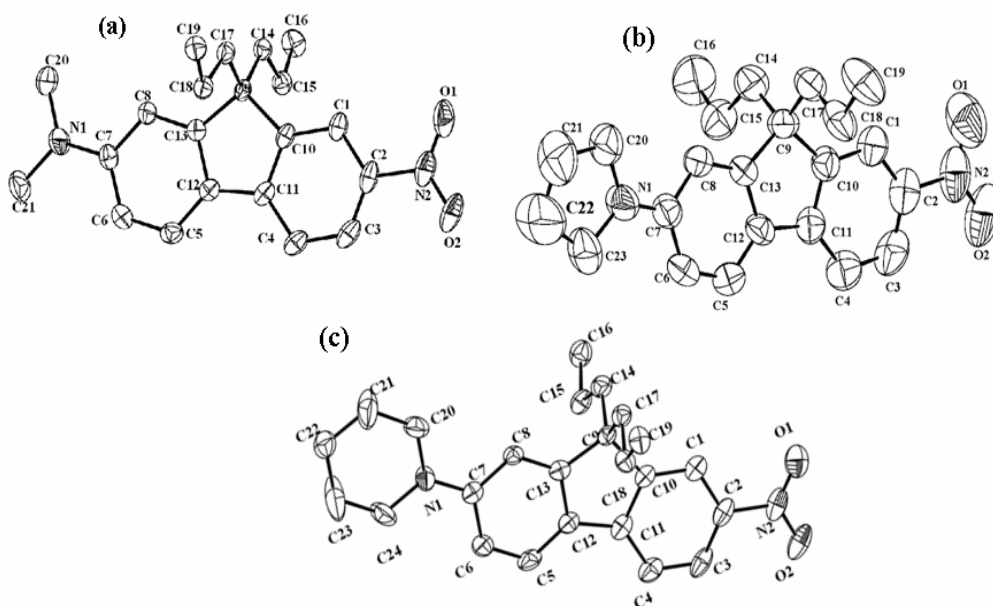
Figure 3.1 (a) ORTEP diagram of **PDMANF** with atoms represented by thermal ellipsoids at 30 % probability level, N(1)-C(7) bond length = 1.376 (9) Å. (b) ORTEP diagram of **5ANF** with atoms represented by thermal ellipsoids at 50 % probability level, N(1)-C(7) bond length = 1.376 (6) Å. (c) ORTEP diagram of **6ANF** with atoms represented by thermal ellipsoids at 30 % probability level, N(1)-C(7) bond length = 1.394 (5) Å.

Table 3.1 Data Collections and Structure Refinement Details of Crystal Structures of **PDMANF**, **5ANF** and **6ANF**

	PDMANF	5ANF	6ANF
Formula	$C_{21}H_{26}N_2O_2$	$C_{23}H_{28}N_2O_2$	$C_{24}H_{30}N_2O_2$
Formula wt	338.40	364.47	378.50
Crystal system	monoclinic	monoclinic	monoclinic
Space group	P2(1)/n	P2(1)/c	P2(1)/c
a (Å)	9.9257(6)	10.001(3)	9.9984(15)
b (Å)	14.9179(9)	16.096(5)	16.020(2)
c (Å)	13.3095(8)	13.613(4)	13.474(2)
α (°)	90	90	90
β (°)	109.413(10)	108.216(7)	107.784(3)
γ (°)	90	90	90
V (Å^3)	1858.70(19)	2081.6(11)	2055.0(5)
Z	4	4	4
F(000)	728	784	816
ρ_{calcd} (g cm^{-3})	1.209	1.163	1.223
μ (mm^{-1})	0.078	0.074	0.078
T (K)	100	100	100
Crystal size	0.33×0.26×0.2	0.24×0.12×0.1	0.27×0.1×0.06
Absorption correction	Multi-scan	Multi-scan	Multi-scan
T_{min}, T_{max}	0.976, 0.985	0.789,0.993	0.932, 0.995
Total no reflections	21394	20035	13250
unique reflections	4487	3754	4795
obs. reflections	3546	1086	1895
θ_{max} (°)	28.24	25.25	28.32
No. of parameters	230	246	255
R indices (obs. data): R, R_w	0.0541, 0.1529	0.0792,0.1609	0.0907, 0.1861
R indices (all data): R, R_w	0.0668, 0.1603	0.2735,0.2452	0.2292, 0.2425
GOF	1.106	0.906	0.974
ρ_{max}, ρ_{min} (e/Å^3)	0.411, -0.223	0.163, -0.204	0.349, -0.359

3.4. Photophysical behavior of the systems

3.4.1. Absorption behavior

The UV-vis absorption spectra of the systems have been studied in various solvents of different polarity and the spectral data have been collected in Table 3.2. Representative absorption spectra of **DMANF** and **5ANF** in different solvents are shown in Figure 3.2. Except in extremely nonpolar solvent like cyclohexane, where the absorption band is somewhat structured, the absorption is characterized by broad band that displays solvatochromic behavior typical of a charge transfer transition in which the amino group acts as a donor and nitro as an acceptor. The bandwidth (fwhm) usually varies between 4600 and 6200 cm^{-1} and the molar extinction coefficient between 20000 and 24000 mol^{-1} cm^{-1} L in acetonitrile. A change in the solvent from toluene to dimethyl sulfoxide (DMSO) typically results in 20-30 nm bathochromic shift of the absorption maximum of the systems. The large magnitude of the shift suggests that the ground state of the systems is significantly polar. This fact is consistent with the estimated ground state dipole moments that are found to be quite high (7.6 D – 8.4 D) for the systems (*vide* section 3.6). Among the propyl group containing systems, **5ANF** shows the most red-shifted absorption band in any solvent. This observation, which suggests that **5ANF** is the most dipolar compound in this series, is consistent with both the AM1 calculated dipole moment (8.42 D) and short C-N bond length (1.376 Å, obtained from the crystal structure) of **5ANF.** Perhaps, the most interesting aspect of our observation in this regard is that the systems show a hypsochromic shift on changing the solvent from DMSO to ethanol despite the fact that ethanol is more polar than DMSO (as evident from the E$_T$(30) values of

the solvent, *vide* Table 3.2). This blue shift can be explained only if we consider the H-bonding interaction between the amino nitrogen of the systems and the hydroxyl group of ethanol, in which the latter serves as H-bond donor. This blue shift of the absorption maximum is also observable in other alcoholic solvents highlighting the generality of the observation. This behavior is consistent with the literature data on aminofluorene.[9]
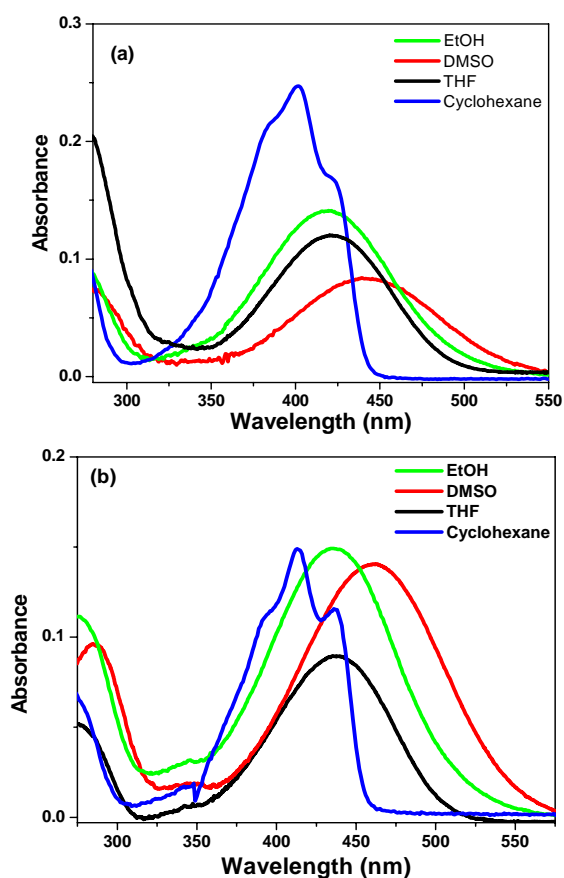
Figure 3.2 Absorption spectra of (a) **DMANF** and (b) **5ANF** in some selected solvents.

Table 3.2 Absorption and Fluorescence Spectral Data of the Systems in Different Solvents at Room Temperature[a]

	Systems												
	ANF		DMANF		PANF		PDMANF		4ANF		5ANF		6ANF	
Solvents[b]	λ^{abs}_{max}	λ^{emis}_{max}	λ^{abs}_{max}	λ^{emis}_{max}	λ^{abs}_{max}	λ^{emis}_{max}	λ^{abs}_{max}	λ^{emis}_{max}	λ^{abs}_{max}	λ^{emis}_{max}	λ^{abs}_{max}	λ^{emis}_{max}	λ^{abs}_{max}	λ^{emis}_{max}
Cyclohexane (33.1)	372	460	402	467	382	460	405	470	396	470	414	470	393	470
Toluene (33.9)	389	504	417	540	394	508	422	550	408	550	433	550	410	550
Dioxane (36.0)	394	538	413	576	400	540	423	562	410	565	430	565	404	565
THF (37.4)	406	572	422	599	410	565	430	595	418	600	435	600	412	604
EtOAc (38.1)	398	572	416	613	404	565	419	602	410	598	427	600	407	604
ACN (45.6)	399	656	424	722	408	650	429	710	419	710	443	710	414	710
DMSO (45.1)	433	690	440	740	434	680	448	720	436	723	461	710	436	720
EtOH (51.9)	401	677	419	705	405	678	428	710	415	708	415	708	408	708

[a] λ^{abs}_{max} and λ^{emis}_{max} values are expressed in nm. λ^{emis}_{max} values reported in this table are for the solvent sensitive ICT emission of the system (λ_{exc} = 375 nm). [b] Quantities in the paranthesis indicate E_T (30) values of the solvents.

3.4.2. Fluorescence spectral behavior

ANF and **DMANF** are known to display a broad emission band due to the intramolecular charge transfer (ICT) transition.[5] The wavelength corresponding to the maximum intensity of the band is known to be remarkably sensitive to the polarity of the media due to enhanced separation of charge in the excited state.[5]
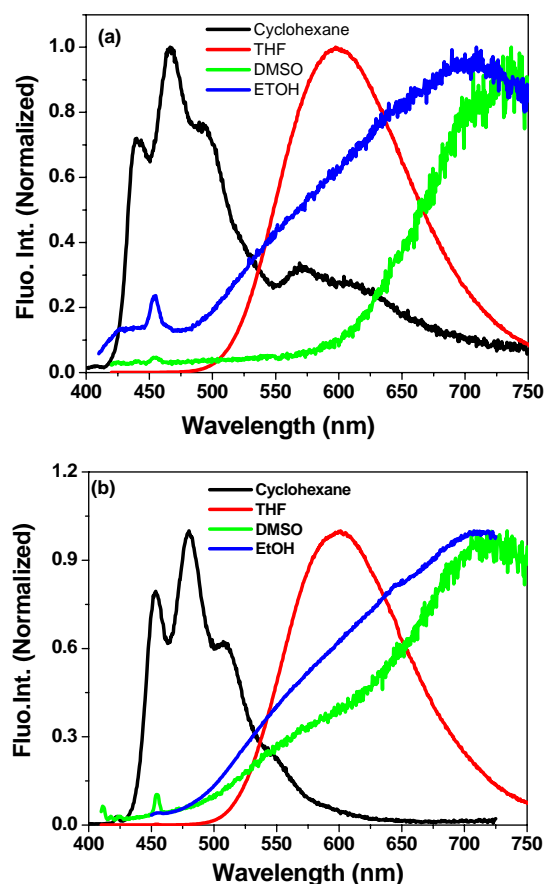
Figure 3.3 Normalized emission spectra of (a) **DMANF** and (b) **5ANF** in some selected solvents. $\lambda_{exc} = 375$ nm.

Interestingly, in the present study, for all the systems we observed multiple emission bands under different experimental conditions. Upon exciting the sample at around 375 nm we could observe dual emission for all the systems. This is clearly evident from the emission behavior of **DMANF** and **5ANF** shown in Figure 3.3. In cyclohexane, the emission of **DMANF** can be best described as a two-component emission, with the high energy structured component (λ_{max} = 470 nm) being essentially the mirror image of the absorption band. The second component, which appears at longer wavelength (~560 nm), is somewhat less in intensity (Figure 3.3 (a)). As the polarity of the medium is increased, the two separate emission profiles merge into a single band. When the polarity of the medium is very high, the ICT component of the emission gets further Stokes-shifted making the 560 nm band observable again. In highly polar solvent, ethanol, a prominent emission hump at around 560 nm is clearly observable in addition to the ICT fluorescence band, which appears at a much longer wavelength (Figure 3.3 (a)). For other systems, the behavior is not found to be very different. For example, in the case of **5ANF**, even though the 560 nm emission component is not so clear in cyclohexane, it shows up prominently as a shoulder in highly polar media such as DMSO or ethanol when the ICT emission has moved away significantly from this rather weak band (Figure 3.3 (b)). Another reason for why this emission is not so obvious in cyclohexane is because the other emission is too strong. In highly polar media, when the fluorescence yield of the ICT emission becomes too low, the 560 nm emission can be clearly seen. Deconvolution of the total emission spectra leads to two separate emission bands with the maxima appearing at 560 nm and 705 nm, as shown in Figure 3.4,

for **DMANF** in ethanol. We refer to the ICT and 560 nm emission bands as **Em$_1$** and **Em$_2$** respectively. The emission maxima corresponding to **Em$_1$** band in different solvents are collected in Table 3.2. As can be seen from the data presented in Table 3.2, the effect of polarity of the medium on the fluorescence maximum is much more pronounced than that on the absorption. While changing the solvent from toluene to DMSO, the absorption maximum of the systems shows around 25 nm bathochromic shift, the fluorescence maximum, shifts by ~200 nm. This observation clearly suggests that the ICT emitting state of the systems is much more polar than the ground state.
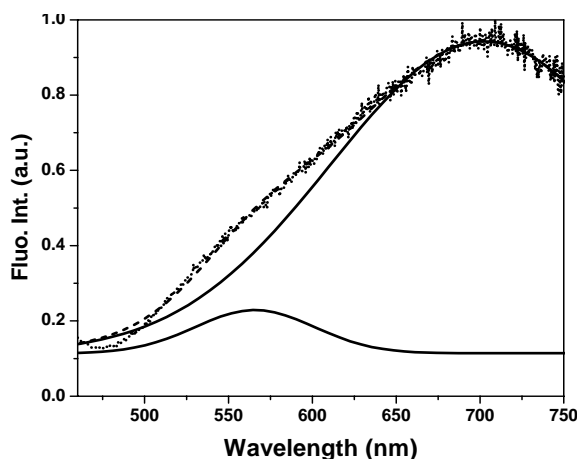
Figure 3.4 Deconvolution of the total fluorescence of **DMANF** in ethanol into two fluorescence bands. Solid lines represent the deconvoluted spectra and the dotted line represents the total emission spectrum. λ_{exc} = 375 nm.

In order to determine the origin of the two emission components, we have carried out a control experiment. Gradual addition of a more polar solvent, ethylacetate to a cyclohexane solution of **DMANF,** leads to intensification of the

470 nm emission band with a bathochromic shift, whereas the 560 nm emission band gets buried under the intense ICT band (Figure 3.5). The results are found to be very similar for other systems. The control experiment clearly confirms that the 470 nm emission in cyclohexane is of charge transfer origin and shifts towards longer wavelength with gradual addition of more polar solvent, whereas the 560 nm emission band can be surmised as originating from a state having negligible charge transfer character.
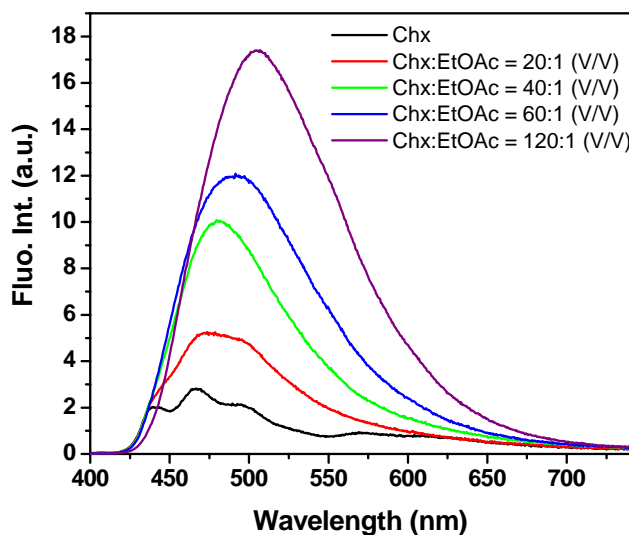
Figure 3.5 Emission spectra of **DMANF** in cyclohexane (Chx) with gradual addition of ethylacetate at room temperature. λ_{exc} = 375 nm.

The excitation spectra corresponding to two different emission bands of **DMANF** and **5ANF** in DMSO are shown in Figure 3.6. For **DMANF**, the excitation maxima corresponding to **Em$_1$** and **Em$_2$** appear at 410 nm and 370 nm respectively, in cyclohexane, while they appear at 440 nm and 370 nm in DMSO.

The observation of two different excitation maxima corresponding to two different emission bands, completely rules out the possible involvement of any excited state process (such as TICT) in giving rise to multiple emission components. Instead, it suggests that **Em$_1$** and **Em$_2$** originate from two locally excited states of the systems.
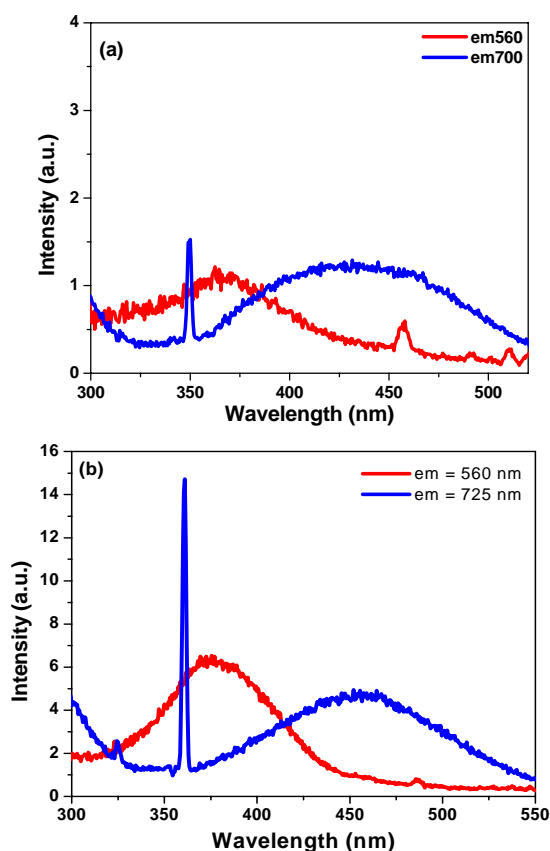
Figure 3.6 Excitation spectra of (a) **DMANF** and (b) **5ANF** in DMSO corresponding to two emission bands.

More interestingly, when excited at a higher energy (e.g. λ_{exc} = 300 nm), another fluorescence of much less intensity is observable at around 350-420 nm for all the systems. Representative emission spectra highlighting this band for **ANF** and **DMANF** in ethyl acetate are shown in Figure 3.7. It is to be noted that for dialkylamino systems, the emission maximum is found to be less sensitive to the polarity of the media compared to the parent system such as **ANF** and **PANF**. One interesting feature of this emission component, referred to as **Em$_3$**, is that the fluorescence maximum corresponding to **DMANF** appears at shorter wavelength relative to that for **ANF** even though the excitation maximum appears at a longer wavelength (Figure 3.8).
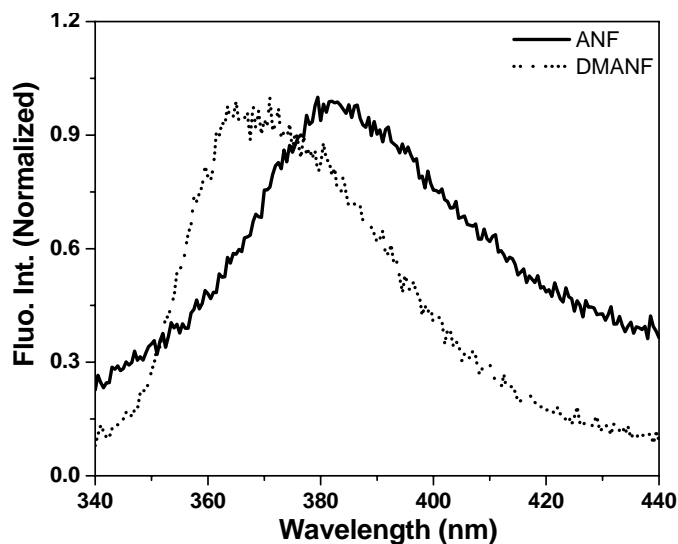
Figure 3.7 Normalized emission spectra of **ANF** (——) and **DMANF** ($\cdots$) in ethyl acetate λ_{exc} = 300 nm.
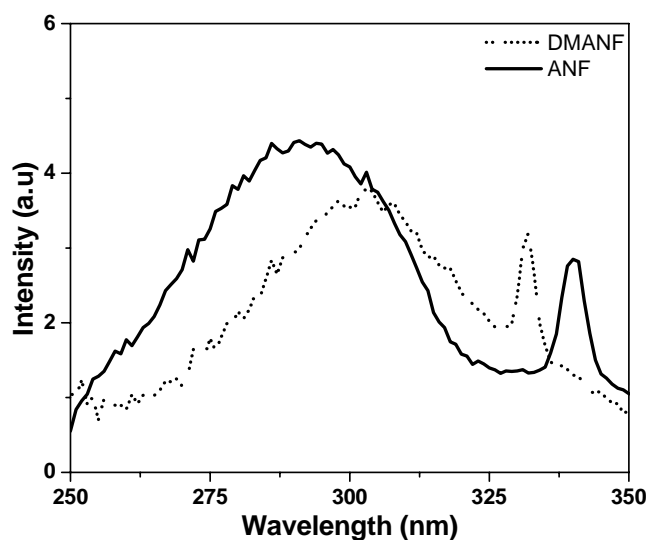
Figure 3.8 Excitation spectra of **ANF** (—) and **DMANF** (···) in ethyl acetate. For **ANF** and **DMANF** emissions were monitored at 380 nm and 370 nm respectively.

This observation implies that photoexcitation to this state leads to decoupling of the electron donor and acceptor moieties presumably due to the internal rotation (twisting) of the dialkylamino or the nitro group.

3.4.3. Fluorescence quantum yield and lifetime

Fluorescence quantum yield of the most prominent emission component (**Em$_1$**) of the **ANF** derivatives measured in a series of solvents of different polarity are collected in Table 3.3.

The fluorescence quantum yield of the systems decreases with increasing polarity of the solvent, presumably due to the decrease in the energy gap between the ground and emitting states, facilitating the internal conversion process.

Table 3.3 Fluorescence Quantum Yields[a] of the Systems at Room Temperature

Solvents	Systems						
	ANF	DMANF	PANF	PDMANF	4ANF	5ANF	6ANF
Toluene	0.100	0.630	0.180	0.440	0.210	0.380	0.330
Dioxan	0.320	0.500	0.390	0.530	0.320	0.500	0.560
THF	0.220	0.660	0.350	0.410	0.240	0.460	0.500
EtOAc	0.150	0.180	0.090	0.110	0.060	0.100	0.090
ACN	0.006	0.130	0.005	0.090	0.008	0.006	0.007
DMSO	0.002	0.002	0.002	0.007	0.008	0.009	0.005

[a]These values are estimated for **Em$_1$**. λ_{exc} = 375 nm.

The fluorescence decay behavior of **Em$_1$** has also been studied in different solvents. The decay parameters associated with the emission profiles of the systems are collected in Table 3.4. A representative decay profile of **ANF** in 1,4-dioxane is shown in Figure 3.9.

For all the systems, the ICT emission shows single exponential decay profile with lifetimes between 0.93–3.88 ns in nonpolar media. In polar solvents like ACN and DMSO, the decay profiles are found to be biexponential in nature with an average lifetime of 95–360 ps (*vide* Table 3.4).

Figure 3.9 Fluorescence decay profile of **ANF** in 1,4- dioxane as monitored at 540 nm. The experimental decay curve is shown by dotted line and the instrument profile by dashed line. The solid line is the fit to the decay curve. A weighted deviation is also shown at the bottom of the decay curve. λ_{exc} = 375 nm.

Table 3.4 Fluorescence Lifetimes (ns) of the Systems at Room Temperature[a]

Solvents	Systems						
	ANF	DMANF	PANF	PDMANF	4ANF	5ANF	6ANF
Toluene	0.93	2.30	1.47	3.00	2.94	3.10	3.00
Dioxan	2.13	3.30	2.68	3.67	3.45	3.72	3.72
THF	2.74	3.27	3.09	3.88	3.60	3.67	3.80
EtOAc	1.00	2.83	2.30	3.50	3.20	3.30	3.50
ACN	0.09	0.20	$0.11^{\dagger}$	$0.25^{\dagger}$	$0.21^{\dagger}$	$0.24^{\dagger}$	$0.22^{\dagger}$
DMSO	-	-	$0.19^{\dagger}$	$0.36^{\dagger}$	$0.32^{\dagger}$	$0.34^{\dagger}$	$0.350^{\dagger}$

[a]The values are estimated for **Em$_1$**. λ_{exc} = 375 nm. †These values represent average lifetime calculated from the prexponential factors and lifetime components of the multiexponential decay profiles. The lifetimes could not be determined accurately in few cases as they are found to be shorter than the time resolution (40 ps) of the instrument.

The nonradiative rate constants (k_{nr}) estimated from the fluorescence quantum yields and the lifetimes of the **Em$_1$** for the systems are collected in Table 3.5. An increase in the nonradiative rate with an increase in the polarity of the medium is evident from this data.

Table 3.5 Nonradiative Rate Constants ($k_{nr}/10^9$ s^{-1}) of the Systems in Various Solvents at Room Temperature[a]

	Systems						
Solvents	ANF	DMANF	PANF	PDMANF	4ANF	5ANF	6ANF
Toluene	0.97	0.16	0.56	0.19	0.27	0.20	0.22
Dioxan	0.32	0.15	0.23	0.13	0.20	0.13	0.12
THF	0.28	0.10	0.21	0.15	0.21	0.15	0.13
EtOAc	0.85	0.29	0.39	0.25	0.29	0.27	0.26
ACN[b]	11.04	4.35	9.04	3.64	4.72	4.14	4.51

[a]The values corresponds to the **Em$_1$**. [b]In ACN, the average lifetime values were used to calculate k_{nr}.

The fluorescence quantum yield associated with the **Em$_2$** component of the systems are collected in Table 3.6. It is evident that the dialkylamino systems exhibit the **Em$_2$** fluorescence more prominently compared to the amino systems, **ANF** and **PANF.**

Table 3.6 Fluorescence Quantum yields ($\phi_f/10^{-3}$) of the **Em$_2$** Component of Fluorescence of the Systems at Room Temperature[a]

Solvents	Systems						
	ANF	DMANF	PANF	PDMANF	4ANF	5ANF	6ANF
ACN	-	-	-	-	6.0	3.0	3.0
DMSO	-	-	0.2	4.0	8.0	6.0	3.0
EtOH	0.4	1.0	0.3	3.0	3.0	4.0	2.0

[a]Fluorescence quantum yields in the table were measured from decnvoluted spectra. λ_{exc} = 375 nm. ϕ_f values could not be determined in some cases as the spectrum due to this emission component was not clearly resolvable.

The fluorescence lifetimes associated with the **Em$_2$** component of the systems in different solvents are collected in Table 3.7. A representative decay profile of **Em$_2$** fluorescence of **5ANF** in acetonitrile is shown in Figure 3.10. The emission decay profiles were found to be multi-exponential in nature. The average fluorescence lifetimes of the systems have been found to vary between 270–810 ps (*vide* Table 3.7).
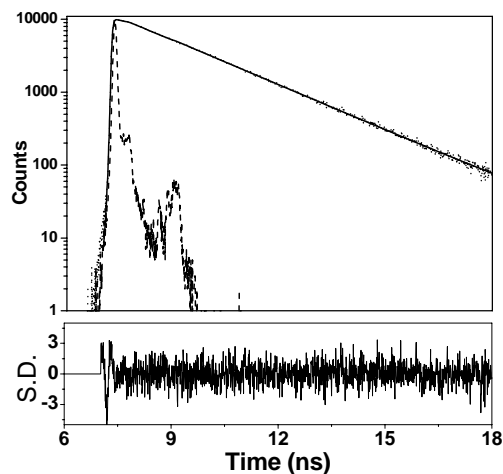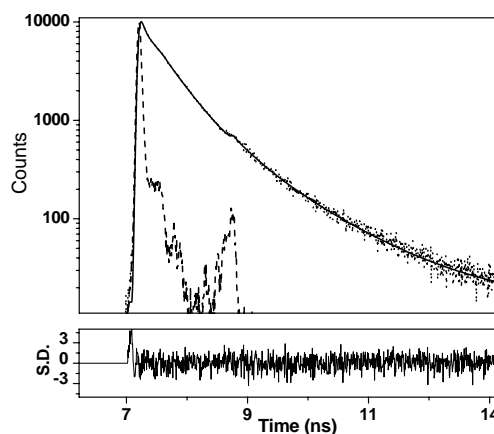
Figure 3.10 Fluorescence decay profile of **5ANF** as monitored at 550 nm in acetonitrile. The experimental decay curve is shown by dotted line and the instrument profile by dashed line. The solid line is the fit to the decay curve. A weighted deviation is also shown at the bottom of the decay curve. λ_{exc} = 375 nm.

Table 3.7 Fluorescence Lifetimes (ps) Corresponding to **Em$_2$** Component at Room Temperature[a]

Solvents	Systems				
	PANF	PDMANF	4ANF	5ANF	6ANF
ACN	-	-	330	325	270
DMSO	-	810	805	660	590

[a]The values represent average lifetime calculated from the preexponential factors and lifetime components of the multi-exponential decay profile. λ_{exc} = 375 nm. The lifetimes could not be determined accurately in few cases as they are found to be shorter than the time resolution of the instrument.

The fluorescence quantum yield and lifetime values corresponding to the highest energy **Em$_3$** emission of the systems in various solvents are collected in

Table 3.8 and Table 3.9 respectively. A representative decay profile of **Em₃** for

ANF in 1,4-dioxane is shown in Figure 3.11.

Table 3.8 Fluorescence Quantum yields ($\phi_f/10^{-3}$) of the **Em₃** Fluorescence at Room Temperature. λ_{exc} = 300 nm

Solvents	Systems						
	ANF	DMANF	PANF	PDMANF	4ANF	5ANF	6ANF
Dioxan	1.0	1.0	9.0	0.6	4.0	4.0	0.6
THF	1.0	2.0	9.0	0.3	5.0	0.5	0.5
EtOAc	2.0	4.0	10.0	0.5	4.0	0.8	0.1
ACN	4.0	4.0	20.0	0.3	5.0	0.3	0.4
DMSO	4.0	3.0	20.0	4.0	3.0	3.0	2.0
ETOH	4.0	3.0	30.0	3.0	4.0	2.0	3.0
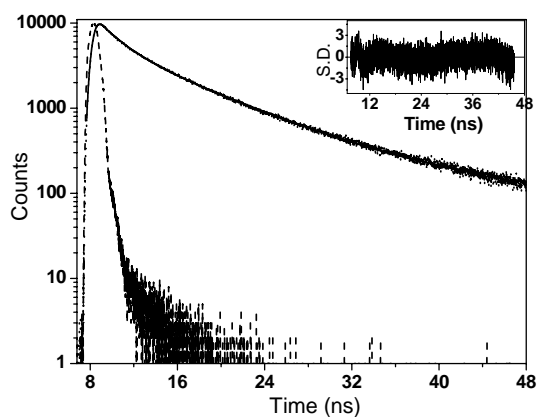
Figure 3.11 Fluorescence decay profile of **ANF** as monitored at 385 nm in 1,4- dioxane. The experimental decay curve is shown by dotted line and the instrument profile by dashed line. The solid line is the fit to the decay curve. Inset shows the weighted deviation. λ_{exc} = 280 nm.

Table 3.9 Fluorescence Lifetimes (τ_f, ns) of **Em$_3$** Fluorescence of the Systems in Different Solvents at Room Temperature.[a]

	Systems						
Solvents	ANF	DMANF	PANF	PDMANF	4ANF	5ANF	6ANF
Dioxane	5.0	3.0	4.8	1.0	1.9	0.8	0.5
THF	3.2	3.6	1.8	0.5	1.7	1.5	0.9
EtOAc	2.6	5.0	1.6	0.2	1.1	0.4	0.1
ACN	2.7	3.0	2.2	0.1	1.48	0.9	0.1
DMSO	3.8	3.5	1.9	0.6	1.1	0.6	0.2

[a]The values represent average lifetime calculated from the preexponential factors and lifetime components of the multi-exponential decay profile. λ_{exc} = 280 nm.

3.5. Theoretical calculation of the Excited State Energies

We have theoretically studied the energetics of the different accessible locally excited states of the systems. These calculations have been carried out on **ANF,** which serves as the reference compound. The hybrid DFT functional B3LYP was used for these calculations. The ground state calculations such as the optimization of the geometry were performed at B3LYP/6-31G* level. Excited state calculations were performed with the time-dependent (TD-DFT) framework at the B3LYP/6-31+G** level in vacuo. In addition to gas phase calculations, the excited state calculations were also performed in different solvents by self-consistent reaction field (SCRF) method and using polarized continuum (PCM)

model at the B3LYP/6-31+G** level. All quantum mechanical calculations were performed using the Gaussian 03 program package.

The excited state calculations were also carried out by semi-empirical ZINDO/S-CI method,[10-13] using configuration interaction by exciting one electron from each of the eight highest occupied orbitals to the eight lowest unoccupied orbitals. Effect of the solvent on the energy states were estimated using Onsager's Formulation.[14] The calculated and experimental excitation energies for the different excited states of **ANF** are collected in Table 3.10. An energy level diagram corresponding to the excitation to different excited states of **ANF** is shown in Figure 3.12. The excitation energy of **ANF** was determined experimentally from the $\lambda_{\max}^{exc}$ of the systems in the respective solvents.

It is evident that the excitation energies for different excited states calculated from TD-DFT and ZINDO/S-CI methods agree reasonably well with the experimentally determined transition energies (*vide* Table 3.10).

Table 3.10 Calculated Excitation Energies of Different Energy States of **ANF**[a]

Methods	Medium			
	Vacuum	Cyclohexane	Toluene	Acetonitrile
TD-DFT	3.07	2.80 (3.19)	2.74 (3.19)	2.54 (3.11)
	4.02	3.94 (3.35)	3.85 [†]	3.59 (3.35)
	4.08	4.09 (4.32)	3.96 (4.30)	3.82 (4.27)
ZIND/S-CI	3.44	3.06	3.01	2.97
	4.16	4.14	4.14	4.14
	4.55	4.41	4.39	4.36

[a]The excitation energy values are expressed in eV unit and quantities in the parenthesis represent the experimentally observed excitation energies of the states. [†]Experimental excitation energy is not reported due to the absence of **Em$_2$** band in this medium.
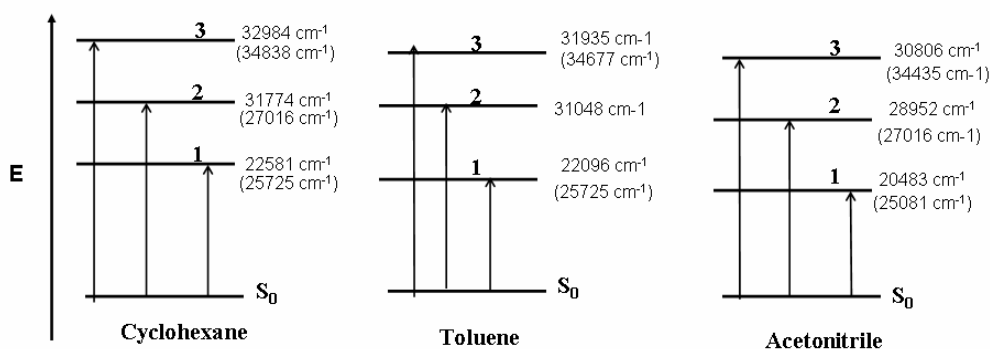
Figure 3.12 Pictorial representation of the energetics of three close-lying energy states of **ANF** in different solvents. Numbers in cm^{-1} represent the TD-DFT calculated transition energies of the respective states; experimentally observed energies have also been shown in the parenthesis.

3.6. Change of Dipole Moment upon Photoexcitation

ANF is reported to undergo drastic change of dipole moment upon photoexcitaion.[4] The change in excited state dipole moment ($\Delta\mu$) for **ANF** is measured to be as high as 25 D by electro-optical measurement.[4] This unusually high $\Delta\mu$ value of **ANF** has motivated us to evaluate the excited dipole moments corresponding to the most polar emitting state of the present systems from the various parameters available to us using a few methods.[15-20]

The ground state dipole moments of the optimized structures of the systems, which are needed for the estimation of excited state dipole moments, have been calculated using semi-empirical AM1 (Austin model 1) calculations. Dipole moments of the most polar excited state of the systems have been calculated from the Stokes shift between the absorption and fluorescence wavenumbers of the systems in different solvents using different methods. Among the different methods employed for this purpose, the first two methods, namely, the popular Lippert-Mataga equation (Eq. 2.2)[15-17] and another one suggested by Ravi et al. (Eq. 2.5),[18] involve the Onsager's cavity radius (a). However, considering the fact that the 'a' is not a well-defined quantity that can be measured accurately, two 'a' independent methods, one suggested by Koti et al. (Eq. 2.6 and Eq. 2.7).[19] and another one by Kawski (Eq. 2.8 and Eq. 2.9)[20] were also employed for the estimation of μ_e.

The ground state dipole moments and the change in dipole moment ($\Delta\mu$) upon photoexcitation of all the systems have been collected in Table 3.11. The $\Delta\mu$ values of the parent system, **ANF** evaluated by all four methods discussed above, are found to be significantly lower compared to the reported $\Delta\mu$ value. It is also

interesting to note that the estimated $\Delta\mu$ values of the dialkylamino systems are much higher for the 'a'- independent methods than those obtained from the 'a'- dependent methods.

Table 3.11 Ground State Dipole Moments (μ_g) and Change in Dipole Moments ($\Delta\mu$) upon Photoexcitation of the Systems

Compounds		$\Delta\mu$			
	μ_g [a]	Method 1[b]	Method 2[c]	Method 3[d]	Method 4[e]
ANF	7.7	12.1	9.6	11.3	12.8
DMANF	8.2	12.2	10.3	20.3	23.2
PANF	7.6	17.7	9.3	19.2	20.1
PDMANF	8.2	19.5	10.0	29.4	31.8
4ANF	7.9	18.9	9.9	26.3	28.6
5ANF	8.4	18.4	9.3	25.1	26.4
6ANF	8.3	18.5	9.5	24.8	26.4

[a] In Debye, from AM1 calculation. Excited dipole moments have been calculated following [b]Eq. 2.2, [c]Eq. 2.5, [d]Eq. 2.6 and Eq. 2.7, [e] Eq. 2.8 and Eq. 2.9. In the cases where applicable, Onsager cavity radius was taken as 7 Å[15].

3.7. Conclusion

Several structurally similar amine-terminated nitrofluorene derivatives have been synthesized and fully characterized by conventional analytical methods and X-ray crystallography. The electronic absorption and fluorescence behavior of the EDA fluorene derivatives in different conventional solvents are found to be rather complex, but quite interesting. The present investigation reveals three different

fluorescence components with the major one having considerable charge transfer in character. The second component, which is weak in intensity and having negligible charge transfer character is observable clearly only in extremely nonpolar and highly polar media, originates from another locally excited state of the systems. A third emission component, weak in intensity, is also observed for the systems. The large energy gap between the first and second excited states in the **ANF** derivatives leads to a decrease in the rate of nonradiative transition between the two states making the rate of the radiative transition from the second excited state possible. The emission from the third excited state appeared unlikely considering the low energy gap between the second and third excited states. It appears that fast internal rotation of the amino or nitro moiety gives rise to this emission.

References

1. Ruthmann, J.; Kovalenko, S. A.; Ernsting, N. P.; Ouw, D. *J. Chem. Phys.* **1998**, *109*, 5466.

2. Belfield, K. D.; Schafer, K. J.; Mourad, W.; Reinhardt, B. A. *J. Org. Chem.* **2000**, *65*, 4475.

3. Maus, M.; Rurack, K. *New. J. Chem.* **2000**, *24*, 677.

4. Baumann, W.; Bischof, H. *J. Mol. Struct.* **1985**, *129*, 125.

5. Catalán, J.; López, V.; Pérez, P.; Martin-Villamil, R.; Rodriguez, J-G. *Liebigs, Ann*. **1995**, 241.

6. Saroja, G.; Pinghu, Z.; Ernsting, N. P.; Leibscher, J. *J. Org. Chem.* **2004**, *69*, 987.

7. Marhevka, V. C.; Ebner, A. N.; Russel, D. S.; Hanna, P. E. *J. Med. Chem.* **1985**, *28*, 18.

8. Belfield, K. D.; Schafer, K. J.; Mourad, W.; Reinhardt, B. A. *J. Org. Chem.* **2000**, *65*, 4475.

9. Saha, S. K.; Dogra, S. K. *J. Mol. Struct.* **1998,** *470*, 301.

10. Ridley, J. E.; Zerner, M. C. *Theo. Chem. Acta* **1973**, *32*, 111.

11. Bacon, A. D.; Zerner, M. C. *Theo. Chem. Acta* **1979**, *21*, 53.

12. Thompson, M. A.; Zerner, M. C. *J. Am. Chem. Soc.* **1991**, *113*, 8210.

13. Hanson, L. K.; Frajer, J.; Thompson, M. A.; Zerner, M. C. *J. Am. Chem. Soc.* **1987**, *109*, 4728.

14. Soujanya, T.; Saroja, G.; Samanta, A. *Chem. Phys. Lett.* **1995**, *236*, 503.

15. Lippert, V. E. *Z. Electrochem.* **1957,** *61*, 962.

16. Mataga, N.; Kaifu, Y.; Koizumi, M. *Bull. Chem. Soc. Jpn.* **1956**, *29*, 465.

17. Mataga, N. *Bull. Chem. Soc. Jpn.* **1963**, *36*, 654.

18. Ravi, M.; Samanta, A.; Radhakrishnan, T.P. *J. Phys. Chem.* **1994**, *98*, 9133.

19. Koti, A. S. R.; Bhattacharjee, B.; Haram, N. S.; Das, R.; Periasamy, N.; Sonawane, N. D.; Rangnekar, D.W. *J. Photochem. Photobiol., A* **2000**, *137*, 115.

20. Kawski, A. *Z. Naturforsch.* **1999,** *54a,* 379.

.

Chapter 4

Photophysical Behavior of Aminomethoxyflavone Derivatives

This chapter describes the synthesis, characterization and photophysical behavior of several structurally similar aminomethoxyflavone derivatives. Copper-mediated Ullmann-type C-N bond formation reaction protocol has been employed for the synthesis of the derivatives. The Systems have been characterized by conventional analytical and single crystal X-ray diffraction techniques. Photophysical behavior of the systems has been studied as a function of the polarity of the medium using steady state and time-resolved spectroscopic techniques. Theoretical calculations have also been carried out with a view to comprehend the experimental findings.

4.1. Introduction

The flavones and its derivatives are widely known for their anti-oxidant property.[1-3] 3-hydroxyflavone and its derivatives in particular have received considerable attention of the photophysicists ever since Sengupta and Kasha reported dual fluorescence of 3-hydroxy flavone.[4-12] A majority of the studies are focused on the excited state intramolecular proton transfer (ESIPT) reaction in this system, which is responsible for the blue and green fluorescence of 3-HF originating from the 'normal' and 'tautomer' forms of the molecule. Specifically, the influence of extraneous factors such as the polarity, viscosity and hydrogen bond donating ability of the solvent and temperature on the dynamics of ESIPT

process and its consequence on the steady state fluorescence response of the molecule have been an area of intense research.[6-11] Several studies also focused on exploring the potential applications of these systems.[13-17] These include estimation of the polarity of various micro environments in organized systems,[13] determination of the depth and potential of a membrane,[14] sensing micro-phase transitions,[15] sensing metal ions [16] and investigation of anti-HIV activities.[17] However, except for a few studies,[12] investigation of the charge/electron transfer phenomenon in flavone derivatives containing electron donor and acceptor groups has still remained largely unexplored.

In order to study the charge/electron transfer process in flavones, we have synthesized a series of amine terminated methoxyflavone derivatives (Chart 4.1), where different amino groups serve as donor and carbonyl group of the flavone moiety serves as acceptor. The choice of the present systems has been governed by the fact that aromatic carbonyls and nitrogen heterocycles possess both n-π* and π-π* states,[18-21] and introduction of charge transfer character into these systems by incorporating an electron donor is expected to influence the fluorescence behavior of these systems considerably. We have used the 3-methoxy derivative of flavone instead of the 3-hydroxy derivative not only to avoid complications from the ESIPT process but more importantly to focus mainly on the change in the fluorescence behavior of the systems due to the charge transfer process. The very idea to study several systems with different amino moieties is to examine the influence of the nature of the amino group, if any, on the fluorescence response of the systems.
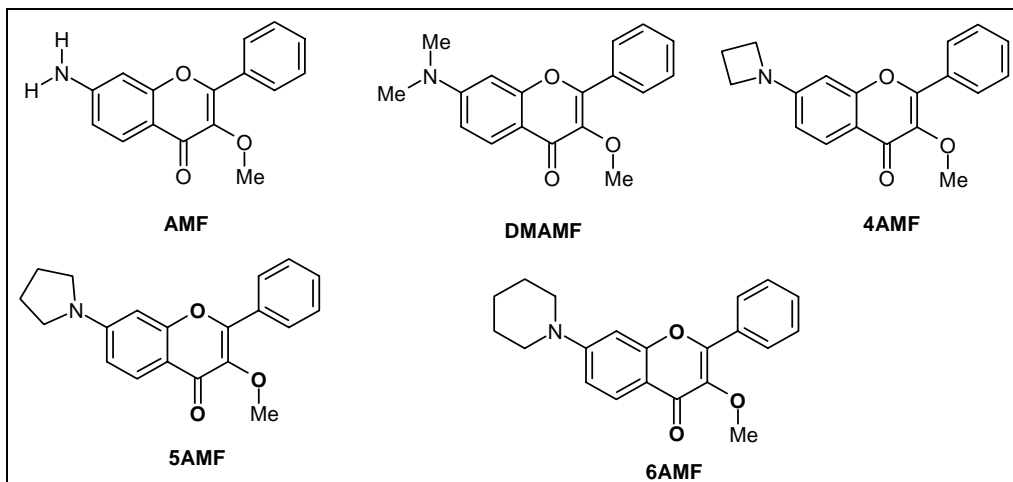
Chart 4.1

The fluorescence properties of the systems, which are found to be strongly dependent on the polarity of the solvent, have been interpreted taking into consideration the nature of the two excited states involved in the emission process. The results seem to suggest that a change in the nature of the state from n-π* to π-π* with increase in the polarity of the medium. Excited state calculations of the frontier orbitals, based on the TD-DFT method, have been carried out to correlate the experimental findings.

4.2. Synthesis of the systems

The methoxyflavone derivatives were synthesized in a multi-step process. First, 7-iodo-3-methoxy-2-phenyl-chromen-4-one (IMF) was synthesized starting from 3-iodo phenol following a procedure published elsewhere (Scheme 4.1).[22-23] The amino containing derivatives were synthesized from IMF following a method based on copper-mediated Ullmann-type reaction (Scheme 4.2). IMF was treated

with appropriate amines, using cuprous iodide and cesium acetate maintaining the reaction temperature 10 °C below the boiling point of the respective amines and stirring the reaction mixture for 24-48 h under nitrogen atmosphere. The acyclic analogues, **AMF**, **DMAMF** and cyclic analogues, **4AMF, 5AMF** and **6AMF** were obtained following this method.

4.2.1. Synthesis of IMF

IMF was synthesized by multi-step process (Scheme 4.1).
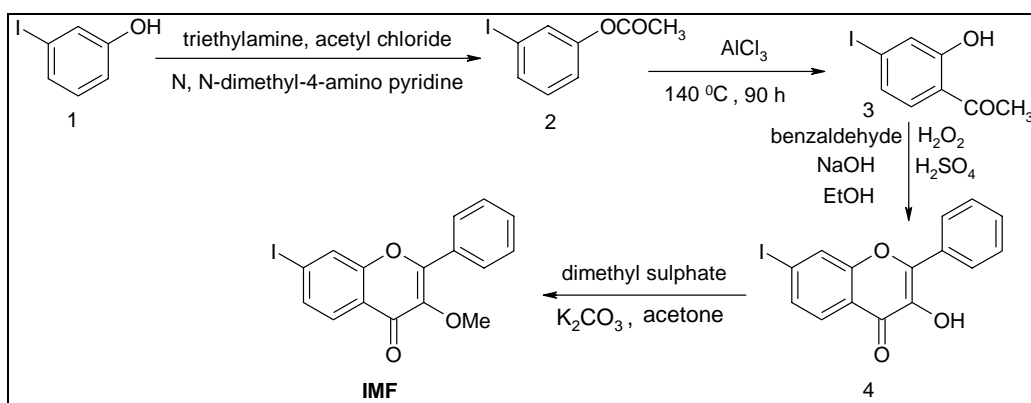
Scheme 4.1 Synthetic route to **IMF**.

Step 1: ***3-iodo-phenyl acetate (2)***. To a stirring solution of 3-iodophenol (26.06 g, 118 mmol), triethylamine (18 mL, 129 mmol) and N,N-dimethyl-4-amino-pyridine (0.62 g, 5 mmol) in dichloromethane (250 mL) under nitrogen was added acetyl chloride (9 mL, 127 mmol) drop-wise over 5 min. The reaction was allowed to stir for 2 h and then washed with water (200 mL) and saturated sodium bicarbonate solution (200 mL). The organic layer was then dried (Na_2SO_4) and

concentrated in vacuo to give 3-iodo-phenyl acetate (30.20 g, 97%). The compound was characterized from the following analytical data.

^{1}H NMR (400MHz, CDCl$_3$): δ 2.29 (s, 3 H), 7.06-7.12 (m, 2 H), 7.43-7.46 (m, 1 H), 7.55-7.58 (m, 1 H).

Step 2: ***2-hydroxy-4-iodo-acetophenone (3).*** To a stirring solution of 3-iodo-phenyl acetate (32.20 g, 123 mmol) in chlorobenzene (250 mL) under nitrogen was added aluminium chloride (31.00 g, 232 mmol). The reaction mixture was heated to 140 ^{0}C for 90 h then allowed to cool. The reaction mixture was poured on to ice/water and then filtered and the residue washed with dichloromethane (DCM). The filtrate was then extracted with DCM and the combined organic layers extracted with 10 % KOH solution (3 × 100 mL). The combined aqueous layer were then acidified with 6 N HCl and extracted with DCM (3 × 75 mL). This organic layer was then dried ((Na$_2$ SO$_4$) and concentrated in vacuo to give 2-hydroxy-4-iodo-acetophenone (22.30 g, 69 %). The compound was characterized from the following analytical data.

^{1}H NMR (400MHz, CDCl$_3$): δ 2.60 (s, 3 H), 7.26-7.28 (m, 2 H), 7.42 (s, 1 H), 12.26 (s, 1 H).

Step 3: ***3-hydroxy-7-iodo-2-phenyl-chromen-4-one (4).*** A solution of NaOH (5 g, 0.25 mol) in 7.50 cc water was added with vigorous stirring to a solution of 2-hydroxy-4-iodo-acetophenone (9.694 g, 0.027 mol) and benzaldehyde (4.32 g, 0.04 mol) in 50 cc ethanol. A heavy greenish yellow precipitate formed immediately. Gradually the mixture became warm and more fluid, eventually setting (after 10 min stirring) to a firm orange paste that was allowed to stand over

night. The orange paste was dissolved in a solution of NaOH (2.50 g), 12.50 cc water and 250 cc ethanol. After cooling to 15 ^{0}C, 40 cc of 15 % H_2O_2 was added slowly with vigorous stirring. An orange-red precipitate formed immediately and temperature rose to 30 ^{0}C. The reaction mixture was stirred for a further 15 min, neutralized with dilute H_2SO_4 and poured into 500 cc of water. Upon standing for 1 h, the orange-yellow solid was filtered by suction, washed with a little ice cold methanol and recrystallized from methanol to yield pale yellow needles (5 g, 50.87 %). The compound was characterized from the following analytical data.

^{1}H NMR (400MHz, CDCl$_3$): δ 7.52-7.54 (m, 3 H), 7.75 (d, *J* = 8.04 Hz, 1 H), 7.93 (d, *J* = 8.01 Hz, 1 H), 8.05 (bs, 1 H), 8.22-8.23 (m, 2 H), 12.30 (s, 1 H).

Step 4: ***7-iodo-3-methoxy-2-phenyl-chromen-4-one (IMF).*** 3-hydroxy-7-iodo-2-phenyl-chromen-4-one (3.276 g, 0.009 mol) was dissolved in 30 cc of acetone and transferred to a flask containing K_2CO_3 (2.50 g, 0.018 mol). Dimethyl sulphate (2.27 g, 0.018 mol) was added and the mixture was heated under reflux for 5 h. Excess dilute ammonia was added to destroy any remaining dimethyl sulphate before removing the acetone on a rotary evaporator. The reddish brown solid formed was filtered, washed with water until the filtrate was neutral and recrystallized from methanol to yield reddish brown solid of IMF (2 g, 58.79 %). The main starting material IMF was characterized by following analytical data.

^{1}H NMR (400MHz, CDCl$_3$): δ 8.06-8.08 (m, 2 H), 7.98 (d, *J* = 8.04 Hz, 1 H), 7.94 (s, 1 H), 7.73 (d, *J* = 8.14 Hz, 1 H), 7.53-7.51 (m, 3 H), 3.89 (s, 3 H), 12.32 (s, 1 H). Elemental analysis: $C_{16}H_{11}O_3I$: calcd.: C 50.82, H 2.93, O 12.69: found: C 50.79, H 2.98%. LCMS: m/z 379 (M+H$^+$).

4.2.2. Synthesis of acyclic analogues: general procedure

The acyclic amino derivatives of methoxyflavone were synthesized by copper-mediated Ullmann-type C-N bond formation reaction (Scheme 4.2).

To a stirred mixture of IMF (100 mg, 0.264 mmol), cesium acetate (120 mg, 0.62 mmol) and CuI (5 mol %) in 1.5 ml dry DMSO, dry NH_3 gas (for the amine derivative or Me_2NH (for dimethylamine derivative) was passed over KOH for 15 minutes. The dry NH_3 or Me_2NH was generated by adding KOH to an aqueous solution of the respective amines and stirring it for 15 minutes. The reaction mixture was kept for stirring at room temperature for 24 hours under sealed condition after purging N_2 and subsequently heated for another six hours at 30 ºC. The resulting solution was taken up in ethylacetate and washed with brine solution. The organic layer was dried over anhydrous Na_2SO_4, filtered, and concentrated. The crude product was then purified by column chromatography on basic alumina (EtOAc/hexane = 20/80) to give the brown materials.
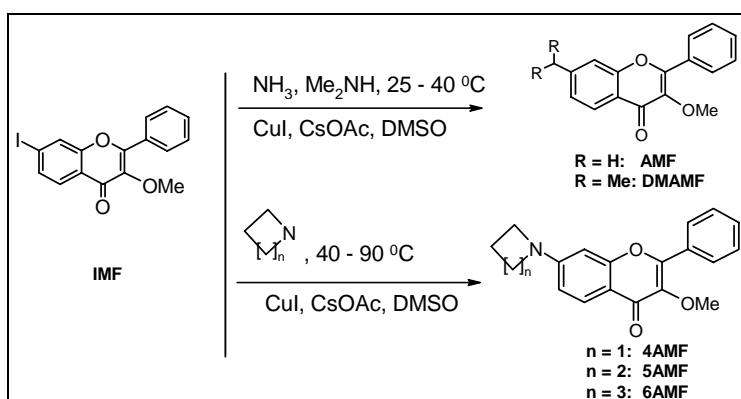
Scheme 4.2 C-N bond formation reaction by Cu-catalyzed amination of **IMF**.

The acyclic analogues, **AMF** and **DMAMF** were characterized by following analytical data.

AMF

^{1}H NMR (400MHz, CDCl$_3$): δ 8.03-8.05 (m, 3 H), 7.48-7.50 (m, 3 H), 6.67-6.69 (m, 1 H), 6.63 (s, 1 H), 4.26 (s, 2 H), 3.87 (s, 3 H). Elemental analysis: C$_{16}$H$_{13}$NO$_3$: calcd.: C 71.90, H 4.90, N 5.24: found: C 71.83, H 4.97, N 5.21 %. LCMS: m/z 268 (M+H$^+$).

DMAMF

^{1}H NMR (400MHz, CDCl$_3$): δ 8.06-8.09 (m, 3 H), 7.48-7.50 (m, 3 H), 6.77(d, *J* = 8.0 Hz, 1 H), 6.31 (s, 1 H), 3.87 (s, 3 H), 3.10 (s, 6 H). Elemental analysis: C$_{18}$H$_{17}$NO$_3$: calcd.: C 73.20, H 5.80, N 4.74: found: C 73.18, H 5.87, N 4.68 %. LCMS: m/z 296 (M+H$^+$).

4.2.3. Synthesis of cyclic analogues: general procedure

The cyclic amino derivatives of methoxyflavone were also synthesized by copper-mediated Ullmann type C-N bond formation (Scheme 4.2).

To a solution 7-iodo-3-methoxy-2-phenyl-chromen-4-one (IMF) (100 mg, 0.264 mmol) in dry DMSO (1.5 ml) the corresponding amine (1.2 mmol) and cesium acetate (120 mg, 0.62 mmol), CuI (5 mol%) were added and the solution was heated to 40-90°C (according to the boiling point of the corresponding amines) under N$_2$ atmosphere for 24 h, the color changed to reddish brown. After being cooled to room temperature, the reaction was quenched with water and extracted with EtOAc (50 mL) and organic layer was washed with brine solution

(100 mL). The organic layer was dried over anhydrous Na_2SO_4 and concentrated through evaporation. The product was purified through column chromatography (basic alumina, EtOAc/hexane = 30/70) as a brown solid.

The cyclic analogues, **4AMF**, **5AMF**, **6AMF** were confirmed by following analytical data.

4AMF

^{1}H NMR (400MHz, CDCl$_3$): δ 8.05-8.08 (m, 3 H), 7.48-7.50 (m, 3 H), 6.43-6.46 (m, 1 H), 6.26 (s, 1 H), 4.02 (t, J = 5.4 Hz, 4 H), 3.87 (s, 3 H), 2.45-2.48 (m, 2 H). Elemental analysis: $C_{19}H_{17}NO_3$: calcd.: C 74.25, H 5.58, N 4.56: found: C 74.19, H 5.61, N 4.53 %. LCMS: m/z 308 (M+H$^+$).

5AMF

^{1}H NMR (400MHz, CDCl$_3$): δ 8.05-8.09 (m, 3 H), 7.48-7.50 (m, 3 H), 6.63 (d, J = 8.0 Hz, 1 H), 6.41 (s, 1 H), 3.87 (s, 3 H), 3.40-3.42 (m, 4 H), 2.06-2.07 (m, 4 H).Elemental analysis: $C_{20}H_{19}NO_3$: calcd.: C 74.75, H 5.96, N 4.36: found: C 74.71, H 6.04, N 4.29 %. LCMS: m/z 322 (M+H$^+$).

6AMF

^{1}H NMR (400MHz, CDCl$_3$): δ 8.05-8.08 (m, 3 H), 7.48-7.51 (m, 3 H), 6.95-6.97 (m, 1 H), 6.74 (s, 1 H), 3.87 (s, 3 H), 3.39-3.40 (m, 4 H), 1.68-1.69 (m, 4 H), 1.63-1.64 (m, 2 H). Elemental analysis: $C_{21}H_{21}NO_3$: calcd.: C 74.20, H 6.31, N 4.18: found: C 74.16, H 6.38, N 4.12 %. LCMS: m/z 336 (M+H$^+$).

4.3. X-ray crystallographic measurements

Among the aminomethoxyflavone derivatives, good single crystals suitable for X-ray diffraction studies could be obtained for **4AMF** and **5AMF** (from chloroform). ORTEP diagrams of the systems are shown in Figure 4.1. The essential crystallographic data are presented in Table 4.1.
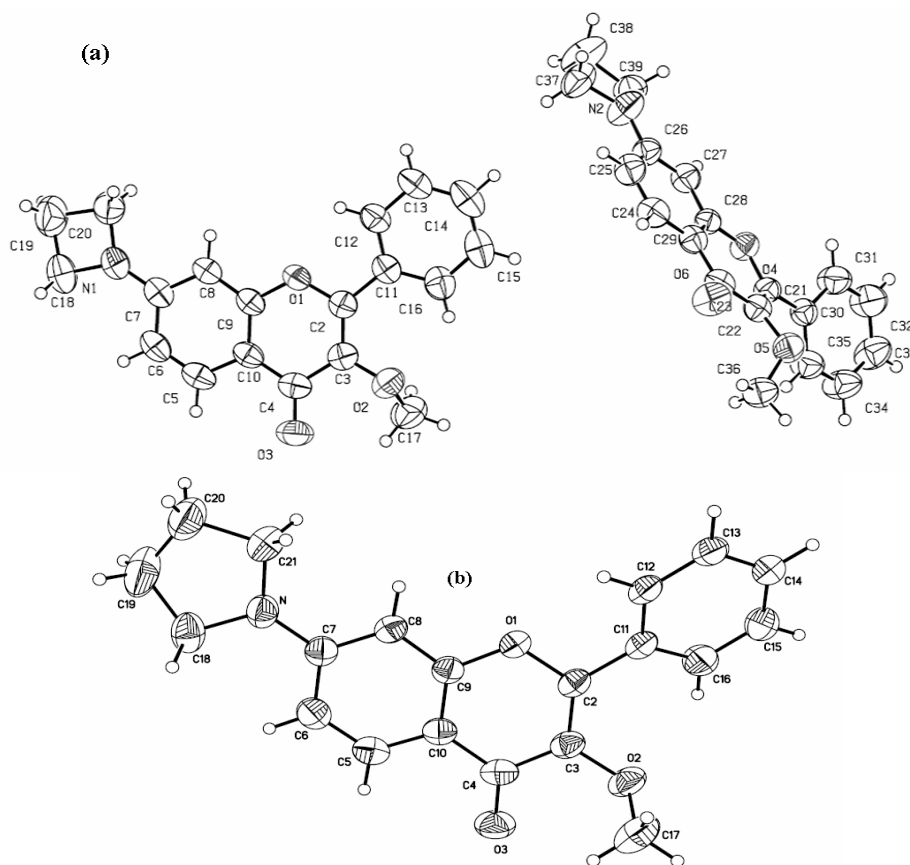
Figure 4.1 (a) ORTEP diagram of **4AMF** with atoms represented by thermal ellipsoids at 35 % probability level, N(1)-C(7) bond length = 1.3459 (3) Å. (b) ORTEP diagram of **5AMF** with atoms represented by thermal ellipsoids at 35 % probability level, N-C(7) bond length = 1.3676 (2) Å.

Table 4.1 Data Collections and Structure Refinement Details of Crystal Structures of **4AMF** and **5AMF**

	4AMF	5AMF
Formula	$C_{19} H_{17} NO_3$	$C_{20} H_{19} NO_3$
Formula wt	307.335	321.36
Crystal system	monoclinic	monoclinic
Space group	P2(1)/c	C2/c
a (Å)	14.899 (4)	13.667 (5)
b (Å)	12.360 (3)	7.954 (3)
c (Å)	17.557(4)	30.913 (12)
α (°)	90	90
β (°)	104.626 (4)	97.345 (6)
γ (°)	90	90
V (Å^3)	3131.9 (13)	3332 (2)
Z	4	8
F(000)	1296	1360
ρ_{calcd} (g cm^{-3})	1.304	1.281
μ (mm^{-1})	0.088	0.086
Temperature (K)	273 (2)	571 (2)
Crystal size	0.21 x0.15 x0.07	0.21 x0.10 x0.05
Color, habit	Brown, needle	Brown, rect.
Absorption correction	Multi scan	Multi scan
T_{min}, T_{max}	0.9938,0.9817	0.9957,0.9821
Total no. of reflections	31201	8253
No. of unique reflections	6201	3251
No. of obs. reflections	6201	3251
θ_{max} (°)	26.10	25.99
No. of parameters	417	218
R indices (obs. data): *R*, R_w	0.0573,0.1271	0.0592,0.1424
R indices (all data): *R*, R_w	0.1063,0.1483	0.0973,0.1629
GOF	1.025	1.019
$\Delta\rho_{max}$, $\Delta\rho_{min}$ (e/Å^3)	0.256, -0.177	0.228, -0.176

One of the structural parameters considered quite useful from the point of view of photophysics of the systems is the dihedral angle between the planes containing amino functionality and flavone moiety. The dihedral angle ($\angle$C21NC7C6) in **5AMF** is found to be 179.01^0 and that ($\angle$C20N1C7C6) in **4AMF** is 173.10^0.

4.4. Photophysical behavior of the systems

4.4.1. Absorption behavior

The UV-vis absorption spectral data of the systems in various solvents of different polarity have been collected in Table 4.2 and representative spectra for **AMF** and **5AMF** in two selected solvents are shown in Figure 4.2.

Figure 4.2 Absorption spectra of (a) **AMF** and (b) **5AMF** derivatives in 1,4-dioxane (—) and acetonitrile (**…**) at room temperature.

Table 4.2 Absorption and Emission Spectral Data of the Systems in Various Solvents at Room Temperature

Solvents[a]	Systems									
	AMF		DMAMF		4AMF		5AMF		6AMF	
	λ^{abs}_{max}	λ^{emis}_{max}	λ^{abs}_{max}	λ^{emis}_{max}	λ^{abs}_{max}	λ^{emis}_{max}	λ^{abs}_{max}	λ^{emis}_{max}	λ^{abs}_{max}	λ^{emis}_{max}
Toluene (33.9)	324	410	355	435	348	443	360	440	350	442
Dioxane (36.0)	324	423	355	450	348	455	360	453	351	455
THF (37.4)	330	442	356	468	349	475	361	472	353	472
EtOAc (38.1)	335	442	353	470	348	476	359	472	349	472
Acetone (42.1)	339	457	359	492	352	497	362	495	355	495
ACN (45.6)	340	465	359	502	353	510	365	505	356	510
DMSO (45.1)	350	495	366	525	362	528	371	527	363	526
EtOH (51.9)	352	495	369	520	365	525	375	522	366	525

[a]Quantities in the parenthesis indicate the $E_T(30)$ values of the solvents. $\lambda_{exc} = 350$ nm.

The parent amino compound, **AMF**, shows a broad band with maximum appearing at 324 nm in toluene. The band maximum shifts to 352 nm in ethanol (Figure 4.2 (a)). The solvent dependence of the absorption data of the systems seems to indicate the dipolar nature of the molecule. The absorption maxima for the dialkylamino systems appear at longer wavelengths compared to the parent amino system in any given solvent (Figure 4.2 (b)). This is a reflection of the inductive influence of the alkyl groups, which enhances the extent of charge

separation in the system. Among the various dialkylamino systems, the inductive influence appears to be same and yet, the $\lambda_{\max}^{abs}$ values vary to some extent (348-360 nm in toluene, 353-365 nm in acetonitrile and 365-375 nm in ethanol). This fact implies that the donor nitrogen atom of the systems is not coplanar with the flavone moiety. Instead, the dihedral angle formed by the amine functionality and the flavone moiety is different from system to system.

A closer look at the $\lambda_{\max}^{abs}$ data of the systems reveals that **5AMF** exhibits the most red-shifted absorption band. This implies that **5AMF** is the most dipolar compound in this series. This behavior of **5AMF** is consistent with the calculated (B3LYP/6-31G*) dipole moment value (5.94 D) of the system (*vide* section 4.5), which is found to be highest among the series. The crystal structure data of the systems is also consistent with the findings.

4.4.2. Fluorescence spectral behavior

Fluorescence spectra of the systems were recorded in various solvents of different polarity. The wavelengths corresponding to the fluorescence peak positions are collected in Table 4.2 and a few representative spectra are shown in Figure 4.3.
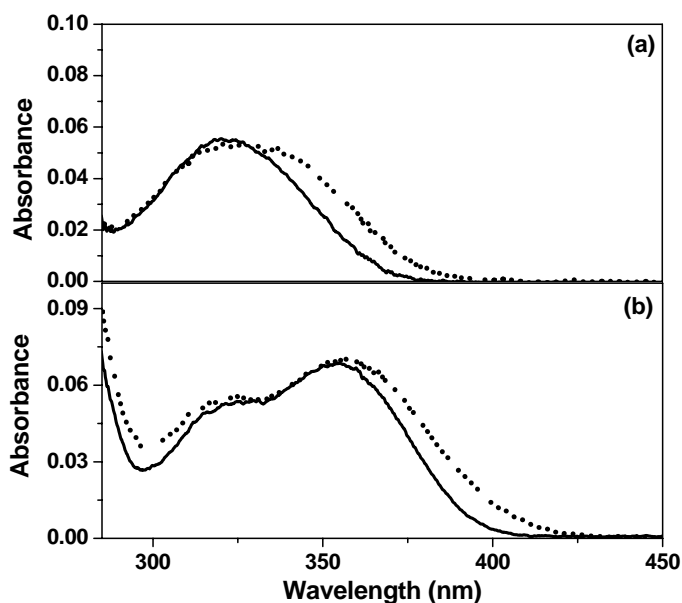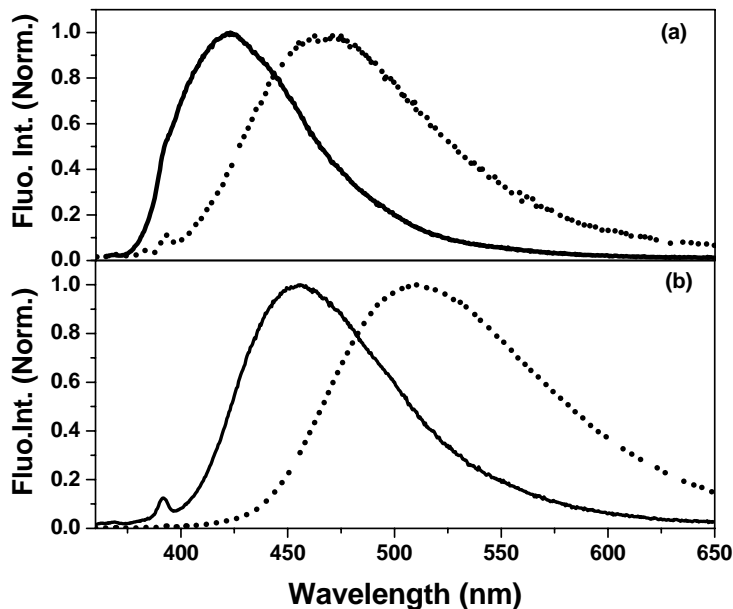
Figure 4.3 Fluorescence spectra of (a) **AMF** and (b) **5AMF** derivatives in 1,4-dioxane (——) and acetonitrile (**...**) at room temperature. λ_{exc} = 350 nm.

An increase in the polarity of the medium results in much more pronounced Stokes shift of the fluorescence maximum compared to the absorption. This implies that the polarity of the medium affects the excited state of the system in much more pronounced way than the ground state. This means that the excited (or emitting) state is more polar than the ground state. For example, in case of **DMAMF**, on changing the solvent from toluene to acetonitrile the absorption maximum shifts by 5 nm, whereas the emission maximum shifts by 67 nm (*vide* Table 4.2). The effect of inductive influence of the different dialkylamino systems is also observable in the emission profile of the derivatives. In any solvent,

fluorescence maxima of the dialkylamino systems appear at much longer wavelength region compared to the parent amino analogue (*vide* Table 4.2).

4.4.3. Fluorescence quantum yield

Fluorescence quantum yields (ϕ_f) of the systems measured in a series of solvents of different polarity are collected in Table 4.3. The variation of the ϕ_f values of the systems with the polarity of the medium is highlighted in Figure 4.4.

Table 4.3 Fluorescence Quantum Yields[a] ($\phi_f/10^{-3}$) of the Systems at Room Temperature

Solvents[b]	Systems (ϕ_f)				
	AMF	DMAMF	4AMF	5AMF	6AMF
Toluene(33.9)	0.5	4.0	4.0	4.0	4.0
Dioxane(36.0)	0.5	6.0	6.0	6.0	7.0
THF(37.4)	0.6	19.0	15.0	20.0	24.0
EtOAc(38.1)	1.0	20.0	18.0	26.0	28.0
Acetone(42.1)	2.0	61.0	55.0	73.0	72.0
ACN(45.6)	20.0	134.0	151.0	173.0	181.0
DMSO(45.1)	70.0	180.0	190.0	200.0	210.0
EtOH(51.9)	150.0	210.0	220.0	210.0	230.0

[a] $\pm$ 10%. [b] Quantities in the parenthesis indicate the $E_T(30)$ values of the solvents. λ_{exc} = 350 nm.
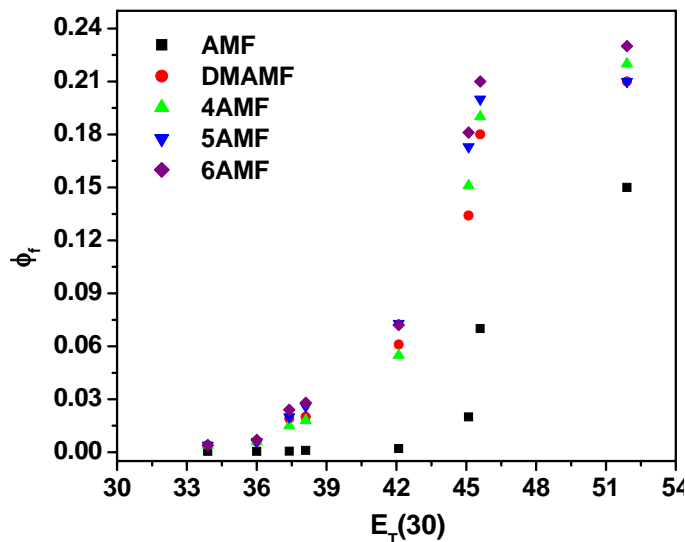
Figure 4.4 Influence of the polarity of the medium on the fluorescence quantum yields of the systems. Solvents used here are toluene, 1,4-dioxane, THF, EtOAc, acetone, ACN, DMSO and EtOH with E_T (30) values 33.9, 36.0, 37.4, 38.1, 42.1, 45.6, 45.1 and 51.9 respectively. $\lambda_{exc} = 350$ nm.

In a given solvent, the dialkylamino analogues are found to be more fluorescent compared to the parent system, **AMF**. Quantum yields of all the systems increase with increase in the polarity of the solvents. In fact, while changing the solvent from toluene to dimethyl sulfoxide (DMSO), a 140-fold enhancement of the quantum yield value of **AMF** is observed, whereas the other systems show nearly 50-fold enhancement of the quantum yields. For systems comprising electron donor and acceptor groups in conjugation, the fluorescence efficiency of the systems commonly decreases with an increase in the polarity of the medium.[24,25] This is because the lowest (emitting) state in these systems is of intramolecular charge transfer in nature, which gets stabilized in polar media. As

a consequence, the energy gap between the emissive state and ground state decreases with increase in the polarity of the media favoring the nonradiative transition to the latter state. Hence, the present observation of the enhancement of quantum yields of the system with increase in the polarity of the media is quite interesting.

4.4.4. Fluorescence decay behavior

The fluorescence decay behavior of the systems has been studied in several solvents of different polarity. The decay parameters of the systems have been presented in Table 4.4 and a representative decay profile of **DMAMF** is shown in Figure 4.5.

Figure 4.5 Fluorescence decay curves for **DMAMF** derivative in (a) acetonitrile and (b) 1,4 –dioxane . Solutions were excited at 374 nm and emission was monitored at emission maximum. The solid lines represent 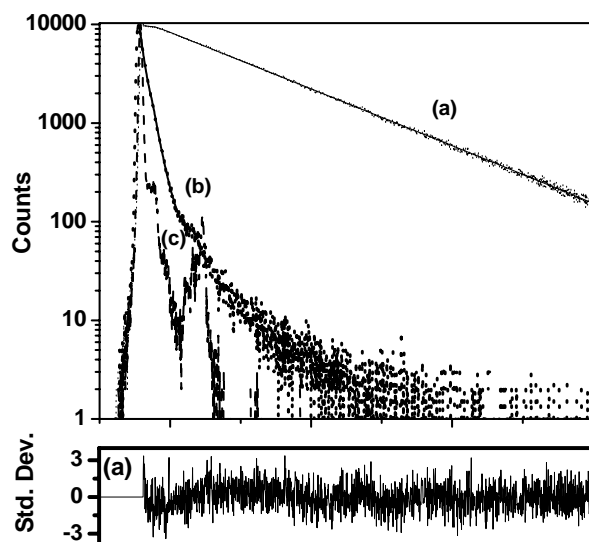the best fit to the data. The instrumental response function (lamp profile) is also shown in (c). The weighted deviation is also shown below the decay curves.

Table 4.4 Fluorescence Decay Parameters[a] of the Systems in Various Solvents at Room Temperature

Solvents	Systems									
	AMF		DMAMF		4AMF		5AMF		6AMF	
	τ_1, τ_2	τ_{avg}	τ_1, τ_2	τ_{avg}	τ_1, τ_2	τ_{avg}	τ_1, τ_2	τ_{avg}	τ_1, τ_2	τ_{avg}
Toluene	910 (0.05), 67 (0.95)	110	60 (0.64), 173 (0.36)	100	132 (0.76), 390 (0.24)	185	92 (0.83), 230 (0.17)	115	98 (0.75), 215 (0.25)	125
Dioxane	50 (0.85), 357 (0.15)	100	110 (0.68), 246 (0.32)	155	224 (0.96), 1120 (0.04)	265	95 (0.49), 236 (0.51)	170	250 (0.54), 105 (0.46)	185
THF	95 (0.96), 587 (0.04)	115	257 (0.73), 545 (0.27)	335	365 (0.48), 805 (0.52)	605	166 (0.34), 463 (0.66)	365	110 (0.27), 450 (0.73)	360
EtOAc	103 (0.85), 485 (0.15)	160	270 (0.46), 471 (0.54)	380	157 (0.41), 1400 (0.59)	890	292 (0.45), 580 (0.55)	450	315 (0.38), 600 (0.62)	490
Acetone	70 (0.38), 272 (0.62)	195	1390		1890		1650		1790	
ACN	365 (0.91), 865 (0.09)	745	3030		3540		3520		3630	
DMSO	1210		3370		3580		3450		3880	
EtOH	2270		3330		3250		3150		3170	

[a]The fluorescence decays were monitored at the respective fluorescence peak maxima of the compounds. Biexponential fitting was resorted when single exponential fitting was found unsatisfactory. The quantities in the parenthesis indicate the relative weight of each component. The lifetimes are expressed in ps. λ_{exc} = 375 nm.

The fluorescence decay behavior can be summarized as follows. In less polar media, all the systems show a biexponential decay behavior, whereas in highly polar solvent a single exponential decay is observed. The effect of polarity on the fluorescence lifetimes of the system is very similar to that observed for the fluorescence quantum yields. The lifetime value (τ_f) for all the derivatives increases with increase in the polarity of the medium.

4.4.5. Radiative and nonradiative rate constants

The radiative (k_r) and nonradiative (k_{nr}) rate constants of the systems in different solvents, estimated from the measured values of ϕ_f and τ_f using $k_r = \phi_f/\tau_f$ and $k_{nr} = (1-\phi_f)/\tau_f$, are collected in Table 4.5 and Table 4.6 respectively. In case of multi-exponential decay profiles, the average lifetime values were used to calculate k_r and k_{nr}. The variation of the nonradiative rate constants with the polarity of the media is also shown in Figure 4.6.

Table 4.5 Radiative ($k_f/10^6$ s^{-1}) Rate Constants of the Systems in Various Solvents at Room Temperature

	AMF	DMAMF	4AMF	5AMF	6AMF
Toluene	4.5	40.0	21.6	34.7	32.0
Dioxane	5.1	38.7	22.6	35.3	37.8
THF	5.3	56.7	24.8	54.8	66.7
EtOAc	6.2	52.6	20.2	57.9	67.0
Acetone	10.2	43.9	29.1	44.2	40.2
ACN	26.9	44.2	42.4	49.1	49.9
DMSO	57.9	63.4	53.1	58.0	54.1
EtOH	66.1	63.1	67.7	66.7	72.5

Table 4.6 Nonradiative ($k_{nr}/10^9$ s^{-1}) Rate Constants for the Systems in Various Solvents at Room Temperature

	AMF	DMAMF	4AMF	5AMF	6AMF
Toluene	9.1	9.96	5.38	8.66	7.97
Dioxane	10.2	6.41	3.75	5.85	5.37
THF	8.8	2.93	1.63	2.70	2.71
EtOAc	6.2	2.59	1.11	2.17	1.98
Acetone	5.1	0.67	0.50	0.56	0.52
ACN	1.3	0.28	0.24	0.23	0.22
DMSO	0.8	0.24	0.23	0.23	0.20
EtOH	0.4	0.24	0.24	0.25	0.24
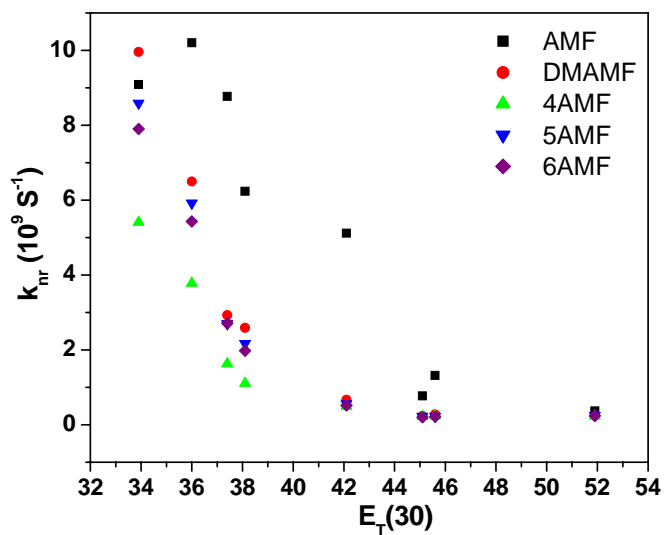
Figure 4.6 Influence of the polarity of the medium on the nonradiative rate constants of the systems. Solvents used here are toluene, 1,4-dioxane, THF, EtOAc, acetone, ACN, DMSO and EtOH with E_T (30) values 33.9, 36.0, 37.4, 38.1, 42.1, 45.6, 45.1 and 51.9 respectively. λ_{exc} = 350 nm.

As can be seen from Table 4.5, the radiative rate constants steadily increase with the increase in the polarity of the medium for all the systems. This increase is however most prominent in the case of **AMF**. For example, **AMF** shows ~13 times increase in the k_f value upon changing the solvent from toluene to DMSO. Naturally, the nonradiative rate constants for all the systems are also found to be higher in nonpolar media compared to those in polar media. For example, **AMF** shows 12 times decrease in the nonradiative rate constant value upon changing the solvent from toluene to DMSO (*vide* Table 4.6). A major change in the radiative and nonradiative rate constants of the systems upon changing the solvent from a nonpolar to a polar one can be accounted for by considering a change in the nature of the emitting state with change in solvent. In the present case, the results imply a more allowed state contributing to the emission process in polar media.

4.4.6. Triplet state study

The results presented in the previous section suggest a change in the nonradiative rate constants of the systems with the change of polarity of the medium (*vide* Table 4.6). In order to find out whether an increase/decrease in the k_{nr} value of the systems is associated with a corresponding increase/decrease of the triplet yield of the systems, we have investigated the triplet state of **AMF** as a function of the polarity of the medium using time-resolved transient absorption technique. Laser flash photolysis ($\lambda_{exc} = 355$ nm) of the **AMF** derivative shows a broad transient absorption band in the 400-550 nm region in both the solvents. That this absorption is due to triplet-triplet transition is evident from the facts that (i) bubbling of O_2 or air leads to the disappearance/diminishing intensity of the

band and (ii) long lifetime (8 µs in toluene and 12 µs in acetonitrile) of the transient. That this transition is characteristic of the triplet state of the system is further supported by the literature data on a similar derivative.[26] While the fluorescence quantum yield of **AMF** in toluene is lower than that in acetonitrile by a factor of 40, we find that the end-of-pulse absorption change, $(\Delta OD)_0$ values for optically matched solutions of **AMF** in two solvents that differ widely in polarity are nearly identical (Figure 4.7).
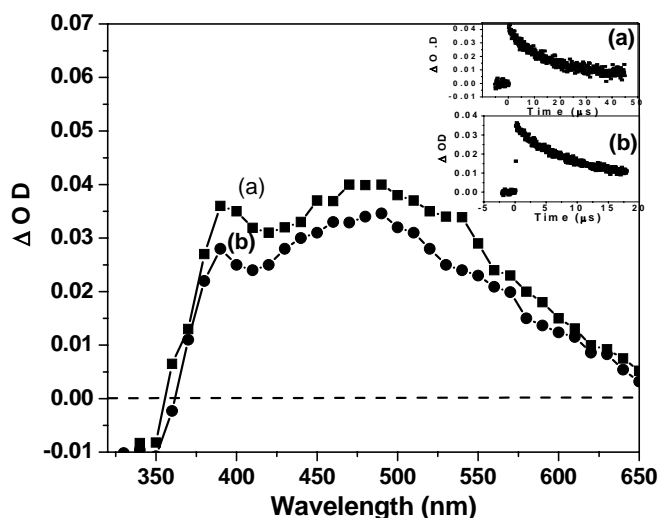
Figure 4.7 Transient absorption spectra of **AMF** in (a) toluene and in (b) acetonitrile. The spectra were obtained 0.5 µs after the laser pulse. Inset shows the decay profile.

Assuming that the molar extinction coefficients for the T-T absorption are very similar in two solvents, the results imply that the triplet yield is very similar in two solvents. Thus the decrease in the nonradiative rate constants with increase in the polarity of the media is not due to any change in the intersystem crossing

efficiency. Clearly, the efficiency of the internal conversion process is affected as the polarity of the media is changed.

4.5. Theoretical calculation

4.5.1. Ground state calculations

The ground state geometries of the systems were optimized in vacuo at B3LYP/6-31G* level. From the optimized structures, the torsion angles between the amino functionality and the flavone moiety of the systems for **AMF**, **DMAMF**, **4AMF**, **5AMF** and **6AMF** are found to be 160.04^0, 175.86^0, 159.09^0, 174.69^0 and 135.84^0 respectively. This observation suggests that the amine functionalities are twisted with respect to the flavone ring and the twist angles vary for different systems. The ground state dipole moments of the systems, **AMF**, **DMAMF**, **4AMF**, **5AMF** and **6AMF** are estimated to be 4.41, 5.41, 5.31, 5.94 and 4.83 D respectively.

4.5.2. Excited state calculations

We have theoretically studied the energetics of different molecular orbitals, which are associated with the lowest excited state of all the systems. The primary objective of this study is to find out whether the increase in the fluorescence efficiency on changing the medium from non polar to polar is associated with a change in the nature/symmetry of the emitting state. Excited state calculations on all the systems were performed using the time-dependent (TD-DFT) framework at the B3LYP/6-31G* level in the gas phase as well as in acetonitrile. The excited state calculations in acetonitrile were performed by self-consistent reaction field (SCRF) method using polarized continuum (PCM) model. All quantum

mechanical calculations were performed using the Gaussian 03 program package. The representative molecular orbital pictures associated with the first excited state for **5AMF** in the gas phase and in acetonitrile are shown in Figure 4.8 and Figure 4.9 respectively.
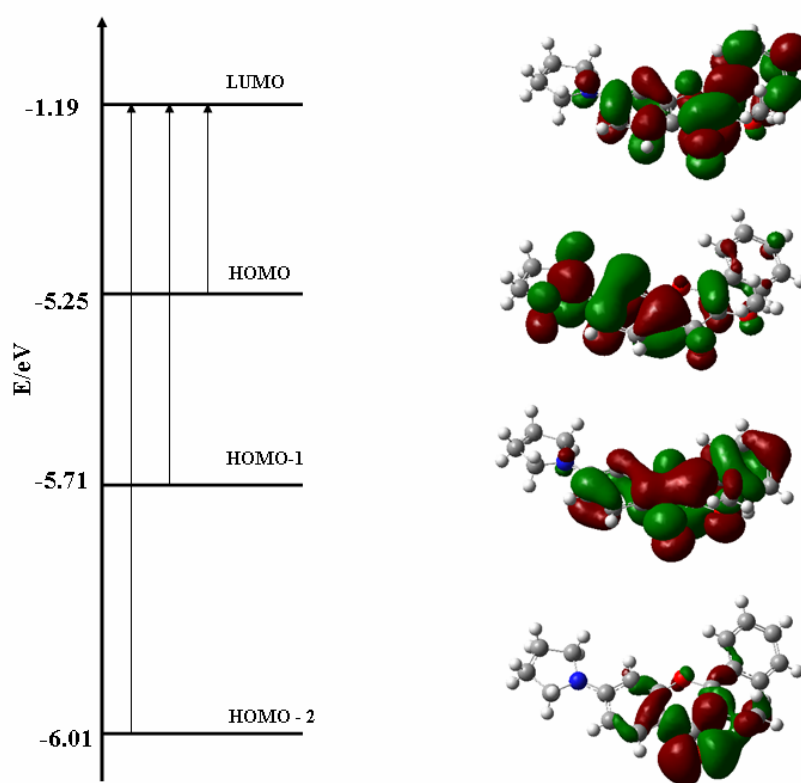
Figure 4.8 The molecular orbital picture associated with the first excited state of **5AMF** in the gas phase. The oribitals were obtained by TD-DFT method at B3LYP/6-31G* level.
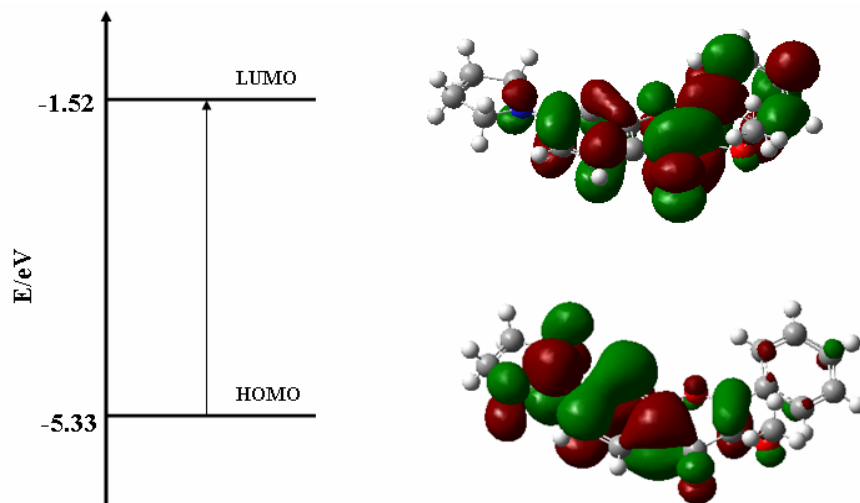
Figure 4.9 The molecular orbital picture associated with the first excited state of **5AMF** in acetonitrile. The oribitals were obtained by TD-DFT method at the 6-31G* level via SCRF/ PCM solvation scheme.

The excitation energies corresponding to the first excited state of the systems have been calculated. We have also determined the nature of the lowest energy transitions by carefully examining the symmetries of the orbitals involved in the transitions. TD-DFT calculated parameters associated with the systems are shown in Table 4.8.

Table 4.8 Lowest Energy Excitations (B3LYP/6-31G*) of the Systems

Systems	Medium	Tr.Energy (eV)	Osc. Strength	MOs involved (Tr. Coeff.)	Nature
AMF	Vacuo	3.535	0.024	HOMO-2 → LUMO (0.612)	$n \to \pi^*$
				HOMO → LUMO (-0.279)	$\pi \to \pi^*$
	Acetonitrile	3.552	0.314	HOMO-2 → LUMO (0.136)	$n \to \pi^*$
				HOMO → LUMO (0.656)	$\pi \to \pi^*$
DMAMF	Vacuo	3.509	0.110	HOMO-2 → LUMO (0.484)	$n \to \pi^*$
				HOMO-1 → LUMO (-0.153)	$\pi \to \pi^*$
				HOMO → LUMO (-0.444)	$\pi \to \pi^*$
	Acetonitrile	3.336	0.302	HOMO → LUMO (-0.675)	$\pi \to \pi^*$
4AMF	Vacuo	3.518	0.086	HOMO-2 → LUMO (0.530)	$n \to \pi^*$
				HOMO-1 → LUMO (-0.162)	$\pi \to \pi^*$
				HOMO → LUMO (-0.384)	$\pi \to \pi^*$
	Acetonitrile	3.358	0.323	HOMO → LUMO (0.674)	$\pi \to \pi^*$
5AMF	Vacuo	3.485	0.192	HOMO-2 → LUMO (-0.336)	$n \to \pi^*$
				HOMO-1 → LUMO (-0.126)	$\pi \to \pi^*$
				HOMO → LUMO (0.571)	$\pi \to \pi^*$
	Acetonitrile	3.254	0.309	HOMO → LUMO (-0.676)	$\pi \to \pi^*$
6AMF	Vacuo	3.487	0.112	HOMO-2 → LUMO (0.489)	$n \to \pi^*$
				HOMO-1 → LUMO (-0.154)	$\pi \to \pi^*$
				HOMO → LUMO (0.439)	$\pi \to \pi^*$
	Acetonitrile	3.311	0.306	HOMO → LUMO (0.677)	$\pi \to \pi^*$

The estimated excitation energy corresponding to the first excited state of the systems agrees well with the experimentally determined quantities. As for example, the calculated lowest energy transition of **DMAMF** is found to be at 3.51 eV in vacuo and the experimental energy estimated from the λ_{max}^{abs} value in toluene is 3.49 eV. The calculation shows that three different excitations, HOMO - LUMO, (HOMO-1) - LUMO and (HOMO-2) – LUMO contribute to the first excited state of the systems in vacuum. The HOMO - LUMO, (HOMO-1) - LUMO and (HOMO-2) – LUMO excitations, as determined from the shapes of the molecular orbitals, are assigned to π-π*, π-π*, n-π* transitions. While three different excitations correspond to the first excited state in the gas phase, the contribution of the (HOMO-2) – LUMO excitation (n-π* transition) is clearly the largest (*vide* Table 4.8). Interestingly, in the polar medium, acetonitrile, the excitation mainly arises from the HOMO - LUMO excitation, having π-π* character of the transition (*vide* Table 4.8). However, in case of **AMF** a minor contribution arises from (HOMO-2) – LUMO excitation, with n-π* character.

Calculations suggest that in the gas phase both n-π* and π-π* states contribute to the photophysical response of the systems with the major contribution arising from the n-π* state. Interestingly, the excited state calculations in acetonitrile reveal that the first excited state is of π-π* in nature. It is to be noted in this context that optical and magnetic resonance studies have established that the n-π* and π-π* states of the flavones are strongly mixed.[27] The present study indicates that the forbidden nature of the first excited state, predominantly due to the n-π* character, is primarily responsible for relatively low radiative efficiency of the

systems in non polar media. However, the π-π* state, which becomes the lowest excited state in polar media, is responsible for enhanced radiative efficiency in these media. Thus it is clearly evident that the relaxation of the symmetry restrictions from nonpolar to polar media is the primary reason for the increase in the radiative efficiency of the systems in polar media.

4.6. Conclusion

Several structurally similar EDA flavone derivatives have been synthesized and fully characterized by conventional analytical methods and X-ray crystallography. The fluorescence properties of the systems are found to be strongly dependent on the polarity of the solvent. Except for the unsubstituted amino derivative, all other amino systems have been found to behave similarly. The nonradiative rate constants evaluated from the quantum yield and lifetime values gradually decrease with increase in the polarity of the solvent. The observations have been interpreted taking into consideration the nature of the two excited states involved in the emission process. The results suggest a change in the nature of the state from n-π* to π-π* with increase in the polarity of the medium. Excited state calculations of the frontier orbitals, based on the TD-DFT method, support the experimental findings.

References

1. Mauricio Duarte-Almeida, J.; Novoa, A. V.; Linares, A. F.; Lajolo, F. M.; Inés Genoves, M. *Plant Foods for Human Nutrition* **2006**, *61*, 187.

2. Brahmachari, G.; Gorai, D. *Curr. Org. Chem.* **2006**, *10*, 873.

3. Sengupta, B.; Uematsu, T.; Jacobsson, P.; Swenson, *J. Biochem and Biophys. Res. Commun.* **2006**, *339*, 355.

4. Sengupta, P. K.; Kasha, M. *Chem. Phys. Lett.* **1979**, *68*, 382.

5. Kasha, M. *J. Chem. Soc., Faraday Trans. 2* **1986**, *82*, 2379.

6. McMorrow, D.; Kasha, M. *J. Am. Chem. Soc.* **1983**, *105*, 5133.

7. Chattopadhyay, N.; Barroso, M.; Serpa, C.; Arnaut, L. G.; Formosinho, S. J. *Chem. Phys. Lett.* **2004**, *387*, 258.

8. Dennison, S. M.; Guharay, J.; Sengupta, P. K. *Spectrochim. Acta Part A* **1999**, *55*, 903.

9. Klymchenko, A. S.; Pivovarenko, V. G.; Demchenko, A. P. *J. Phys. Chem. A* **2003**, *107*, 4211.

10. Oncul, S.; Demchenko, A. P. *Spectrochim. Acta Part A* **2006**, *65*, 179.

11. Ameer-Beg, S.; Ormson, S. M.; Brown, R. G.; Matousek, P.; Towrie, M.; Nibbering, E. T. J.; Foggi, P.; Neuwahl, F. V. R. *J. Phys. Chem. A* **2001**, *105*, 3709.

12. Chou, P.T.; Huang, C. H.; Pu, S. C.; Cheng, Y. M.; Liu, Y. H.; Wang, Y.; Chen, C.T. *J. Phys. Chem. A* **2004**, *108*, 6452.

13. Klymchenko, A. S.; Demchenko, A. P. *Phys. Chem. Chem. Phys.* **2003**, *5*, 461.

14. Klymchenko, A. S.; Duportail, G.; Ozturk, T.; Pivovarenko, V. G.; Mély, Y.; Demchenko, A. P. *Chemistry and Biology* **2002**, *9*, 1199.

15. Lü, F.; Gao, L.; Fang, Y. *Progress in Chemistry* **2005**, *17*, 773.

16. Poteau, X.; Saroja, G.; Spies, C.; Brown, R. G. *J. Photochem. Photobiol. A: Chem.*, **2004**, *162*, 431.

17. Mishra, L.; Sing, A. K.; Trigun, S. K.; Sing, S. K.; Pandey, S. M. *Ind. J. Exp. Biol.* **2004**, *42*, 660.

18. Becker, R. S. *Theory and Interpretation of Fluorescence and Phosphorescence,* John Willey and Sons, New York , 1969.

19. Kalyanasundaram, K.; Thomas, J. K. *J. Phys. Chem.* **1977**, *81*, 2176.

20. Turro, N. J.; Okubo, T. *J. Phys. Chem.* **1982**, *86*, 159.

21. de Melo, J. S.; Becker, R. S.; Elisei, F.; Macanita, A. L. *J. Chem. Phys.* **1997**, *107*, 6062.

22. Meyer, N. D.; Haemers, A.; Mishra, L.; Pandey, H.; Pieters, L. A. C.; Dirk, A.; Berghe, V.; Vlietinck, A. J. *J. Med. Chem.* **1991**, *34*, 736.

23. Ormson, S. M.; Brown, R. G.; Vollmer, F.; Rettig, W. *J. Photochem. Photobiol. A: Chem.* **1994**, *81*, 65.

24. Saha, S.; Samanta, A. *J. Phys. Chem. A* **1998**, *102*, 7903.

25. Saha, S.; Samanta, A. *J. Phys. Chem. A* **2002**, *106*, 4763.

26. Christoff, M.; Toscano, V. G.; Badder, W. J. *J. Photochem. Photobiol. A: Chem.* **1996**, *101*, 11.

27. Gallivan, J. B.; Brinen, J. S. *Chem. Phys. Lett*. **1971**, *10*, 455.

Photophysical and Signaling Behavior of a Flavone-based Chemosensor

This chapter deals with the synthesis, characterization, photophysical and signaling behavior of a flavone-based chemosensor. The system has been designed and developed with a view to sensing fluoride ion selectively. The absorption and fluorescence behavior of this system have been investigated in absence and presence of halides and other commonly encountered anions. NMR and density functional studies on this system have been carried out to determine the nature of interaction between the present system and the halides.

5.1. Introduction

The flavones have not yet been studied for signaling of the anionic species. This may not be surprising as the coordination chemistry of the anions has received much less attention compared to the cations and it is only very recently studies are being targeted towards the recognition and signaling of the various anions taking into consideration the important role of several inorganic anions in industrial processes, energy transduction and enzyme activity in organisms, clinical treatment of disease states, etc.[1-3] Fluoride ion is one of the central species of attraction in this regard because of its both beneficial (e.g., treatment of osteoporosis)[4-5] and detrimental (e.g., fluorosis)[6] roles.

With a view to exploring the potential of the flavones in anion signaling applications, in particular, for signaling of fluoride ion, we have developed 3-methoxy-7-aminoflavone derivative, **LH** incorporating the essential design components required for this purpose. While targeting the present system, we have taken cognizance of the fact that molecular systems that contain a polarized N-H fragment are ideally suited for the recognition and signaling of the anionic species.[7] The benzoyl moiety is specifically appended to the amino nitrogen to make the N-H fragment more polarizable. We have used the 3-methoxy derivative of flavone instead of the 3-hydroxy derivative to avoid complications from the excited state intramolecular proton transfer (ESIPT) process.

LH
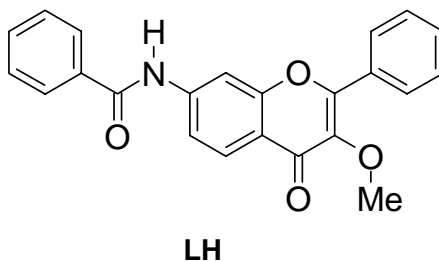
In this chapter we report on the synthesis and photophysical behavior of **LH** both in the absence and presence of the halide salts in aprotic media. Since both H-bonding and proton transfer mechanisms often give rise to a very similar kind of optical response of the receptor, one of the main objectives of this study is to obtain insight into the mechanism of the signaling process with the help of theoretical calculations based on the density functional method. For this purpose, the calculations have been carried out on **LH**, **L⁻** and **LH:X⁻**. The results suggest

that the absorption and fluorescence response of **LH** in the presence of F⁻can be best described by the abstraction of the acidic proton from **LH**.

5.2. Synthesis of LH

The main precursor compound, 7-amino-3-methoxy-2-phenyl-chromen-4-one (AMF) was synthesized from IMF following the method described in the previous chapter (Section 4.2.2). AMF was reacted to benzoylchloride in dichloromethane to obtain the desired chemosensor, **LH.** The details of the synthetic procedures of **LH** are described below (Scheme 5.1).

To a 50 ml round-bottom flask, AMF 100 mg (0.374 mmol) was dissolved in a small amount of DCM then 0.1 ml of benzoyl chloride was also added to it. The reaction mixture was stirred for about 24 h at room temperature. The reaction mixture was taken out, filtered and washed several times with dichloromethane. White compound was formed after recrystallization in acetonitrile. Yield 40 mg (29%). The following analytical data were used for the characterization of **LH**.

^{1}H NMR (400MHz, DMSO-d_6): δ 10.78 (s, 1 H), 8.37 (s, 1 H), 7.98-8.04 (m, 5 H), 7.76-7.78 (m, 1 H), 7.55-7.58 (m, 6 H), 3.82 (s, 3 H).

Elemental analysis: $C_{23}H_{17}NO_4$: calcd.: C 74.38, H 4.61, N 3.77: found: C 74.28, H 4.71, N 3.68%.

LCMS: m/z 370 (M-H$^+$).
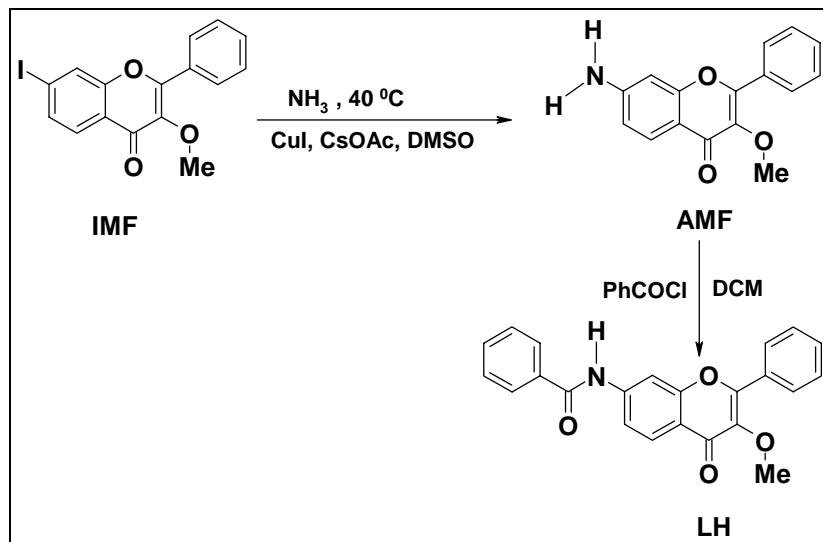
Scheme 5.1 Synthetic route to **LH**.

5.3. Absorption and fluorescence behavior of LH

AMF exhibits a broad absorption band that can be assigned to intramolecular charge transfer (ICT) transition from the amino group to the keto functionality of the fluorophore. The ICT character is evident from the solvatochromic nature of the absorption band of AMF. Upon changing the solvent from 1, 4 dioxane to acetonitrile (ACN) the absorption maximum shifts from 324 nm to 340 nm. This is consistent with the dipolar nature of AMF. The DFT calculation suggests a ground state dipole moment (μ_g) of 4.44 D for this system. Interestingly, the absorption maximum of **LH** is found rather insensitive to the polarity of the solvent. Irrespective of the polarity of the medium, the maximum appears at 317 nm (Figure. 5.1). The DFT calculation suggests a μ_g value of 4.29 D for **LH.** A blue shift of ~23 nm of the absorption maximum of **LH** compared to AMF in

acetonitrile is also a reflection of small charge transfer character of **LH.** Low dipole moment of **LH** can be rationalized taking into consideration the fact that charge separation in the AMF moiety (from the 7-amino group to the flavone carbonyl group) is significantly reduced on replacement of one of the amino hydrogen by electron withdrawing C_6H_5CO- group.
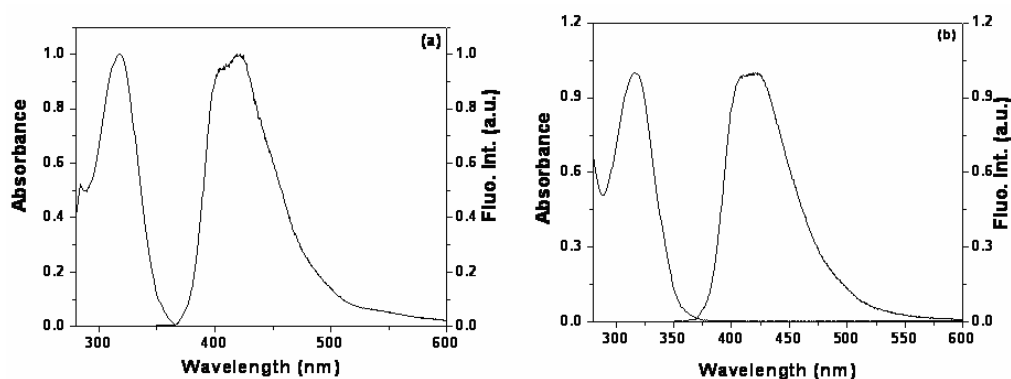
Figure 5.1 Absorption and emission spectra of **LH** (a) in 1,4-dioxane and (b) in acetonitrile. $\lambda_{exc} = 335$ nm.

While AMF exhibits a broad solvent sensitive emission band (λ_{max} observed at 442 and 465 nm in 1, 4-dioxane and acetonitrile, respectively), the emission spectrum of **LH** is characterized by a solvent insensitive broad band ($\lambda_{max} = 422$ nm in both 1, 4-dioxane and acetonitrile). The solvent insensitivity of the fluorescence (or absorption) band position (Figure 5.1) of **LH** is a reflection of reduced charge separation from the nitrogen atom to the flavone ring system on introduction of the benzoyl moiety. Both AMF and **LH** display a biexponential fluorescence decay behavior. The average fluorescence lifetime of AMF and **LH** has been calculated to be 740 and 460 ps, respectively.

5.3.1. Absorption titration of LH with anions

The interaction between **LH** and halide ions has been investigated in acetonitrile through UV-visible absorption and fluorescence measurements. Spectrophotometric titration was performed on dilute solution of compound **LH** with gradual addition of a freshly prepared tetrabutylammonium salt of required anions (F⁻, Cl⁻, Br⁻, I⁻). In particular, to a dilute solution of **LH,** solution of tetrabutylammonium salt was added in a stepwise fashion. Upon progressive addition of tetrabutylammonium fluoride (TBAF) solution, the 317 nm band intensity is slightly decreased and a small bathochromic shift (~4 nm) of the maximum could be observed (Figure 5.2). Interestingly, a completely new band at 408 nm is developed with a clear isosbestic point at 335 nm indicating the formation of a second species (Figure 5.2).
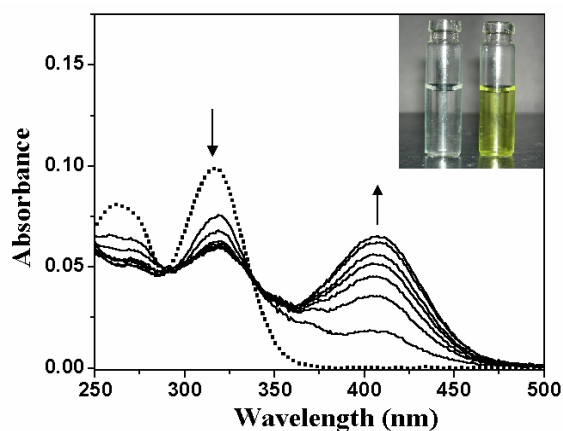

Figure 5.2 Absorption spectra of acetonitrile solution **LH** (8.5×10^{-6} M) upon progressive addition of TBAF (6.9×10^{-5} to 5.4×10^{-4} M). The dotted curve represents the absorbance spectrum of the free compound. Inset shows naked eye response of the signaling event.

It is obvious that the new species can either be a hydrogen-bonded complex between **LH** and F⁻ represented by **LH**…F⁻ or the deprotonated form of **LH**, namely **L**⁻. The naked eye observation shows the colorless solution of **LH** turning into yellow in the presence of F⁻ (Figure 5.2). Even though there have been several instances where a similar change has been attributed to the formation of a hydrogen-bonded complex between **LH** and F⁻, we propose the change in the spectral behavior of **LH** in the presence of the fluoride to be due to the deprotonation of the acidic amido proton by F⁻ for the fact that spectral change similar to the one seen in the presence of F⁻ is also observed in presence of stronger bases such as Bu₄NOH (Figure 5.3), while weaker base such as NEt₃ cannot induce any spectral change. In this context we note that fluoride recognition by a deprotonation mechanism has recently been established in the case of a naphthalene-urea based chemosensor by Nam et al.[8] As far as the influence of other halides is concerned, no significant change in the optical behavior of **LH** is observed when the halide concentration is similar to that used for fluoride. However, when the halide concentration is almost 10 times more than that used for the fluoride, a weak shoulder at around 360 nm can be observed presumably due to the formation of a weak H-bonding complex[7] between **LH** and other halides (Figure 5.3). Other anions such as ClO₄⁻, NO₃⁻, AcO⁻ have not shown any significant responses in the optical behaviors.

Additional supporting evidence in favor of the deprotonation mechanism, which has been obtained from NMR titration experiments and theoretical calculations, is presented latter.
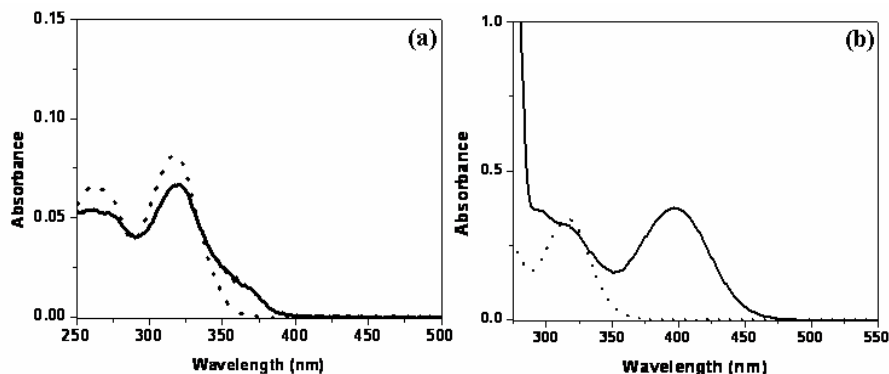
Figure 5.3 Effect of Bu$_4$NCl and Bu$_4$NOH on the absorption spectrum of **LH.** (a) Addition of 1×10^{-3} M Bu$_4$NCl to acetonitrile solution of **LH** (7×10^{-6} M), (b) addition of 2×10^{-4} M Bu$_4$NOH to acetonitrile solution of **LH** (2.9×10^{-5} M). The dashed spectra are recorded in the absence of any external reagent.

In essence, one can write the following reaction to explain the fluoride signaling mechanism of **LH**.

$$\textbf{LH} + F^- \Leftrightarrow \textbf{L}^- + HF$$
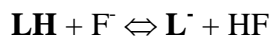
According to this mechanism, the new 408 nm absorption band observed in the presence of F^- is due to **L$^-$.** Much higher basicity of the fluoride ion compared to the other halides is responsible for the fact that the equilibrium is shifted towards right only in the case of the former species and hence, recognition is selective.

5.3.2. Fluorescence titration of LH with anions

The fluorescence spectrum of free **LH** displays a broad band with maximum at 422 nm in acetonitrile. Upon gradual addition of F^- to a solution of **LH**, a significant decrease in the intensity of this fluorescence band accompanied by the

emergence of a new emission band centered at 590 nm,[9] is observed with a clear isoemissive point at 518 nm (Figure 5.4).
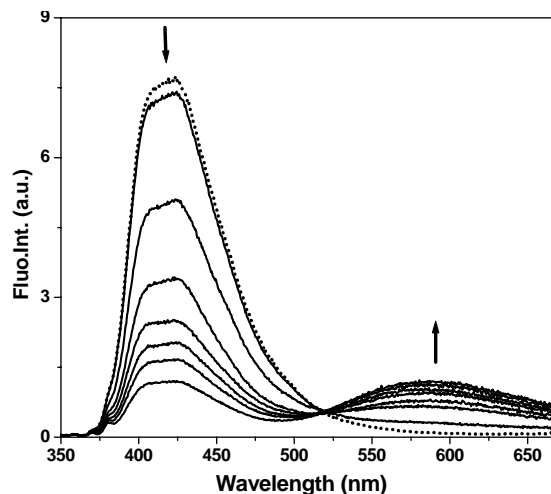
Figure 5.4 Fluorescence spectra of acetonitrile solution of **LH** (8.5×10^{-6} M) upon progressive addition of TBAF (6.9×10^{-5} to 5.4×10^{-4} M). Dotted curve represents the fluorescence spectrum of the free compound. $\lambda_{exc} = 335$ nm.

Upon addition of the other anions, no significant change other than fluorescence quenching of the original band is observed. The fact that F⁻ '*switches off*' the 422 nm emission band and simultaneously '*switches on*' the 590 nm emission band is an important point to note. Essentially, this means that **LH** not only allows colorimetric signaling of F⁻, but also its fluorescence signaling. What is even more interesting to note here is that the fluorescence response of **LH** in the presence of F⁻ allows its ratiometric signaling when the ratio of the fluorescence output at two different wavelengths is plotted as a function of the concentration of F⁻. Figure 5.5 shows a plot of the ratio of the fluorescence

intensities at 590 and 422 nm versus concentration of F⁻. As can be seen from Figure 5.5, I_{590}/I_{422} increases linearly with the concentration of fluoride ions in the concentration range shown. A comparative fluorescence ratiometric response of **LH** with different anions is also shown in Figure 5.6.
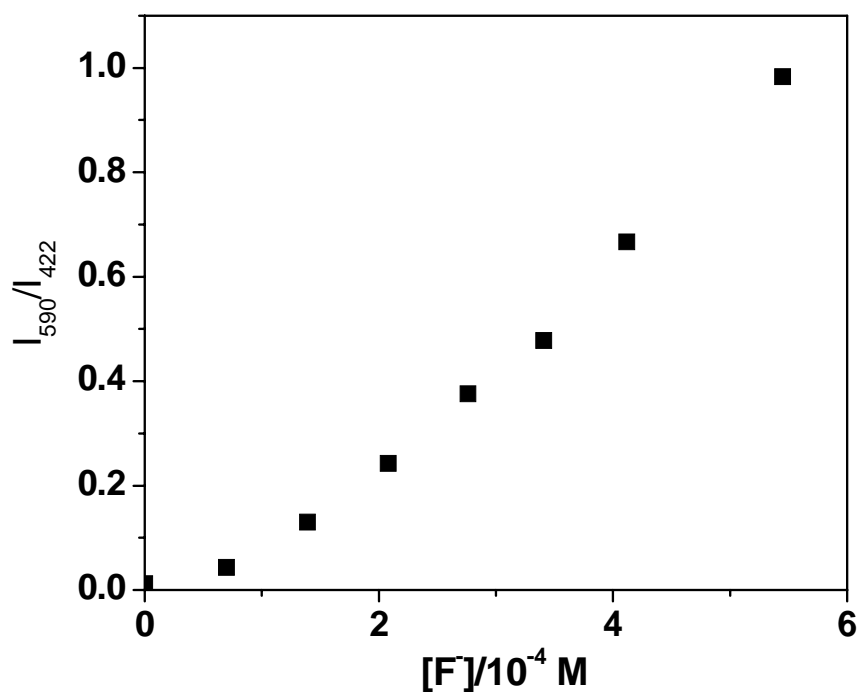
Figure 5.5 Plot of the ratio of the fluorescence intensities at 590 and 422 nm as a function of [F⁻] in acetonitrile. λ_{exc} = 335 nm.
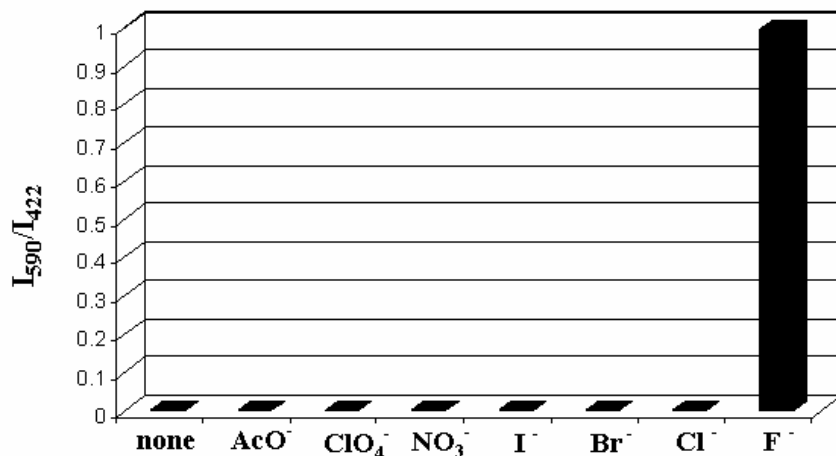
Figure 5.6 Ratiometric fluorescence response of **LH** to selected anions in acetonitrile.

It should be noted that modulation of fluorescence intensity of the sensor system has been exploited in the past for the recognition and sensing of the anions.[10,11] Only a few sensors show anion-induced enhancement of fluorescence intensity.[11] It is however well-known that single wavelength intensity-based fluoresensors suffer from a number of drawbacks because of the fluctuation of the fluorescence intensity of the system on various factors. Ratiometric fluorosensors, on the other hand, provide built-in correction for the environmental effects, intensity fluctuations, etc. and hence, are preferred to the single wavelength counterpart. While ratiometric fluorescence sensors are available for various cations[12], very few systems of this type are available for fluoride ions.[13] In this respect, the present observation with the flavone derivative is significant.

5.4. NMR experiment of LH with fluoride

The amido proton of **LH** is abstracted in the presence of F⁻ is also evident from the results of proton NMR titration experiment (Figure 5.7). As can be seen from Figure 5.7, the imide proton signal of **LH** appears at 10.85 ppm due to strong electron withdrawing influence of the carbonyl group present in the system. Upon, gradual addition of the fluoride salt, the amide proton signal first gets broadened and finally disappears. This result when considered along with those discussed previously confirms the abstraction of the imide proton of **LH** to form HF.

Figure 5.7 Proton NMR spectra of sensor **LH** in DMSO-d_6 in the presence of (a) 0 equiv., (b) 5 equiv. and (c) 15 equiv. of TBAF.
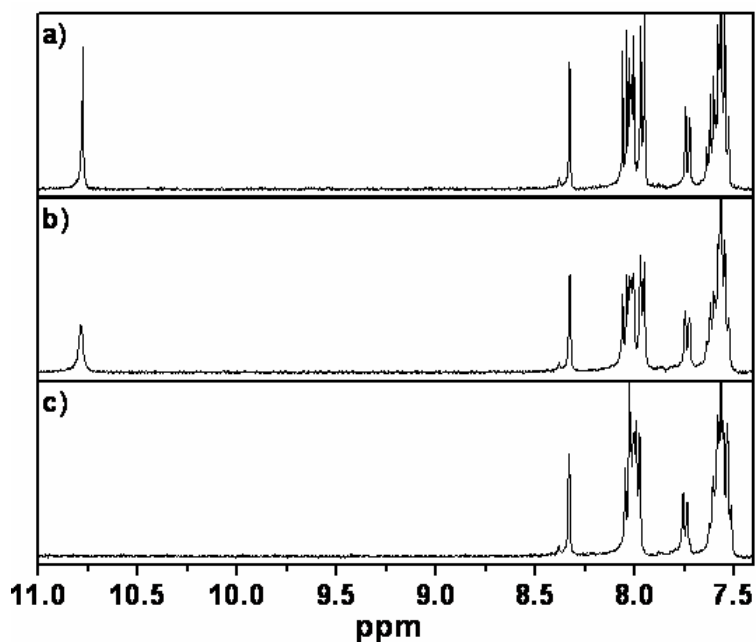
5.5. Theoretical calculations

5.5.1. Ground state structures

Very recently, DFT studies have been successfully exploited in predicting the ground state structures of different receptor-halogen complexes.[14] However, all these studies end-up with the result that the recognition process goes through a hydrogen bonded species. In order to obtain insight into the anion-sensing mechanism, in particular, to determine whether the recognition process in our system is mediated through the H-bonding interaction between **LH** and F^- or proton abstraction from the imide hydrogen of **LH** to the fluoride ion, we have carried out theoretical calculations exploiting the density functional method. The system consisting of **LH** and F^-, with an initial $NH…F^-$ distance set around 1.75 Å (as typical $NH…F^-$ hydrogen bond distance ranges between 1.73 and 1.77 Å)[15] and an $NH…F^-$ linear geometry, when optimized using the density functional method at the B3LYP/6-31G* level yielded a final geometry (Figure 5.8) with the H-F distance of 1.033 Å and N…H distance of 1.475 Å. Since a typical N-H bond distance is 0.983 Å one can conclude deprotonation of the acidic imide hydrogen from **LH** and formation of HF. The theoretical calculations when carried out with Cl^- and Br^- (which do not induce significant changes in the absorption and fluorescence properties of **LH**) yielded optimized structures that correspond to hydrogen-bonded complexes between **LH** and Cl^- and **LH** and Br^-, rather than formation of **L⁻** (Figure 5.8). This is clearly evident from the optimized structural parameters, in particular, the various bond distances shown in Table 5.1. For example, the calculated H…Cl and H…Br distances (2.217 and 2.403 Å, respectively) are much higher than common gas phase distances of 1.27 and 1.41

Å respectively and the N-H distance (1.040 or 1.037 Å) simply represents an elongated N-H bond. The N…H…Cl and N…H…Br angles are found to be 168.78° and 168.43° respectively.
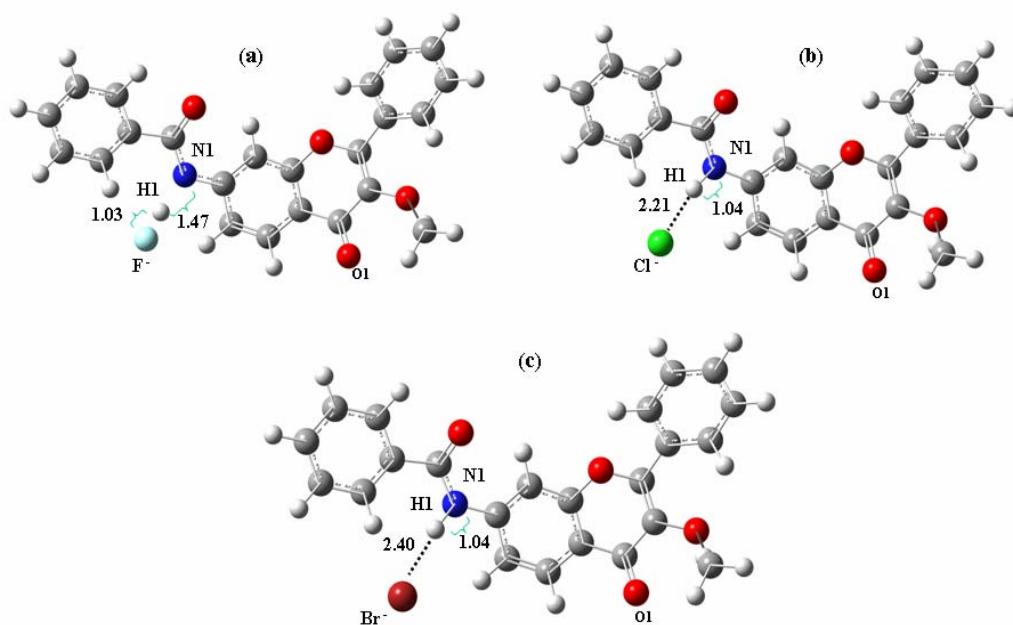
Figure 5.8 Geometries of the (a) **LH**:F⁻, (b) **LH**:Cl⁻ and (c) **LH**:Br⁻ after optimization at the B3LYP/6-31G* level. The selected bond-distances of the respective species are also shown in Å unit.

Table 5.1 Calculated (B3LYP/6-31G*) Structural Parameters of Different **LH**:X$^-$ Species[a]

Complex	X	d(N1-H1)	d(H1···X)	α(N1H1X)
	F	1.475	1.033	171.665
LH:X$^-$	Cl	1.040	2.217	168.779
	Br	1.037	2.403	168.433

[a]Bond lengths (d) and angles (α) are in angstroms and degrees, respectively.

5.5.2. Charge density analysis

A charge density analysis of the receptor-halide systems has also been made by natural bond order (NBO) calculation[16] on the optimized geometries of the complexes. The calculated charge densities collected in Table 5.2 clearly show that the negative charge centred on the most electronegative atom, fluorine, is the lowest (-0.647) among the halides. This is obviously a reflection of partial neutralization of the negative charge by the abstracted proton. This aspect is best borne out when one considers the sum of the charges centred on X and H. Ideally, if HX is indeed formed and if it does not interact with the rest of the system (**L**$^-$), the sum of the charges is expected to be zero. One can see, the sum is only -0.12 in the case of F$^-$, whereas the sum is much higher -0.41 in the case of Cl$^-$or Br$^-$. Hence, the NBO charge analysis also indicates that the proton is almost completely abstracted by F$^-$.

Table 5.2 Calculated (B3LYP/6-31G*) NBO Atomic Charges (q_x) on Selected Atoms of Different **LH**:X$^-$ Species

Complexes	X$^-$	q_x (X$^-$)[a]	q_x (H1)[a]	q_x (N1)[a]	q_x (O1)[a]
	F	-0.647	0.528	-0.685	-0.631
LH:X$^-$	Cl	-0.857	0.448	-0.619	-0.613
	Br	-0.850	0.442	-0.615	-0.608

[a]Parenthesis shows the symbol of different selected atoms (*vide* Figure 5.8).

5.5.3. Interaction energy calculations

The energies of **LH**, halides and **LH**:X$^-$ were obtained from the B3LYP/6-31G* optimized geometries. The interaction energy (ΔE_{int}) of the receptor-halide (X$^-$ = F$^-$, Cl$^-$) species was computed as the difference between the energy of the species ($E_{[R\text{-}X^-]}$) and the total energy of the two free monomers, i.e. receptor (E_R) and halide ion (E_X^-)[14] using the following equation:

$$\Delta E_{int} = (E_{[R\text{-}X^-]}) - (E_R + E_X^-)$$

The interaction energy calculated for the receptor-fluoride complex is - 417.52 kJ mol^{-1}, while that for the receptor-chloride complex is -148.19 kJ mol^{-1}. This also indicates that the receptor-fluoride interaction is much stronger than the receptor-chloride interaction.

5.5.4. Electronic excitation energies

We have also calculated the transition energies of the **LH**, **L**$^-$ and the hydrogen-bonded complex, **LH**…F$^-$ (Table 5.3). It can be seen that the agreement between the experimental and calculated excitation energy is quite good for **LH**. Only the anionic form of the receptor (**L**$^-$) shows the transition observed in the

longer wavelength region on addition of F^-. For the hydrogen-bonded complex, no transition in the long wavelength region could be observed. Thus the calculated spectral data also unambiguously suggest that the intermolecular proton transfer from amide nitrogen to fluoride is responsible for the fluoride ion selective recognition event rather than the hydrogen bonding interaction. Hydrogen bonded complexes of the other halides (Cl^- and Br^-) also do not exhibit any transition in the long wavelength region (Table 5.4).

Table 5.3 Calculated and Experimental Transition Energies of **LH,** its Anionic form, **L⁻** and its Hydrogen-bonded Complex with F^-

Species	Calculated transition energy (eV)[a]	Oscillator strength	Experimental transition energy (eV)[b]
LH	$S_1 = 3.57$ $S_2 = 3.76$ $S_3 = 3.96$	0.46 0.14 0.21	3.48
L⁻	$S_1 = 2.84$ $S_2 = 3.30$ $S_3 = 3.78$	0.35 0.06 0.04	2.84
LH...F⁻	$S_1 = 3.52$ $S_2 = 3.75$ $S_3 = 3.92$	0.54 0.08 0.16	-

[a] Transition energies are calculated using ACN as solvent by TD-DFT method at the 6-31+G* level via SCRF/ PCM solvation scheme. [b]Experimental transition energies are calculated from the crossing point of the absorption and emission spectra of the respective compounds in acetonitrile.

Table 5.4 Calculated Transition Energies of the Hydrogen-bonded Complexes of **LH** with Cl⁻and Br⁻

Complexes	X⁻	Calculated transition energy (eV) [a]	Oscillator strength
		$S_1 = 3.53$	0.54
	Cl	$S_2 = 3.74$	0.09
		$S_3 = 3.93$	0.17
LH...X⁻			
		$S_1 = 3.53$	0.53
	Br	$S_2 = 3.74$	0.10
		$S_3 = 3.92$	0.03

[a] transition energies are calculated using ACN as solvent by TD-DFT method at the 6-31+G* level via SCRF/ PCM solvation scheme.

5.6. Conclusion

A flavone derivative, **LH**, has been specifically designed and developed with a view to explore its potential in specific recognition of fluoride ion and to determine the mechanism of the signaling response of the system. Both colorimetric and fluorescence response of the system in the presence of the halide salts is found to be distinctly different in the case of the fluoride salt indicating possible usage of this flavone derivative in fluoride recognition studies. The fluoride can be detected by naked eye observation as well as by ratiometric fluorescence intensity measurements at two different wavelengths in acetonitrile solution. The fluoride selectivity of the system is attributed to higher basicity of the fluoride compared to the other halides and the spectral changes observed in its presence has been interpreted in terms of a proton abstraction mechanism rather than using commonly invoked hydrogen bonding mechanism. The results of the

theoretical calculations based on the density functional methods presented here fully support the proton abstraction mechanism of the signaling of fluoride ion.

References

1. *Reigel's Handbook of Industrial Chemistry*, 9th ed.; Kent, J. A., Ed.; Van Nostrad Reihold-International Thomson Publising: New York, 1992.

2. Mason, C. F. *Biology of Freshwater Pollution,* 2nd ed.; Longman: New York, 1991.

3. *Chemical Sensors and Biosensors for Medical and Biological Applications,* U. E. Spichiger-Keller ,Wiley-VCH: Weinheim, Germany, 1998.

4. Kirk, K. L. *Biochemistry of the Halogens and Inorganic Halides*; Plenum Press: New York, 1991; p 58.

5. Kleerekoper, M. *Endochrinol. Metab. Clin. North Am.* **1998**, *27*, 441.

6. Wiseman, A. *Handbook of Experimental Pharmacology XX/2, Part 2*; Springer-Verlag: Berlin, 1970; pp. 48–97.

7. Amendola, V.; Esteban-Gomez, D.; Fabbbrizzi, L.; Lecchelli, M. *Acc. Chem. Res.* **2006**, *39*, 343.

8. Cho, E. J.; Moon, J. W.; Ko, S. W.; Lee, J. Y.; Kim, S. K.; Yoon, J.; Nam, K. C. *J. Am. Chem. Soc.* **2003**, *125*, 12376.

9. The fluorescence profile of the new band is characterized by single exponential decay with a lifetime of 285 ps.

10. (*a*) Recent examples of luminescent anion sensing include: Kim, K. N.; Singh, J.; Kim, S. J.; Kim, H. G.; Kim, J. K.; Lee, L. W.; Kim, K. S.; Yoon, J. A.*Org. Lett*. **2003**, *54*, 2083. (b) Cho, E. J.; Ryu, B. J.; Lee, Y. J.; Nam, K. C. *Org. Lett.* **2005**, *7*, 2607. (c) Kim, K.; Yoon, J. T. *Chem. Commun.* **2002**, 770. (d) de Silva, A. P.; McClean, G. D.; Pagliari, S. *Chem. Commun.* **2003**, 2010. (e) Jose, D. A.;

Kumar, D. K.; Ganguly, B.; Das, A. *Tetrahedron Lett.* **2005**, 4*6*, 5343. (f) Gunnlaugsson, T.; Glynn, M.; Tocci (née Hussey), G. M.; Kruger, P. E.; Pfeffer, F. M. *Coord. Chem. Rev.* **2006**, *250*, 3094.

11. (a) Xu, G.; Tarr, M. A. *Chem. Commun.* **2004**, 1050. (b) Kovalchuk, A.; Bricks, J. L.; Reck, G.; Rurack, K.; Schulz, B.; Szumna, A.; Weiβhoff, H. *Chem. Commun.* **2004**, 1946.

12. (a) Taki, M.; Wolford, J. L.; O'Halloran, T. V. *J. Am. Chem. Soc.* **2004**, *126*, 712. (b) Yang, R.; Li, K.; Wang, K.; Zhao, F.; Li, N.; Liu, F. *Anal. Chem.* **2003**, *75*, 612. (c) Yang, R.; Chan, W.; Lee, A. W. M.; Xia, P.; Zhang, H.; Li, K. *J. Am. Chem. Soc.* **2003**, *125*, 2884. (d) Maruyama, S.; Kikuchi, K.; Hirano, T.; Urano, Y.; Nagano, T. *J. Am. Chem. Soc.* **2002**, *124*, 10650. (e) Tong, H.; Wang, L.; Jing, X. X. B.; Wang, F. *Macromolecules* **2002**, *35*, 7169. (f) Banthia, S.; Samanta, A. *J. Phys. Chem. B* **2006**, *110*, 6437.

13. (a) Liu, B.; Tian, H. *J. Mater. Chem.* **2005**, *15*, 2681. (b) Coskun, A.; Akkaya, E. *Tetrahedron Lett.* **2004**, *45*, 4947.

14. (a) Ghosh, T.; Maiya, B. G.; Wong, M. W. *J. Phys. Chem. A* **2004**, *108***,** 11249. (b) Jose, D. A.; Kumar, D. K.; Ganguly, B.; Das, A. *Org. Lett.* **2004**, *6*, 3445.

15. Brooks, S. J.; Evans, L. S.; Gale, P. A.; Hursthouse, M. B. *Chem. Commun*. **2004**, 734.

16. Reed, A. E.; Curtiss L. A.; Weinhold, F. *Chem. Rev.* **1988**, *88*, 899.

Chapter 6

Photophysical and Signaling Behavior of an Aminophthalimide based Chemosensor

This chapter deals with synthesis, characterization, photophysical and signaling behavior of a 4-aminophthalimide-based system, bearing a *fluorophore-spacer-receptor* architecture. The system has been designed and developed with a view to sensing chromium(III) ion selectively. The absorption and fluorescence behavior of this system have been investigated in the absence and presence of different metal ions to explore the signaling potential of the system.

6.1. Introduction

Trivalent chromium, Cr(III) is an essential component of a balanced human and animal diet in amounts of 50 - 200 µg per day (WHO 1988) and its deficiency causes disturbances in the glucose levels and lipid metabolism. On the other hand, chromium is an environmental pollutant and its build up due to various industrial and agricultural activities is a matter of concern.[1] Thus, there is an urgent need to develop chemical sensors[2,3] that are capable of detecting chromium ions in biological and environmental samples. While detection of Cr(III) employing electrochemical[4] and potentiometric[5] techniques has been reported recently, selective detection of Cr(III) by fluorimetric methods,[6] which are known for their simplicity, high sensitivity and instantaneous response, has so far not been made possible primarily due to two reasons. Firstly, paramagnetic Cr(III) is described as

one of the most efficient fluorescence quenchers among the transition metal ions and secondly, the lack of a selective ligand system for Cr(III). In the past few years, considerable effort has been directed towards the development of fluorescence chemosensors for the detection of paramagnetic metal ions using different design strategies[7-18] and selective detection has been achieved only on a few occasions.[19-26] Among the first row transition metal ions, Zn(II) stands out because of its completely filled d-orbitals and thus several systems have been reported for selective detection of Zn(II) ions.[19-21]

Selective detection of Cu(II), which occupies the highest position in the Irving-Williams series, has also been possible because of its strong complexation properties among its relatives.[22-26] It is important to note that molecular recognition can result from selective binding or selective response, but in the latter case, interfering substances will competitively inhibit the optical response to the desired analyte. Unfortunately, most of the systems are guest-selective rather than guest-specific because metal ions of the same family show quite similar binding properties.

We have designed and developed a 4-aminophthalimide-based system, **APCr,** bearing a *fluorophore-spacer-receptor* architecture for selective sensing of chromium(III). Electronically deficient fluorophore, 4-aminophthalimide has been used as the fluorescing moiety in the three-component system. We have used di(2-ethylsulfanylethyl)amine (SNS) ligand,[27] a mixed soft and hard donor ligand, as the receptor unit as it is known to form strong complex with Cr(III)[28]. The fluorophore and the receptor units are connected by an ethyl spacer.
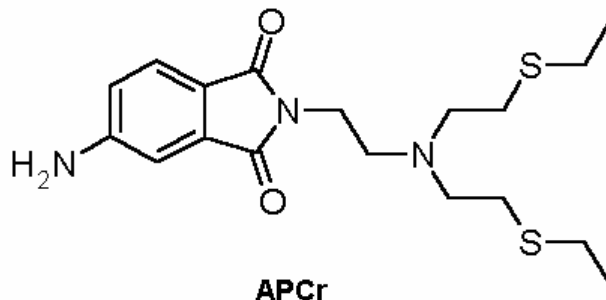
APCr

The synthesis and photophysical behavior of **APCr** both in the absence and presence of the different metal salts in tetrahydrofuran (THF) have been studied. With the present system, an "off-on" fluorescence signaling of Cr(III) has been achieved exploiting the guest-induced inhibition of photoinduced electron transfer signaling mechanism. The system shows ~17-fold Cr(III)-selective chelation-enhanced fluorescence response in tetrahydrofuran and the system is found to be highly selective against the background of environmentally and biologically relevant metal ions.

6.2. Synthesis of APCr

APCr, in which the mixed soft and hard donor ligand (SNS) wherein the electron density of the central nitrogen atom of the ligand system is available for binding with the metal ions, was synthesized in three steps (Scheme 6.1).
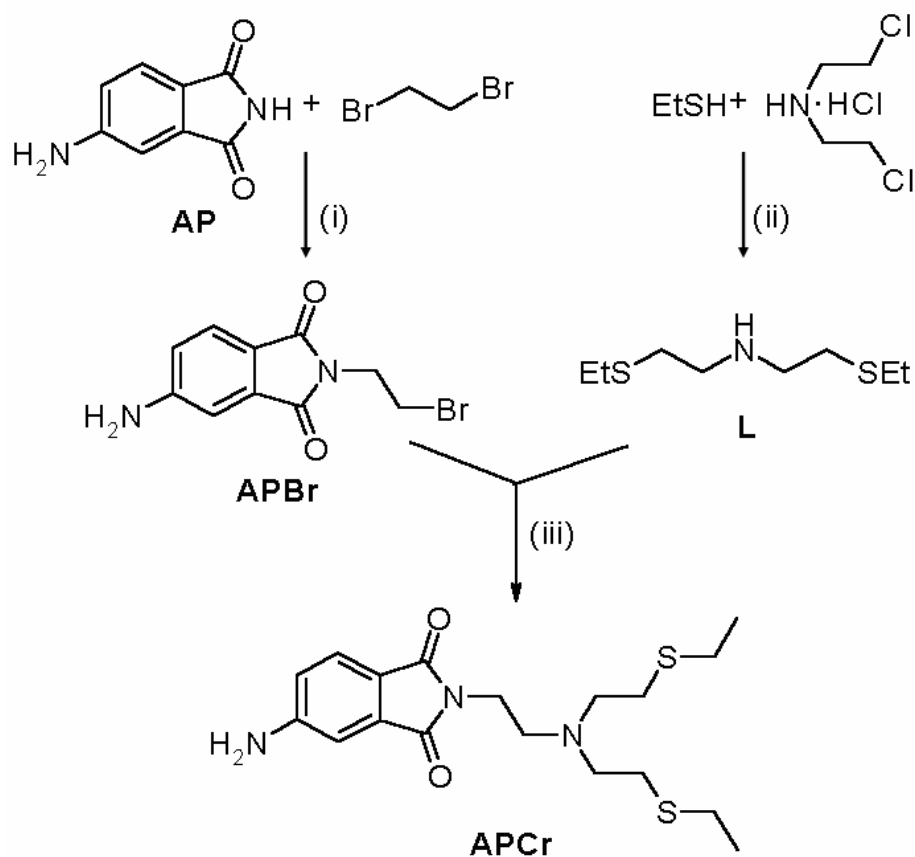
Scheme 6.1 Synthetic route to the fluorescence chemosensor **APCr**. Conditions: (i) NaH, DMF, room temperature, 24 h; (ii) Na, ethanol, reflux, 2 h; (iii) Na_2CO_3, KI, acetonitrile, reflux, 48 h.

In the first two steps, the starting materials **APBr** and **L** (SNS) were synthesized according to the reported procedures.[13,27] In the third step, **APBr** was reacted with **SNS** to obtain the desired chemosensor.

Step 1: N-bromoethyl-4-aminophthalimide (APBr). 4-Aminophthalimide (0.81 g, 5 mmol) was treated with previously washed NaH (0.6 g, 25 mmol) in dry DMF (10 mL) at room temperature with constant stirring for 1 h. Subsequently, 1,2-dibromoethane (0.87 mL, 10 mmol) was added to the reaction mixture and stirred for 24 h at room temperature. The excess NaH present in the reaction mixture was destroyed with water (5–15 mL), and the product was extracted with chloroform (3 × 20 mL). The chloroform extract was dried over anhydrous Na_2SO_4 and evaporated under vacuum. The resulting solid was purified by column chromatography (neutral alumina, 1:1 hexane/ethylacetate). Yield 60%. The purified compound was characterized by the following ^{1}H NMR spectral data.

^{1}H NMR (CDCl$_3$, 400 MHz): δ 3.58 (t, $J = 7.0$ Hz, 2 H), 4.05 (t, $J = 7.0$ Hz, 2 H), 4.45 (bs, 2 H), 6.82 (m, 1 H), 7.05 (m, 1 H), 7.71 (m, 1 H).

Step 2: di(2-ethylsulfanylethyl)amine) (L). Under a nitrogen atmosphere, sodium (4.60 g, 200 mmol) was dissolved in ethanol (200 mL), and ethanethiol (7.44 g, 120 mmol) was added to the solution. An ethanol solution (100 mL) of bis(2-chloroethyl)-amine hydrochloride (7.14 g, 40 mmol) was added dropwise with refluxing, and the reaction mixture was refluxed for 2 h under a nitrogen atmosphere. The residue obtained by solvent evaporation was poured into water, and the product was extracted with chloroform twice. The product was purified by vacuum distillation to give colorless liquid (84 %). The purified compound was characterized by the following ^{1}H NMR spectral data.

^{1}H NMR (CDCl$_3$, 400 MHz): δ 1.27 (t, $J = 7.2$ Hz, 6 H), 1.68 (s, 1 H), 2.55 (q, $J = 7.3$ Hz, 4 H), 2.70 (t, $J = 6.4$ Hz, 4 H), 2.83 (t, $J = 6.6$ Hz, 4 H).

Step 3: 5-amino-2-[2-di(2-ethylsulfanylethyl)aminoethyl]-1,3-isoindolinedione (APCr). APBr (0.74 mM) was added to 50 mL of dry acetonitrile in a 100-mL three-necked round-bottom flask and to this was added L (0.7 mM), potassium carbonate (1 mM), and a catalytic amount of KI. The mixture was allowed to reflux under a nitrogen atmosphere for 48 hours with constant stirring. Subsequently, the solvent was evaporated and the solid residue was extracted with chloroform (4 x 40 mL). The chloroform extract was dried over anhydrous Na_2SO_4 and evaporated to obtain a pale yellow solid that was purified by column chromatography (neutral alumina, 40:60 EtOAc/hexane). Yield 40%. The purified compound was characterized by the following analytical data.

^{1}H NMR (400 MHz, CDCl$_3$): δ 1.20 (t, *J* = 7.40 Hz, 6 H), 2.49-2.61 (m, 8 H), 2.72-2.85 (m, 6 H), 3.68 (t, *J* = 5.32 Hz, 2 H), 4.41 (s, 2 H), 6.80 (d, *J* = 8.04 Hz, 1 H), 7.01 (s, 1 H), 7.59 (d, *J* = 8.12 Hz, 1 H). CHN analysis calculated for $C_{18}H_{27}N_3O_2S_2$: C, 56.66%; H, 7.13%; N, 11.01%. Found: C, 56.38%; H, 7.46%; N, 10.68%. LCMS m/z 382 (M+H$^+$).

6.3. Absorption and fluoresecence behavior of APCr in absence and presence of different metal ions

The optical absorption and fluorescence spectra of **APCr** are characterized by structureless bands centered at 366 nm and 455 nm, respectively in tetrahydrofuran (Figure 6.1). Intramolecular charge transfer (ICT) in the fluorophore moiety gives rise to these bands. The fluorescence quantum yield of **APCr** in tetrahydrofuran (THF) is measured to be 0.026, which is 96% lower than that of the fluorophore, AP (ϕ_f = 0.70 in THF)[29] indicating an efficient

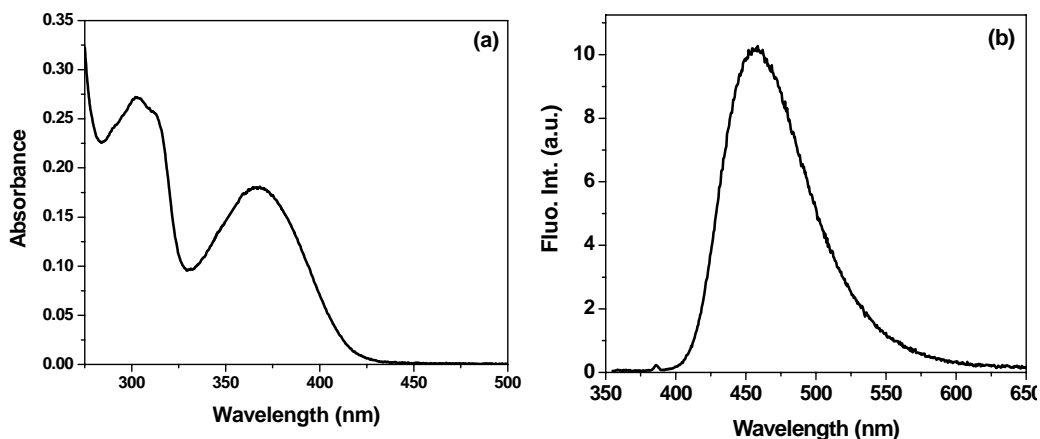photoinduced electron transfer (PET) between the fluorophore and receptor moieties.

Figure 6.1 Absorption (a) and fluorescence (b) spectra of **APCr** (1.75×10^{-5}M) in THF. The fluorescence spectrum was obtained by exciting the sample at 345 nm.

The PET in this system may appear unexpected when the influence of the internal electric (dipolar) field on the PET process, as indicated by de Silva and coworkers,[30] is taken into account. However, we have previously demonstrated that through-space PET in several aminophthalimide and aminonaphthalimide derivatives is not hampered by the electric dipole of the AP moiety.[8,13,31,32] A multiexponential fluorescence decay behavior (Figure 6.2) is observed for the system yielding the following decay parameters: $\tau_1 = 0.17$ ns (64%), $\tau_2 = 0.9$ ns (23%) and $\tau_3 = 15$ ns (13%). The complex nature of the fluorescence decay behavior is a reflection of the flexibility of the molecule, which can exist in several conformations. Two limiting situations can be considered here. One in which the spatial disposition of the fluorophore and receptor moieties is favorable

for PET, which can give rise to components (0.17 ns and 0.9 ns) that are much shorter than the fluorescence lifetime of AP (12.4 ns in THF).[29] The other limiting situation in which the spatial arrangement of the receptor and fluorophore moieties is unfavorable for PET can contribute to the 15 ns component. The time-resolved data suggests that nearly 87% of the molecules are in PET communication with the receptor moiety.
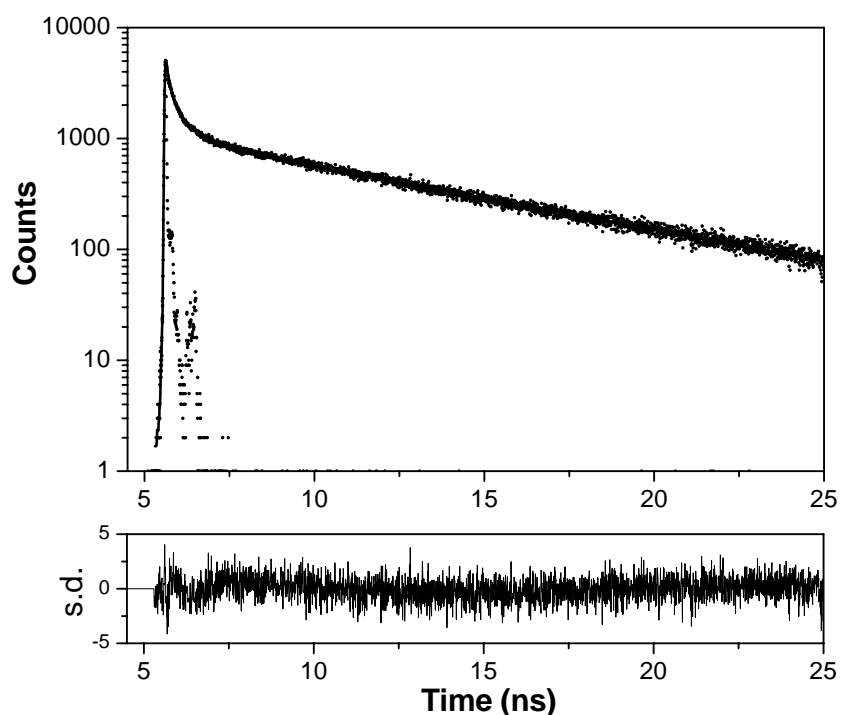

Figure 6.2 Fluorescence decay profile of **APCr** in THF. The solution was excited at 375 nm and the fluorescence monitored at 455 nm. The solid line represents the best fit to the decay profile. The decay parameters are $\tau_1 = 0.17$ ns (64%), $\tau_2 = 0.9$ ns (23%), $\tau_3 = 15.0$ ns (13%).
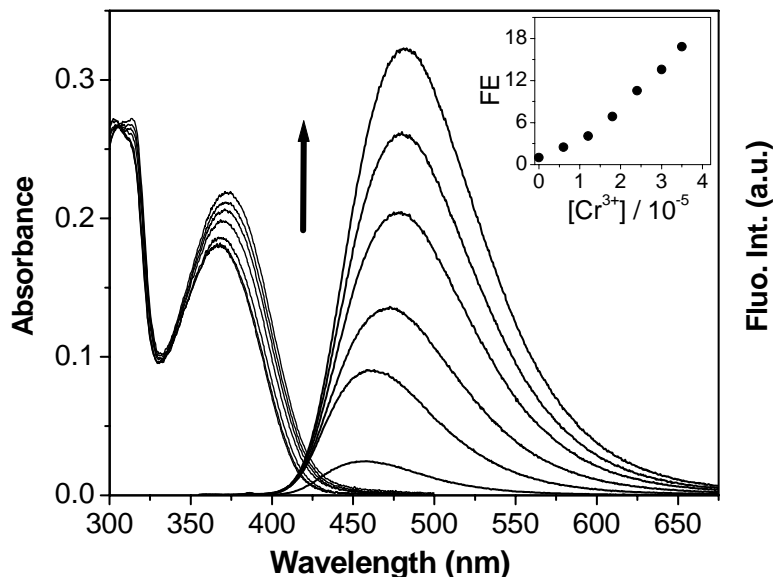
Figure 6.3 Absorption and fluorescence spectra of **APCr** in THF upon progressive addition of Cr(III). [**APCr**] = 1.7×10^{-5} M, [Cr^{3+}] = $(0–3.5) \times 10^{-5}$ M. Inset: fluorescence enhancement vs. concentration of Cr(III).

We have examined the effects of various metal ion additives on the spectral features of **APCr**. It was found that among the metal ions studied, only Cr(III) significantly modulated the absorption and fluorescence spectra of **APCr**. Progressive addition of Cr(III) to a solution of **APCr** led to a gradual bathochromic shift of the absorption maximum with a slight increase in absorbance (Figure 6.3). The presence of an isosbestic point in the absorption spectra at around 345 nm indicated that the optical response arises from the formation of 1:1 complex between **APCr** and Cr(III).

The interaction of **APCr** with Cr(III) causes 27 nm Stokes shift of the emission band and a ~17-fold increase in the fluorescence quantum yield (Table

6.1). The enhancement of fluorescence is clearly due to the disruption of PET communication between the receptor and fluorophore moieties on introduction of metal ions into the coordination sphere of SNS.

Binding constant values (*vide* Table 6.1) evaluated from the absorption titration data assuming 1:1 stoichiometry indicate that **APCr** forms a strong complex with Cr(III) in solution. This is consistent with the literature where it is reported that SNS ligand forms a stable complex with Cr(III) that can be used as a catalyst.[28]

Table 6.1 Maximum Fluorescence Enhancement (FE) Observed and the Binding Constant Values for Selected Metal Ions with **APCr**

Metal ion	FE	$K / 10^4 \text{ M}^{-1}$
None	1.0	-
Cr(III)	16.8	11.3
Mn(II)	1.3	-
Fe(III)	4.3	8.0
Co(II)	1.5	-
Ni(II)	1.2	-
Cu(II)	1.6	-
Zn(II)	1.5	-
Hg(II)	1.0	-
Pb(II)	1.4	-
H^+	5.1	-

[a] λ_{exc} = 345 nm; *K* values, estimated from the absorption spectral data, can be evaluated accurately only for Cr(III) and Fe(III). These values could not be estimated for the other metal ions because of small change in the absorption behavior.

It is known that late first-row transition metal ions such as Ni(II) and Cu(II) form strong complexes with nitrogen donor ligands and in some cases with sulfur

donor ligands. However, in the present case, effective binding occurred only with Cr(III). While Stokes shifted emission with only ~4-fold increase in the quantum yield can be observed in the presence of Fe(III), all other environmentally and biologically relevant metal ions did not show any significant change of the optical response of the system (*vide* Table 6.1). Representative absorption and emission spectra of **APCr** in absence and presence of Co(II) are shown in Figure 6.4. Comparative emission spectra of **APCr** in absence and presence of different metal ions are also shown in Figure 6.5.
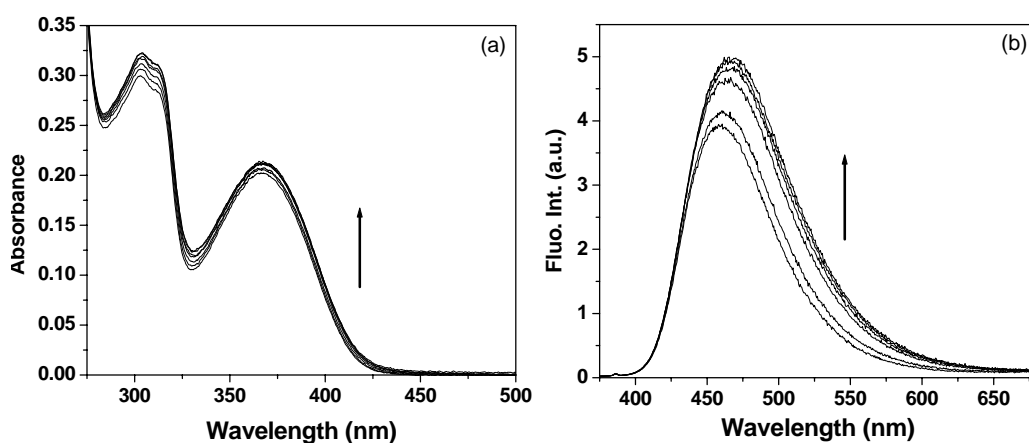

Figure 6.4 Absorption (a) and fluorescence (b) spectra of **APCr** in THF upon progressive addition of Co(II). [**APCr**] $= 1.75 \times 10^{-5}$ M, [Co^{2+}] $= (0 - 1.75) \times 10^{-5}$ M.
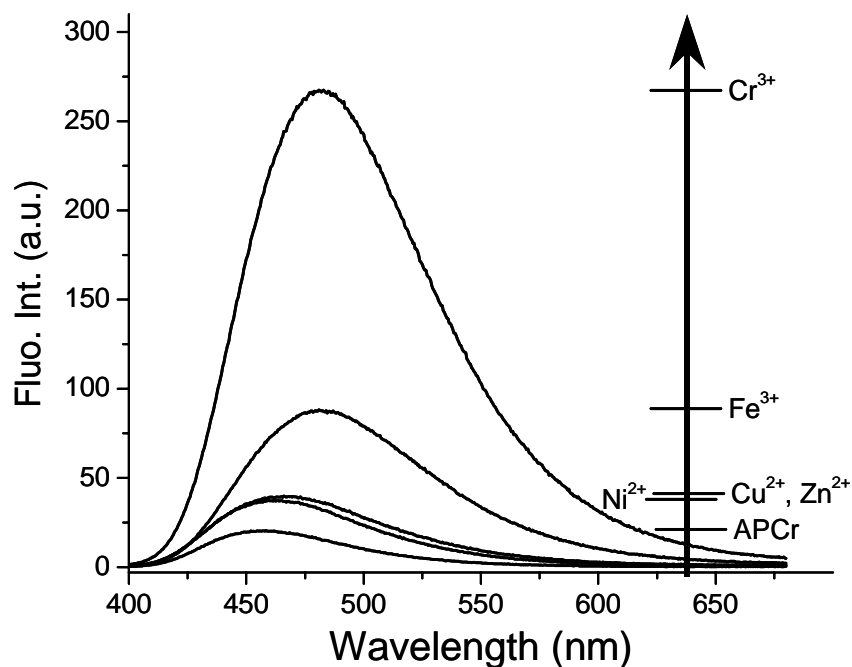
Figure 6.5 Fluorescence spectra of **APCr** (1.8 × 10^{-5} M) in the absence and presence of selected metal ions in THF. In the presence of other remaining metal ions, the spectrum overlaps either with that of the free sensor or with that of Ni(II), Cu(II) or Zn(II). The metal ion concentrations required for the observance of maximum fluorescence enhancement are in the range of (3.5 – 5) × 10^{-5} M. λ_{exc} = 345 nm.

We have also studied the effect of Cr(III) on the fluorescence decay behavior of the chemosensor. In the presence of Cr(III), the sub-nanosecond component of the decay disappears completely confirming the inhibition of the PET quenching pathway upon Cr(III) binding. The decay profile in the presence of Cr(III) can be fitted to a mono-exponential model yielding a lifetime of 10.8 ns (Figure 6.6).
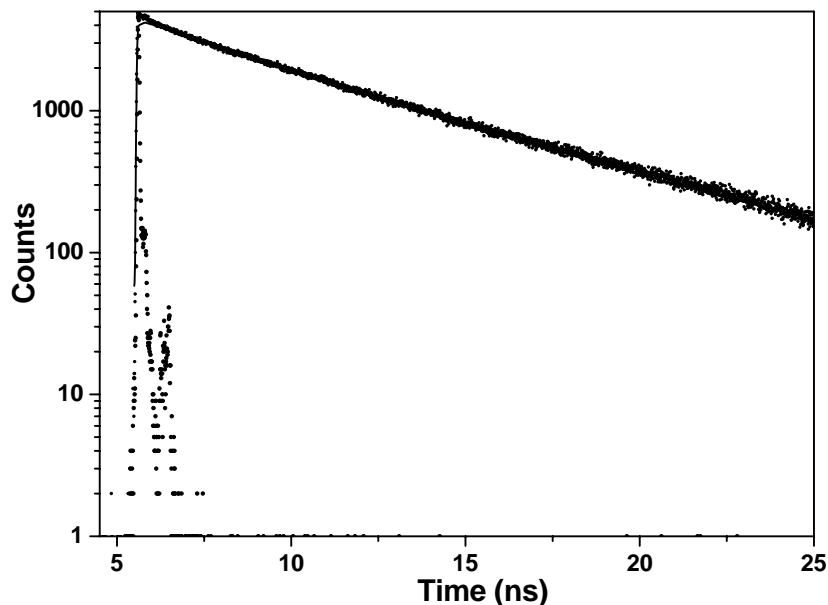
Figure 6.6 Fluorescence decay profile of **APCr** in the presence of Cr(III) in THF. The solution was excited at 375 nm and monitored at 455 nm. The solid line represents the mono-exponential fit to the decay profile with lifetime $\tau = 10.8$ ns.

The selectivity of **APCr** for Cr(III) over alkali and alkaline earth metal ions, other transition and post-transition metal ions was further investigated and the results are depicted in Figure 6.7. The "off-on" signaling of **APCr** for Cr(III) is not affected in the presence of excess alkali and alkaline earth metal ions such as Na(I), K(I), Mg(II) and Ca(II). The chemosensor is also selective for Cr(III) over the divalent first-row transition metal ions and post-transition metal Cd(II), Hg(II) and Pb(II) ions. However, Cr(III) cannot displace Fe(III) from the coordination sphere of **APCr**.

Figure 6.7 A bar diagram highlighting the fluorescence "off-on" signaling response of **APCr** to Cr(III) in the presence of 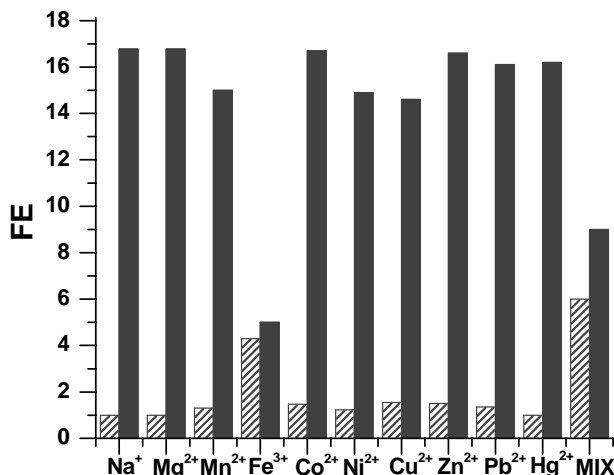selected metal ions and in the presence of all the twelve metal ions (**MIX**). The patterned bars represent enhancement of fluorescence upon addition of 2 equiv. of individual metal ions and the solid bars represent the fluorescence enhancement that occurs upon the introduction of two equiv. of Cr(III) to the solutions containing **APCr** and the selected metal ion. λ_{exc} = 345 nm.

Thus, we have tested the Cr(III) selectivity by analyzing a sample containing all the metal ions except Fe(III). Introduction of two equiv. of Cr(III) to a solution of APCr containing two equiv. each of Na(I), K(I), Mg(II), Ca(II), Mn(II), Co(II), Ni(II), Cu(II), Zn(II), Cd(II), Hg(II) and Pb(II) produced 50% increase in the fluorescence yield.

6.4. Conclusion

In summary, we have developed an 'off-on' fluorescence chemosensor for selective detection of Cr(III) exploiting the selective binding ability of the SNS ligand. A ~17-fold Cr(III)-selective chelation enhanced fluorescence response in

THF is attributed to disruption of PET communication between the receptor and the fluorophore moieties. It is also demonstrated that this system in THF is highly selective over other environmentally and biologically relevant metal ions such as alkali and alkaline earth metal ions, divalent first-row transition metal ions, Group 12 metal ions and Pb(II). However, the present system can be studied further to explore the fluorescence signaling ability of the system in other solvents.

References

1. Zayed, M.; Norman, T. *Plant Soil* **2003**, *249*, 139

2. *Chemosensors of Ions and Molecular Recognition;* eds. Desvergene, J. P.; Czarnik, A. W.; NATO ASI Series; Kluwer Academic, Dordrecht. **1997**, *C492*.

3. Spichiger-Keller, U. S. *Chemical Sensors and Biosensors for Medical and Biological Applications*; Wiley-VCH. 1998**.**

4. Singh, A. K.; Singh, R.; Saxena, P. *Sensors* **2004**, *4*, 187.

5. Hassan, S. S. M.; El-Shahawi, M. S.; Othman, A. M.; Mosaad, M. A. *Anal. Sci.* **2005**, *21*, 673.

6. de Silva, A. P.; Gunaratne, H. Q. N.; Gunnlaugsson, T.; Huxley A. J. M.; McCoy, C. P.; Rademacher, J. T.; Rice, T. E. *Chem. Rev.* **1997**, *97*, 1515.

7. Ghosh, P.; Bharadwaj, P. K; Mandal, S.; Ghosh, S. *J. Am. Chem. Soc.* **1996**, *118*, 1553.

8. Ramachandram, B.; Samanta, A. *Chem. Commun*. **1997**, 1037.

9. Rurack, K.;. Kollmannsberger, M.; Resch-Genger, U.; Daub, J. *J. Am. Chem. Soc.* **2000**, *122*, 968.

10. Prodi, L.; Bolletta, F.; Montalti, M.; Zaccheroni, N. *Coord. Chem. Rev.* **2000**, *205*, 59.

11. Rurack, K. *Spectrochim. Acta, Part A* **2001**, *57*, 2161.

12. Sankaran, N. B.; Banthia, S.; Das, A.; Samanta, A. *New J. Chem.* **2002**, *26*, 1529.

13. Banthia, S.; Samanta, A. *J. Phys. Chem. B* **2002**, *106*, 5572.

14. Sankaran, N. B.; Banthia, S.; Samanta, A. *Proc. Indian Acad. Sci.: Chem. Sci.* **2003**, *114*, 539.

15. Banthia, S.; Samanta, A. *Org. Biomol. Chem.* **2005**, *3*, 1428.

16. Banthia, S.; Sarkar, M.; Samanta, A. *Res. Chem. Intermed.* **2005**, *31*, 25.

17. Royzen, M.; Dai, Z.; Canary, W. J. *J. Am. Chem. Soc.* **2005**, *127*, 1612.

18. Banthia, S.; Samanta, A. *J. Phys. Chem. B* **2006**, *110*, 6437.

19. Hirano, T.; Kikuchi, K.; Urano, Y.; Higuchi, T.; Nagano, T. *Angew. Chem., Int. Ed. Engl.* **2000**, *39*, 1052.

20. Burdette, S. C.; Frederickson, C. J.; Bu, W.; Lippard, S. J. *J. Am. Chem. Soc.* **2003**, *125*, 1778.

21. Banthia, S.; Samanta, A. *Eur. J. Org. Chem.* **2005**, 4967.

22. Boiocchi, M.; Fabbrizzi, L.; Licchelli, M.; Sacchi, D.; Vasquez, M.; Zampa, C. *Chem. Commun.* **2003**, 1812.

23. Gunnlaugsson, T.; Leonard, J. P.; Murray, N. S. *Org. Lett.* **2004**, *6*, 1557.

24. Banthia, S.; Samanta, A. *New J. Chem.* **2005**, *29*, 1007.

25. Kaur, S.; Kumar, S. *Chem. Commun.* **2002**, 2840.

26. Wen, Z.-C.; Yang, R.; He, H.; Jiang, Y.-B. *Chem. Commun.* **2006**, 106.

27. Tanaka, M.; Nakamura, M.; Ikeda, T.; Ikeda, K.; Ando, H.; Shibutani, Y.; Yajima, S.; Kimura, K. *J. Org. Chem.* **2001**, *66*, 7008.

28. McGuinness, D. S.; Wasserscheid, P.; Keim, W.; Morgan, D.; Dixon, J. T.; Bollmann, A.; Maumela, H.; Hess, F.; Englert, U. *J. Am. Chem. Soc.* **2003**, *125*, 5272.

29. Soujanya, T.; Fessenden, R. W.; Samanta, A. *J. Phys. Chem.* **1996**, *100*, 3507.

30. de Silva, A. P.; Gunaratne, H. Q. N.; Habib-Jiwan, J. L.; McCoy, C. P.; Rice, T. E.; Soumillion, J. P. *Angew. Chem., Int. Ed. Engl.* **1995**, *34*, 1728.

31. Sankaran, N. B.; Mandal, P. K.; Bhattacharya, B.; Samanta, A. *J. Mater. Chem.* **2005**, *15*, 2854.

32. Ramachandram, B.; Saroja, G.; Sankaran N. B.; Samanta, A. *J. Phys. Chem. B* **2000**, *104*, 11824.

Photophysical and Signaling Behavior of a Nitrobenzoxa-diazole based Chemosensor

This chapter deals with synthesis, characterization, photophysical and signaling behavior of a nitrobenzoxadiazole-based system. The system has been designed and developed with a view to sensing both cations and anions. The absorption and fluorescence behavior of this system have been investigated in the absence and presence of different metal ions and anions. The cation sensing events have been exploited to construct a two-input molecular IMP logic gate.

7.1. Introduction

Design and development of fluorescence "off-on" chemosensors for various neutral and ionic analytes is an area of considerable current interest because of its biological and environmental importance.[1,2] The most commonly used design principle for metal ion fluorosensors is based on photoinduced electron transfer (PET) mechanism, wherein normally the neutral amine functionalities, termed as receptors, serve as the metal-host and communicate with the fluorophore to report the arrival of the guest.[3] In this context, the transition metal ions as analytes present an inherent challenge because of their notorious fluorescence quenching abilities.[4-6] While this problem has been overcome by utilizing either an electronically deficient fluorophore or a macrocyclic receptor in the sensor system,[7-11] one of the major drawbacks of these systems is their inability to

perform in aqueous medium, which is of biological and environmental interest, as the water molecules compete with the built-in receptor moiety of the sensor system for coordination.

Inspired by the extensive use of the protonated amine and transition metal based receptors for optical sensing of anions[12-15] and recognizing the fact that the anionic receptors are expected to bind the transition metal ions much more strongly compared to their neutral counterparts in aqueous media, we thought that metal ion recognition in water could be made efficient by employing an anionic (deprotonated amine) binding site. Although transition metal ion coordination chemistry with anionic receptors is extensive, surprisingly, this concept of utilization of an anionic receptor moiety has not been actively exploited so far perhaps due to the fact that amino hydrogen atoms are not acidic and cannot be deprotonated under mild conditions.

Since this problem can easily be overcome by having a strong electron acceptor group in conjugation with the amino nitrogen, we have designed 4-amino-7-nitrobenzoxa[1,3]diazole (ANBD) fluorophore-based sensor system **NBDEP** in which the 4-amino hydrogen can easily be abstracted generating *in-situ* anionic binding site for the transition metal ions. A pyridine moiety is purposefully introduced to facilitate the binding process. The initial fluorescence of the designed sensor **NBDEP** is switched "off" at the alkaline pH due to the deprotonation of 4-NH proton. Addition of transition metal ions to the deprotonated fluorophore results into complete recovery of fluorescence due to the formation of strong complex between the two. The spectral features of the

neutral **NBDEP**, however, remain unaffected by the presence of transition metal ions. Very importantly, these events yield the first molecular IMP logic gate.
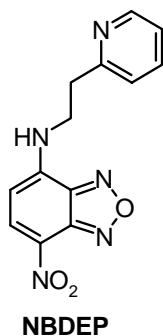
NBDEP

As an additional feature, the acidity of 4-NH proton has further been exploited for selective detection of fluoride ions. The present system also acts as a fluorescence "on-off" chemosensor for fluoride ions.

7.2. Synthesis of NBDEP

4-(2-pyridinylethyl)amino-7-nitrobenzoxa[1,3]diazole (**NBDEP**) has been synthesized in a single step process (Scheme 7.1).
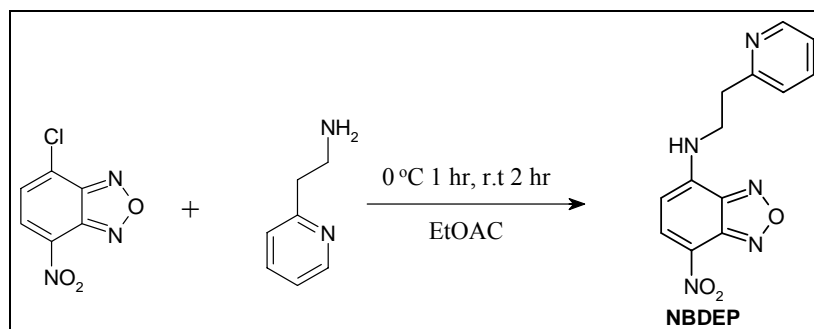
Scheme 7.1 Synthetic route to the fluorescence chemosensor **NBDEP**.

2-(2-Aminoethyl)pyridine (0.2 ml, 1.65 mmol) was added drop-wise to the solution of 4-chloro-7-nitro-benzoxa[1,3]diazole (0.3 g, 1.5 mmol) in ethylacetate at 0 – 5 ºC. The reaction mixture was stirred for 1 hour at 0 – 5 ºC and then for another 2 hours at room temperature. Subsequently, the solvent was evaporated under vacuum and the crude product was purified by column chromatography (basic alumina, 50% ethylacetate/hexane). Yield 70%. The compound was characterized from the following analytical data.

IR: 3200 cm^{-1} (NH); ^{1}H NMR (CDCl$_3$, 400 MHz): δ 3.24 and 3.90 (t, J = 7.0 Hz each, 4 H), 6.17 (d, J = 8.3 Hz, 1 H), 7.21-7.24 (m, 2 H), 7.65-7.67 (m, 1 H), 8.09 (s, 1 H), 8.47 (s, 1 H), 8.63 (d, J = 8.2 Hz, 1 H); CHN analysis calculated for C$_{13}$H$_{11}$N$_5$O$_3$: C, 54.74; H, 3.89; N, 24.55. Found: C, 54.10; H, 3.85; N, 24.44; LCMS: m/z 286 (M+H$^+$).

7.3. X-ray crystallographic measurements

The present chemosensor was further characterized by single crystal X-ray diffraction. Single crystals suitable for X-ray diffraction were grown from slow evaporation of the CDCl$_3$ solvent. ORTEP diagram of the system is shown in Figure 7.1. Structure solution and refinement was carried out with orthorhombic space group, *Pbca*. It has been found that C-N4 bond length (Figure 7.1) is significantly shorter (1.335 Å) than the C(sp^3)-N bond length (1.47 Å). The shortening of the bond is indicative of considerable charge transfer from the N4 nitrogen to the nitro group of the benzoxadiazole moiety.
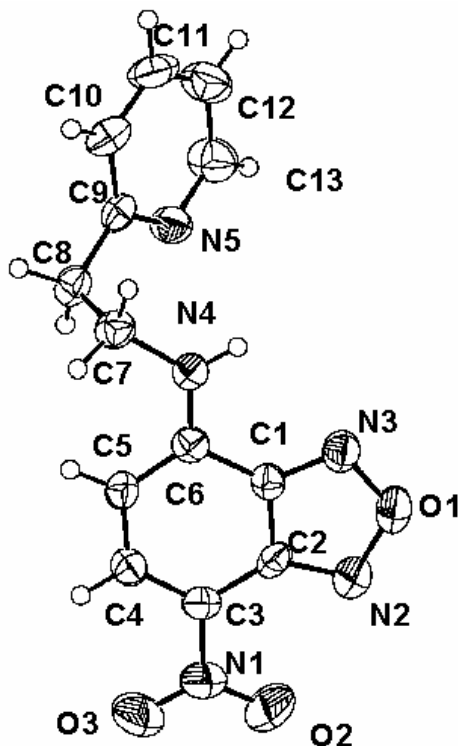
Figure 7.1 ORTEP diagram of **NBDEP** with atoms represented by thermal ellipsoid at the 50% probability level.

Selected crystallographic data: $C_{13}H_{11}N_5O_3$: *M* = 285.26; orthorhombic, space group *Pbca*; cell dimensions *a* = 13.560(11) Å, *b* = 7.385(6) Å, *c* = 26.06(2) Å, *V* = 2609(4) Å^3, *Z* = 8, ρ_{calc} = 1.452 g cm^{-3}, μ (Mo-Kα radiation) = 0.108 mm^{-1}, λ = 0.71073 Å, *T* = 293 K. Reflections collected: 23234 (CCD area detector diffractometer), 2322 unique, 193 parameters refined using 1221 reflections with *I* > 2σ(*I*) to final R indices: R1 = 0.0567, wR2 = 0.1495, GOF = 0.950.

7.4. Absorption and fluorescence behavior of NBDEP in absence and presence of transition metal ions
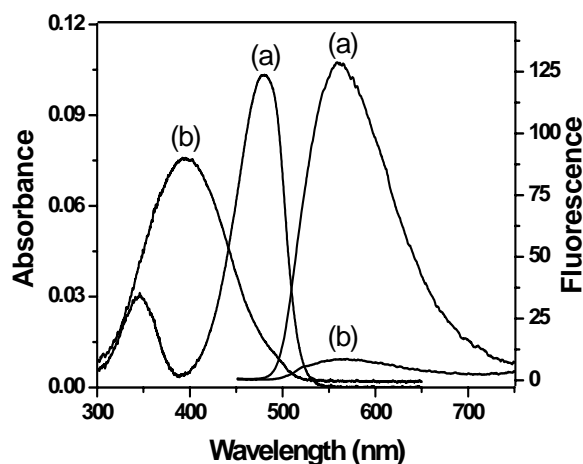
Figure. 7.2 Absorption and fluorescence spectra ($\lambda_{exc.}$ = 440 nm) of **NBDEP** in aqueous solution (a) at pH = 7.4 (b) at pH= 10.7.

The absorption and fluorescence spectra of **NBDEP** at pH 7.4 (buffered water) consist of broad structureless band centered at 480 nm and 558 nm, respectively (Figure 7.2), which is typical of the intramolecular charge transfer (ICT) transition between the amino and nitro groups of the fluorophore.[16] Even though **NBDEP** bears an architecture (*fluorophore-spacer-receptor*) similar to that of commonly used photoinduced electron transfer (PET) sensor systems,[17] PET quenching communication between the pyridyl and ANBD moieties is not significant in the system. This is evident from the fact that the fluorescence quantum yield (0.05) of **NBDEP** is comparable to that of the parent fluorophore, ANBD, (0.06). The lack of PET interaction in **NBDEP** is consistent with the observations made in similar systems.[18-20] In fact, we chose the pyridyl moiety as

an additional binding site for it does not enter into communication with the fluorophore. The absorption and fluorescence spectra of **NBDEP** are slightly dependent on pH in the acidic pH range. A small shift (~400 cm^{-1}) of the absorption maximum accompanied by small change in absorption and fluorescence intensities between pH 3 and 5 can be ascribed to the protonation of the pyridyl nitrogen atom (pK_a = 3.9).[21] However, the spectra are strongly dependent at higher pH values (9.2-10.6) due to the deprotonation of the 4-NH proton leading to the formation of the anionic species. Due to this deprotonation event, a large hypsochromic shift is expected due to the redistribution of electron density. The ground state dipole moment of **NBDEP** and its deprotonated form (**NBDEP⁻**) is 10.9 D and 8.5 D respectively, as calculated by semi-empirical AM1 method on the optimized molecular geometry.[22] The formation of the anionic species is associated with the appearance of a new absorption band at 395 nm at the expense of the 480 nm band (Figure 7.2). That the fluorescence of the system is significantly quenched and no new fluorescence band is observed suggest that the deprotonated form of **NBDEP** is very weakly fluorescent or nonfluorescent (Figure 7.2). In this connection, we note that recently Xu and coworkers have observed emission from a deprotonated species at a longer wavelength compared to the parent system and has suggested this as a general strategy for colorimetric and ratiometric fluorescence signaling purpose.[23] However, since a deprotonated fluorophore is a completely new chemical entity, all deprotonated species need not be fluorescent. The pK_a values for the deprotonation event evaluated from the absorbance and fluorescence changes are 10.4 (±0.1) and 10.6 (±0.1) respectively.[21]

The effect of the d-block metal ions on the absorption and fluorescence behaviour of the systems at neutral (pH=7.4) and mildly alkaline media (pH=10.7, carbonate-bicarbonate buffer, 100 mM KCl) is found quite interesting. Addition of the metal perchlorate salts in neutral aqueous solution of **NBDEP** does not result in any significant change of the absorption or fluorescence spectrum of **NBDEP** (Figure 7.3) indicating poor affinity of the system towards the transition metal ions.

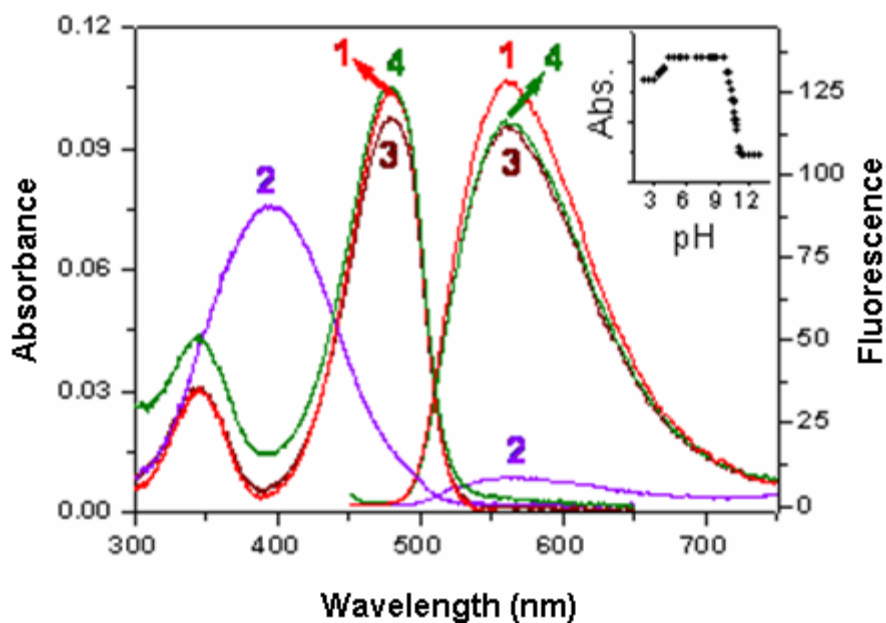**Figure 7.3** Absorption (left axis) and fluorescence (right axis) spectra ($\lambda_{exc.}$ = 440 nm) of **NBDEP** in water under different input conditions: (1) none, pH = 7.4; (2) only OH⁻, pH = 10.7; (3) only Zn^{2+}, pH = 7.4; (4) OH⁻ (pH = 10.7) and Zn^{2+}. Inset: absorbance at 480 nm vs. pH.
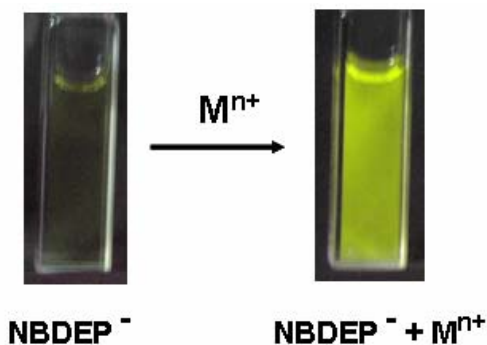
Figure 7.4 Naked eye observation of the effect of metal ions on the fluorescence output of **NBDEP** at pH=10.7.

This is not surprising considering the fact that the electron density at the 4-N atom, which is in conjugation with the electron withdrawing nitro group, is low,[16] and that there is very little communication between the pyridyl moiety and the fluorophore. Interestingly, addition of the d-block metal ions in alkaline media (pH=10.7) results in the recovery of the 480 nm absorption band as well as the fluorescence of the system (Figure 7.3). In highly alkaline aqueous media, metal salts of Ni^{2+} and Cu^{2+} are known to form precipitate of their hydroxides and those of Zn^{2+} form $[Zn(OH)_4]^{2-}$. However, at pH=10.7, no precipitation could be observed and this observation is consistent with the literature.[24] The pyridyl moiety of **NBDEP** is a cation receptor and under conditions such as in basic media the deprotonated 4-N atom along with the pyridine nitrogen atom should form strong complexes with transition metal ions (Scheme 7.2).
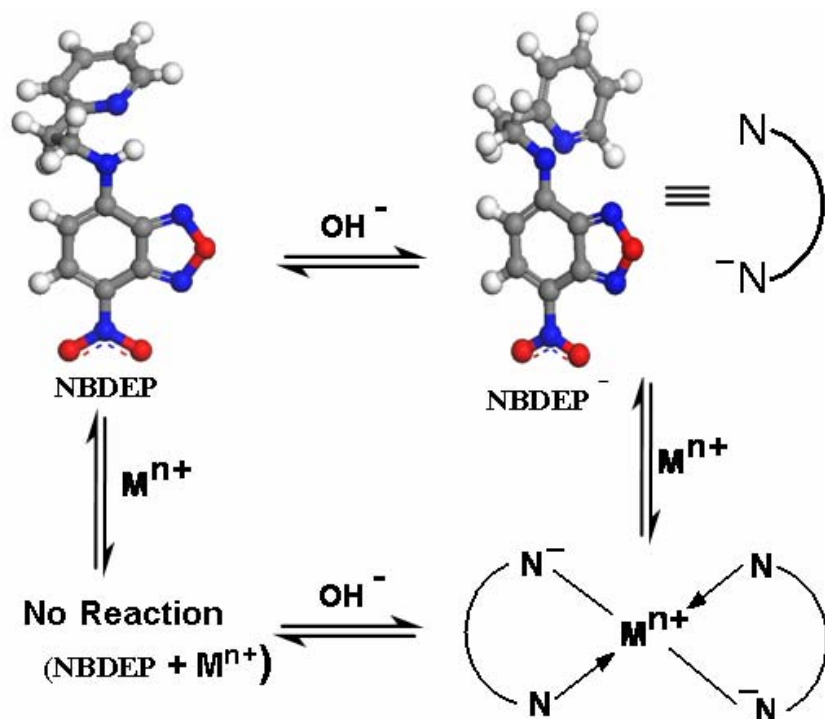
Scheme 7.2 Proposed scheme for the molecular states after various logical events. The optimized molecular structure of **NBDEP** and its deprotonated form **NBDEP⁻** generated using MS Modelling (version 3.0) are shown.

Thus, in the presence of transition metal ions, the spectral features of the system are re-modulated to the original. A typical absorption and fluorescence titration of **NBDEP** at pH=10.7 with the metal salt has been illustrated in Figure 7.5. The effect is quite similar for different transition metal ions. The binding constant values for various transition metal ions are evaluated to be in the range of $(1\text{-}5) \times 10^3 \text{ M}^{-1}$.
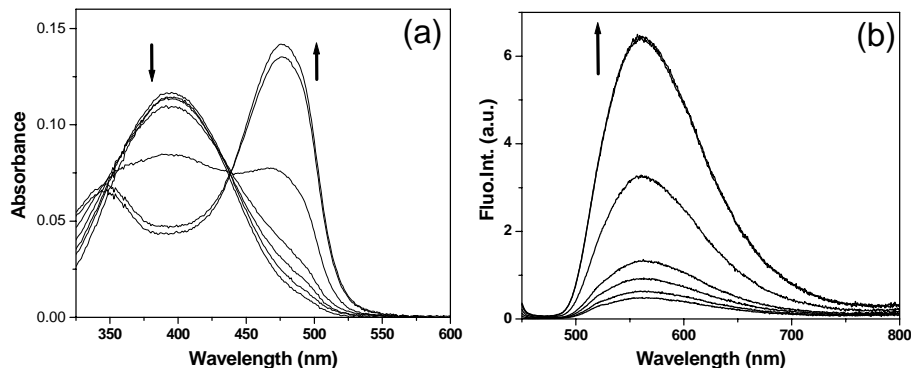
Figure 7.5 Typical changes in the absorption (a) and fluorescence (b) spectra of **NBDEP** (4.9 x 10^{-6} M) upon subsequent addition of metal salts. Data shown in the plot are for Ni^{2+}; $[Ni^{2+}] = (1.8 \times 10^{-4} - 7 \times 10^{-4})$ M.

An important perspective of the fluorescent signaling systems is to establish their input-output relationships in terms of logic gate operations.[25-28] For applications, such as molecule-based logic circuitry, the devices are molecular analogues of those based on the conventional silicon-based circuitry.[25-28] The logic gate implementation of the present events is shown in Figure 7.6 and the corresponding optical outputs observed at the absorption and emission wavelength maxima produce the truth table, Table 7.1.
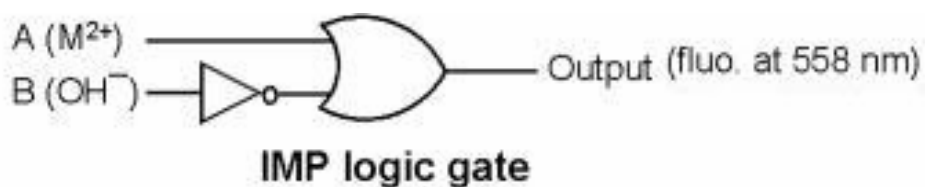
Figure 7.6 Logic circuit for the two-input IMP gate.

Table 7.1 Truth Table for IMP Logic Operation for **NBDEP**[a]

Input		Output
A (M^{+2})	B (OH^-)	Fluorescene (ϕ_f)
0	0	1 (0.051)
0	1	0 (0.003)
1	0	1 (0.046)[b]
1	1	1 (0.046)[b]

[a] 1×10^{-5} M. 0 and 1 represent none and maximum input concentrations, respectively. The maximum concentration for OH^- is 2×10^{-3} M and for M^{2+} is 1×10^{-3} M. Samples excited at 440 nm, fluorescence maximum is at 558 nm.[b] these values are for Zn^{+2} as metal ion input.

High fluorescence output is produced under all circumstances except in the presence of *only* base. This behavior can be conveniently described using logic notation, A+B′ (IMP function),[29] where A and B represent input concentrations of metal ions and the base, respectively. While different molecular logic gates based on chemical inputs and optical outputs including the INH logic has been demonstrated previously,[30-32] the IMP logic has remained elusive.

7.5. Absorption and fluorescence behavior of NBDEP in absence and presence of halides

It is important to note that systems capable of detecting cations and anions simultaneously are very rare.[33-37] As can be seen from our early discussion on this chapter, the 4-NH prtoton of the present system is highly acidic. Literature suggests that a polarized N-H fragment can effectively be used as an efficient receptor for anion recognition and sensing events. Thus we have exploited the acidic nature of the 4-NH proton of the present system for selective detection of fluoride in acetonitrile.

The anion sensing event has been shown in Figure 7.6 and Figure 7.7 respectively. The system operates through both absorption and emission enabling optical detection of fluoride.

On addition of fluoride to an acetonitrile solution of **NBDEP**, the ICT absorption band gradually loses intensity with a slight blue shift. Interestingly, a new structured band centered at 400 nm appears with a clear isosbestic point at 350 nm indicating 1:1 stoichiometry of the complex. The binding constant from the absorption data is estimated to be 6.5×10^4 M^{-1}. The emission spectrum of **NBDEP** is also substantially modified with large quenching of fluorescence on addition of F$^-$ (Figure 7.7). In the presence of other halide ions, only slight quenching of fluorescence has been observed (Figure 7.7). Considering the acidic nature of 4-NH proton, its hydrogen bonding interaction with F$^-$ is attributed to the changes in the optical properties of **NBDEP.**
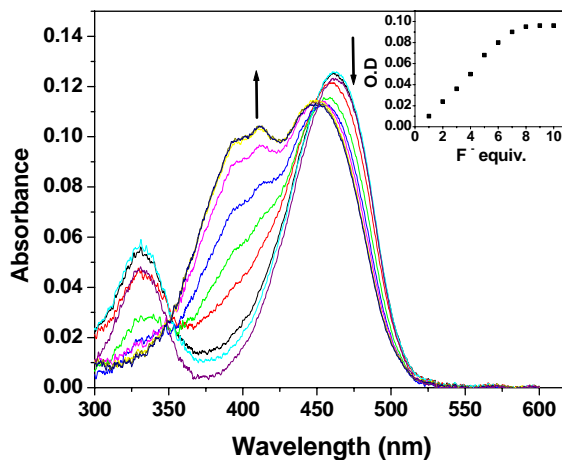
Figure 7.6 Absorption spectra of **NBDEP** (4×10^{-6} M) with gradual addition F$^-$ (4×10^{-6} to 4×10^{-5} M) in acetonitrile. Inset shows the OD vs. F$^-$ equiv. plot.
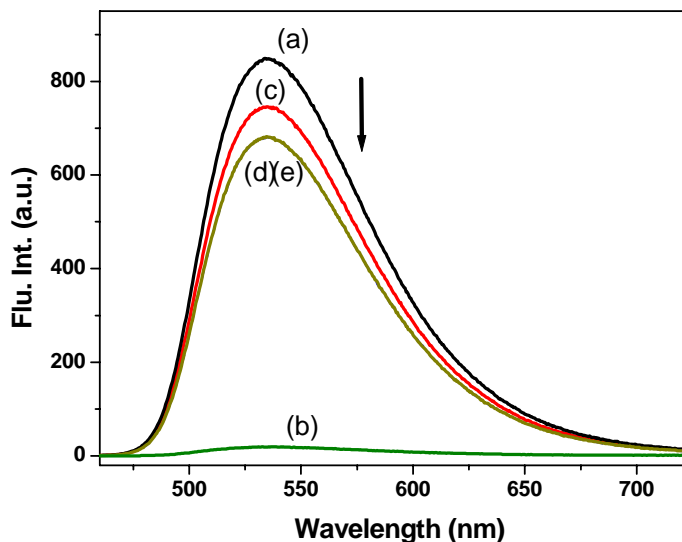
Figure 7.7 Fluorescence spectra of **NBDEP** in acetonitrile (a), and after addition of 10 equivalents of F$^-$ (b), Cl$^-$ (c), Br$^-$ (d) and I$^-$ (e).

7.6. Conclusion

We have shown that *in-situ* generation of an anionic binding site in a ICT fluorophore offers fluorescence detection of transition metal ions in aqueous media, otherwise not possible with the neutral species. The concept described here can easily be extended for the construction of practical sensor systems for metal ions in aqueous solution utilizing specific ionophores. The ICT-based system reported herein is an example of a two-input IMP molecular logic gate and thus an important contribution towards the development of molecular logic devices. The present system is also capable of reporting fluoride ions in non-aqueous media.

Refererences

1. Spichiger-Keller, U. S. *Chemical Sensors and Biosensors for Medical and Biological Applications*; Wiley-VCH: Weinheim, 1998.

2. *Chemosensors of Ion and Molecular Recognition*; Desvergene, J. P.; Czarnik, A. W., Eds.; Kluwer Academic: Dordrecht, 1997; Vol. C492.

3. de Silva, A. P.; Gunaratne, H. Q. N.; Gunnlaugsson, T.; Huxley, A. J. M.; McCoy, C. P.; Rademacher, J. T.; Rice, T. E. *Chem. Rev.* **1997**, *97*, 1515.

4. Rurack, K. *Spectrochim. Acta, Part A* **2001**, *57*, 2161.

5. Prodi, L.; Bolletta, F.; Montalti, M.; Zaccheroni, N. *Coord. Chem. Rev.* **2000**, *205*, 59.

6. Valeur, B.; Leray, I. *Coord. Chem. Rev.* **2000**, *205*, 3.

7. Ghosh, P.; Bharadwaj, P. K.; Mandal, S.; Ghosh, S. *J. Am. Chem. Soc.* **1996**, *118*, 1553.

8. Rurack, K.; Kollmannsberger, M.; Resch-Genger, U.; Daub, J. *J. Am. Chem. Soc.* **2000**, *122*, 968.

9. Banthia, S.; Samanta, A. *J. Phys. Chem. B* **2002**, *106*, 5572.

10. Banthia, S.; Sarkar, M.; Samanta, A. *Res. Chem. Intermed.* **2005**, *31*, 25.

11. Banthia, S.; Samanta, A. *Org. Biomol. Chem.* **2005**, *3*, 1428.

12. Beer, P. D. *Acc. Chem. Res.* **1998**, *31*, 71.

13. Fabbrizzi, L.; Lichelli, M.; Rabaioli, G.; Taglietti, A. *Coord. Chem. Rev*. **2000**, *205*, 85.

14. Parker, D. *Coord. Chem. Rev.* **2000**, *205*, 109.

15. Martinez-Manez, R.; Sancenon, F. *Chem. Rev.* **2003**, *103*, 4419.

16. Saha, S.; Samanta, A. *J. Phys. Chem. A* **1998**, *102*, 7903.

17. Callan, J. F.; de Silva, A. P.; Ferguson, J.; Huxley, A. J. M.; O'Brien, A. M. *Tetrahedron* **2004**, *60*, 11125.

18. Sankaran, N. B.; Banthia, S.; Das, A.; Samanta, A. *New J. Chem.* **2002**, *26*, 1529.

19. Banthia, S.; Samanta, A. *Inorg. Chem.* **2004**, *43*, 6890.

20. Banthia, S.; Samanta, A. *New J. Chem.* **2005**, *29*, 1007.

21. Using: $\log[(A_{max} - A)/(A - A_{min})] = pH - pK_a$ and $\log[(\phi_{max} - \phi)/(\phi - \phi_{min})] = pH - pK_a$.

22. Molecular geometry was optimized using MS Modeling v.3.0.

23. Xu, Z.; Qian, X.; Cui, J. *Org. Lett.* **2005**, *7*, 3029.

24. Doman, T. N.; Williams, D. E.; Banks, J. F.; Buchanan, R. M.; Chang, H.-R.; Webb, R. J.; Hendrickson, D. N. *Inorg. Chem.* **1990**, *29*, 1058.

25. de Silva, A. P.; McClenaghan, N. D.; McCoy, C. P. *Molecular Switches*; Wiley-VCH: Weinheim, 2000.

26. Balzani, V.; Venturi, M.; Credi, A. *Molecular Devices and Machines*; Wiley-VCH: Weinheim, 2003.

27. de Silva, A. P.; McClenaghan, N. D. *Chem. Eur. J.* **2004**, *10*, 574.

28. Raymo, F. M.; Giordani, S. *J. Am Chem. Soc.* **2002**, *124*, 2004.

29. Burger, P. *Digital Design: A Practical Course*; Wiley: New York, 1988.

30. Banthia, S.; Samanta, A. *Eur. J. Org. Chem.* **2005**, 4967.

31. Gunnlaugsson, T.; Mac Donaill, D. A.; Parker, D. *J. Am. Chem. Soc.* **2001**, *123*, 12866.

32. Gunnlaugsson, T.; Mac Donaill, D. A.; Parker, D.; *Chem. Commun.* **2000**, 93.

33. Shukla, R.; Kida, T.; Smith, B. D. *Org. Lett.* **2000**, *2*, 3099.

34. Kubik, S.; Goddard, R. *J. Org. Chem.* **1999**, *64*, 9475.

35. Beer, P. D.; Hopkins, P. K.; Mckinney, J. D. *Chem. Commun.* **1999**, 1253.

36. Beer, P. D.; Cooper, J. B. *Chem. Commun.* **1998**, 129.

37. Tozawa, T.; Misawa, Y.; Tokita, S.; Kubo, Y. *Tetrahedron Lett.* **2000**, *41*, 5219.

Concluding Remarks

This chapter summarizes the results of the investigations delineated in this thesis. The scope of further studies based on the findings of the present work and the challenges ahead have also been outlined.

8.1. Overview

The work embodied in this thesis has been undertaken with a two-fold objective: firstly, to understand the basic photophysics relating to the charge/electron transfer phenomenon of some new electron donor-acceptor (EDA) systems and secondly, to envisage the utility of some EDA systems in recognition and sensing of metal ions and anions exploiting the charge/electron transfer phenomenon. In this context, several EDA systems have been designed and subsequently developed. Thus, synthesis and characterization of the systems constitute a major part of the thesis. Once developed, the systems have been studied thoroughly to investigate the different photophysical processes associated with them and also some of their applications towards the signaling of cations and anions. For these purposes, several instrumental techniques and methodologies such as IR, NMR and mass spectroscopy, CHN analysis, UV-vis absorption, steady-state and time-resolved fluorescence spectroscopy, laser flash photolysis, X-ray crystallography and theoretical calculations have been employed. The results obtained from the investigations are outlined below.

Several structurally similar 2-amino-7-nitrofluorene derivatives, in which different amino groups serve as the electron donor and a nitro group serve as the acceptor, have been synthesized and fully characterized by conventional techniques and X-ray crystallography. The primary objective of this study is to examine the influence of various amino functionalities on the energetics and consequent changes in the radiative and nonradiative processes of the systems. Photophysical behavior of the systems has been studied using steady state and time-resolved absorption and fluorescence techniques in solvents of varying polarity. The fluorescence behavior of all the systems is found to be strongly dependent on the polarity of the solvent. Unlike the commonly encountered electron-donor-acceptor (EDA) systems, several fluorescence bands have been identified under various experimental conditions for these systems. The results point to the existence of multiple close-lying excited states, internal motion and their influence on the photophysical behavior of the systems. Theoretical calculations based on TD-DFT method support our experimental findings.

Another set of EDA systems, aminomethoxyflavone derivatives, have been synthesized and fully characterized. The spectral and temporal behavior of the systems has been studied in solvents of different polarity. The fluorescence properties of the systems are found to be strongly dependent on the polarity of the solvent. Except for the unsubstituted amino derivative, all other amino systems have been found to behave similarly. In these systems, the nonradiative rate constants evaluated from the quantum yield and lifetime values gradually decrease with an increase in the polarity of the solvent. The observations have been interpreted taking into consideration the nature of the two excited states

involved in the emission process. The results suggest a change in the nature of the emitting state from n-π^* to π-π^* with an increase in the polarity of the medium. Excited state calculations of the frontier orbitals based on the TD-DFT method, support the experimental results.

The aminomethoxyflavone derivatives are strongly fluorescent in polar medium. However, as the flavones have not been exploited for signaling of anions we have attempted to design and develop a flavone-based chemosensor for selective-signaling of fluoride ion. The photophysical, NMR, and density functional studies have been carried out to determine the nature of the interaction between sensor system and X^- (X = halogen atom) responsible for fluoride-induced dramatic changes in the absorption and emission properties of the sensor. The color change of the sensor, which can be observed by naked eye, is found specific to fluoride ion and is unaffected by the presence of a large excess of Cl^-, Br^-, I^- thus rendering the present system as a selective sensor for micromolar concentration of fluoride in the visible region. The changes in the fluorescence behavior of the sensor, specifically, the formation of an additional long-wavelength emission band in the presence of fluoride ion allows ratiometric fluorescence signaling of the fluoride ion as well. The results suggest that abstraction of the acidic proton of the sensor by F^- leading to the formation of the anionic form of the sensor is responsible for the spectral changes that allow signaling of the F^-. Density functional calculations confirm the proton abstraction mechanism of signaling of F^-.

As fluorosensor for selective detection of Cr(III) is rare, we have designed and developed a 4-aminophthalimide-based "off-on" fluorosensor with a view to

sensing Cr(III) ion selectively. The fluorosensor is designed on the *fluorophore-spacer-receptor* architecture. A SNS ligand, (di(2-ethylsulfanylethyl)amine), has been used as the receptor unit as it is known to form a strong complex with Cr(III) ion in nonaqueous medium. The effects of various metal ion additives on the spectral behavior of the present sensor system have been examined in tetrahydrofuran**.** It is found that among the metal ions studied, only Cr(III) significantly modulates the absorption and fluorescence spectra of the system**.** A ~17-fold Cr(III) selective chelation-enhanced fluorescence response in THF is attributed to the disruption of PET communication between the receptor and fluorophore moieties. It is shown that the system is highly selective over other environmentally and biologically relevant metal ions such as alkali and alkaline earth metal ions, divalent first-row transition metal ions, Group 12 metal ions and Pb(II).

Systems that are capable of detecting both cations and anions simultaneously are rare. With a view to sensing both cations and anions utilizing a single system, we have designed and developed 4-amino-7-nitrobenzoxa[1,3]diazole-based system integrated with a 2-(2-aminoethyl) pyridine ligand and studied the colorimetric and fluorescence response of the systems towards transition metal ions and F^- at different pH values. The absorption and fluorescence spectra of the system at neutral pH consist of broad band typical of the intramolecular charge transfer (ICT) nature of the system. The system remains almost silent in the acidic pH range, but at basic pH, the initial fluorescence of the system is switched "off" due to the deprotonation of 4-NH proton. Interestingly, addition of transition metal ions at this stage results in complete recovery of fluorescence due to the

formation of a strong complex between the deprotonated fluorophore and the metal ions leading to a base-triggered "off-on" signaling of transition metal ions. The cation sensing events have been exploited further to construct a two-input IMP molecular logic gate. As an additional feature, the fluoride-selective signaling behavior of the system in acetonitrile has also been studied. A hydrogen bonding interaction between acidic 4-NH proton and F^- is primarily attributed for the fluoride-selective signaling behavior.

8.2. Future scope and challenges

The observation of multiple emission bands of the aminonitrofluorene derivatives is a highly interesting observation. More detailed and sophisticated theoretical calculations (based on methods such as CASSCF, SAC-CI, CCSD (T), etc) of the excited state structure and energetics of the systems appear necessary to unravel the complex photophysical behavior of these derivatives. Since these systems exhibit fluorescence that is highly sensitive to the surrounding environment, exploitation of these systems as fluorescence probe molecule for probing the organized assemblies such as proteins, membranes, polymer matrices is an obvious possibility that needs to be explored. These systems are expected to serve as fluorosensor for metal ions or anions by exhibiting a shift of the fluorescence maxima and also possibly by modulation of the fluorescence intensity.

Aminomethoxyflavone derivatives are also expected to serve as reporter molecules for the estimation of polarity of various microenvironments in organized systems. The triplet states of the systems have rarely been investigated.

Study of the triplet state of these systems using time-resolved absorption technique is necessary for a complete understanding of the photophysics of the systems. Excited state intramolecular charge transfer coupled excited state intramolecular proton transfer reactions can be an interesting theme of study in aminomethoxyflavone derivatives containing a hydroxyl functionality instead of the methoxy group.

The fluoride-selective behavior of the flavone-based sensor reported here is observable only in organic medium. An improved designing strategy employing a highly pre-organized receptor or using a polymer support for the sensor system can be explored further for practical purposes.

The present study on the signaling behavior of the 4-aminophthalimide-based system shows that efficient fluorescent signaling systems for the transition metal ions can be developed by employing an electron deficient fluorophore like AP in the *fluorophore-spacer-receptor* design format. However, as stated earlier, this fluorophore is particularly not suitable for aqueous environment. Therefore, we need to develop systems employing other fluorophores that perform better in aqueous environment.

The nitrobenzaoxadiazole-based sensor systems can be effectively used for the signaling of transition metal ions in aqueous medium. However, the present system is not selective to any particular metal ion. Thus, appropriate receptor unit should be integrated with this fluorophore to achieve selective signaling behavior. Although it has been possible to mimic some of the logic functions (in the present case, IMP) at the molecular level by combining chemical and photonic signals, molecular scale logic gates for real world applications are quite far from

the reality. Combined efforts from both the chemist and the electronic engineers are necessary to construct molecular logic gates for actual applications.

Appendix

Publication numbers and atomic coordinates for X-ray structures reported in the thesis

I. Publication numbers for the published compounds

Compounds **DMANF**, **5ANF** and **6ANF**:

Publication no. 4 (Contents, pp vii)

Compound **NBDEP**:

Publication no. 6 (Contents, pp vii)

Table A.1 Atomic coordinates ($\times 10^4$), equivalent isotropic displacement parameters ($\text{Å}^2 \times 10^3$) for **4AMF**. U(eq) is defined as one third of the trace of the orthogonalized U_{ij} tensor.

Atoms	x	y	z	U(eq)
O(1)	9460(1)	4567(1)	1389(1)	54(1)
O(2)	9779(1)	1671(1)	1467(1)	72(1)
O(3)	11239(1)	2355(2)	884(1)	77(1)
N(1)	11009(2)	7498(2)	588(1)	74(1)
C(2)	9347(2)	3494(2)	1536(1)	51(1)
C(3)	9947(2)	2750(2)	1381(1)	55(1)
C(4)	10727(2)	3044(2)	1060(1)	57(1)
C(5)	11569(2)	4640(2)	688(2)	63(1)
C(6)	11635(2)	5717(2)	577(2)	64(1)
C(7)	10961(2)	6431(2)	725(1)	57(1)
C(8)	10236(2)	6011(2)	997(1)	54(1)
C(9)	10190(2)	4917(2)	1114(1)	50(1)
C(10)	10836(2)	4194(2)	960(1)	52(1)

C(11)	8519(2)	3348(2)	1839(1)	53(1)
C(12)	7894(2)	4194(2)	1789(2)	60(1)
C(13)	7111(2)	4095(3)	2069(2)	71(1)
C(14)	6937(2)	3139(3)	2410(2)	80(1)
C(15)	7545(2)	2296(3)	2470(2)	80(1)
C(16)	8328(2)	2391(2)	2189(2)	71(1)
C(17)	10494(2)	1126(3)	2042(2)	94(1)
C(18)	11710(2)	8171(2)	380(2)	79(1)
C(19)	11154(3)	9157(3)	511(2)	103(1)
C(20)	10466(2)	8397(2)	762(2)	74(1)
O(4)	6512(1)	6160(1)	10199(1)	55(1)
O(5)	6234(1)	8614(1)	9071(1)	65(1)
O(6)	5453(1)	7077(2)	7919(1)	75(1)
N(2)	5662(2)	2518(2)	9676(2)	86(1)
C(21)	6596(2)	7199(2)	9974(2)	51(1)
C(22)	6243(2)	7525(2)	9220(1)	51(1)
C(23)	5798(2)	6776(2)	8604(2)	55(1)
C(24)	5440(2)	4819(2)	8338(2)	63(1)
C(25)	5407(2)	3771(2)	8597(2)	66(1)
C(26)	5715(2)	3544(2)	9400(2)	58(1)
C(27)	6077(2)	4363(2)	9927(2)	58(1)
C(28)	6118(2)	5402(2)	9654(1)	46(1)
C(29)	5790(2)	5661(2)	8856(1)	53(1)
C(30)	7080(2)	7875(2)	10647(1)	51(1)
C(31)	6929(2)	7709(2)	11388(2)	72(1)
C(32)	7377(2)	8340(3)	12016(2)	84(1)
C(33)	7981(2)	9136(2)	11923(2)	81(1)
C(34)	8146(2)	9291(2)	11201(2)	81(1)
C(35)	7711(2)	8659(2)	10567(2)	69(1)
C(36)	6682(2)	8947(2)	8479(2)	73(1)
C(37)	5536(2)	1492(2)	9291(2)	87(1)
C(38)	5908(3)	979(3)	10101(2)	115(1)
C(39)	6094(2)	2097(2)	10441(2)	73(1)

Table A.2 Atomic coordinates ($\times 10^4$), equivalent isotropic displacement parameters ($\text{Å}^2 \times 10^3$) for **5AMF**. U(eq) is defined as one third of the trace of the orthogonalized U_{ij} tensor.

Atoms	x	y	z	U(eq)
O(1)	2392(1)	872(2)	5965(1)	57(1)
O(2)	4526(1)	2106(2)	6726(1)	74(1)
O(3)	5252(1)	2288(2)	5929(1)	83(1)
N	1895(2)	-637(3)	4467(1)	64(1)
C(2)	2985(2)	1331(3)	6342(1)	53(1)
C(3)	3947(2)	1711(3)	6340(1)	57(1)
C(4)	4394(2)	1805(3)	5934(1)	60(1)
C(5)	4056(2)	1154(3)	5135(1)	64(1)
C(6)	3463(2)	520(3)	4782(1)	66(1)
C(7)	2495(2)	-23(3)	4820(1)	56(1)
C(8)	2163(2)	111(3)	5228(1)	56(1)
C(9)	2785(2)	750(3)	5577(1)	51(1)
C(10)	3746(2)	1270(3)	5549(1)	53(1)
C(11)	2406(2)	1363(3)	6715(1)	54(1)
C(12)	1598(2)	313(3)	6720(1)	58(1)
C(13)	1042(2)	373(3)	7064(1)	64(1)
C(14)	1284(2)	1478(4)	7402(1)	73(1)
C(15)	2074(2)	2532(4)	7398(1)	82(1)
C(16)	2633(2)	2484(4)	7058(1)	84(1)
C(17)	5259(2)	866(4)	6862(1)	102(1)
C(18)	2215(2)	-918(4)	4039(1)	78(1)
C(19)	1307(3)	-1558(5)	3765(1)	119(1)
C(20)	539(3)	-1815(5)	4033(1)	105(1)
C(21)	901(2)	-1237(4)	4486(1)	73(1)